

RECLAMATION OF CLEAN WATER AND VALUABLE MINERALS FROM MUNICIPAL WASTEWATER BY CHEMICAL PRECIPITATION AND FILTRATION TECHNOLOGIES

Rhulani Shingwenyana; John Khalo; Aphiwe Sicwebu; Emission Lebepe; Ntelekoa Mohasi; Jeffrey Baloyi; Ryneth Mbhele; Vhangwele Masindi; Spyros Foteinis



TT 949/24



Reclamation of clean water and valuable minerals from municipal wastewater by chemical precipitation and filtration technologies

Report
to the
Water Research Commission

by

Rhulani Shingwenyana¹; John Khalo¹; Aphiwe Sicwebu¹; Emission Lebepe¹;
Ntelekoa Mohasi¹; Jeffrey Baloyi¹; Ryneth Mbhele¹; Vhahangwele Masindi¹; Spyros
Foteinis²

¹Council for Scientific and Industrial Research (CSIR), Smart Places, Water Centre, Water and
Wastewater research group, South Africa

²Research Centre for Carbon Solutions, School of Engineering and Physical Sciences, Heriot-Watt
University, Edinburgh EH14 4AS, United Kingdom.

WRC report no. TT 949/24

ISBN 978-0-6392-0679-0

October 2024



This is the final report of WRC project no. C2023/2024-01387.

DISCLAIMER

This report has been reviewed by the Water Research Commission (WRC) and approved for publication. Approval does not signify that the contents necessarily reflect the views and policies of the WRC, nor does mention of trade names or commercial products constitute endorsement or recommendation for use.

EXECUTIVE SUMMARY

This project comprehensively examined the introduction of the circular economy in wastewater treatment through a zero liquid discharge (ZLD) process that comprised nutrient removal and recovery from wastewater in the form of struvite along with clean water reclamation. The results and economic viability of this approach were further underpinned through a cost-benefit analysis (CBA). Specifically, raw and poorly treated municipal wastewater (MWW) is rich in microbial, organic, and inorganic contaminants. Of major concern is the elevated concentrations of nutrients, such as ammonia and phosphate, which when released to receiving environments are highly conducive to eutrophication. Oligotrophic water bodies might initially benefit from nutrients releases, but inevitably a vicious cycle is set off where excess aquatic plants and algae will eventually decompose, producing large amounts of carbon dioxide, lowering the pH, and depleting the available water-dissolved oxygen. These anoxic and harsher conditions will then lead to the death of aquatic organisms, thus reducing the biodiversity of that ecosystem and its intrinsic ability to foster life. Therefore, there is a pressing need to develop technologies that effectively manage nutrients for the benefit of downstream ecosystems and their inherent integrity. The introduction of the circular economy, and waste beneficiation and valorisation has inspired a new paradigm in wastewater management, and this was the main driver of the current project. Specifically, cryptocrystalline magnesite an abundant mineral in South Africa, was thermally activated and was solely used for the chemical precipitation of phosphate and ammonia from municipal wastewater. A co-product of this treatment process is struvite, which is a valuable slow-release fertiliser for use in agriculture. In addition, reclamation of the treated wastewater were further considered, examining different defined purposes, as stipulated in South Africa's and global regulatory frameworks, guidelines, and standards.

High accuracy analytical measurements confirmed the optimum conditions for struvite crystallisation as pH in the range 8 to 9, mixing (agitation) speed 150 rpm, reaction time 60 min, and activated magnesite dosage of 2 g per L of MWW (S/L ratio). This enabled the efficient recovery of nutrients from MWW, with complete phosphate removal (~100%) and ~71% of ammonia removal being achieved within 40 minutes and 210 minutes of interaction, respectively, thus denoting that multiple mechanisms are at play in nutrients removal from MWW. The treated MWW (supernatant from struvite synthesis) was further polished using filtration (membrane distillation) through hydrophobic polytetrafluoroethylene (PTFE) and polyvinylidene fluoride (PVDF) membranes. The membrane materials exhibited varying performances, while pre-treatment enhanced flux and minimized the permeation of ammonia,

prevented scaling, and increase in pH to be in accordance with SANS 241 specifications. Specifically, after pre-treatment, the PTFE membranes achieved an average mass flux of 1.4 g/cm²/h over extended periods, thus suggesting viability for direct agricultural application with appropriate re-mineralisation since the product water is high quality demineralised water. The CBA of the integrated system revealed a capital expenditure (CapEx) of R14.2 million and operational expenditure (OpEx) of R2.3 million. Revenue from water and struvite sales were estimated at R18.50/kL and R18.45/kg, respectively. This has yielded a 20-year net present value (NPV) of -R29.57 million and a benefit-cost ratio (BCR) of 0.19, therefore indicating that the project is currently not self-sustainable. Sensitivity analysis identified electricity costs, product pricing, and equipment costs as significant factors affecting financial viability of the integrated system. Results from this study emphasize the great need for a bespoke “barometer” for wastewater treatment cost and monetary value appreciation of struvite and water that fits defined purposes. This could focus on using more cost effective treatment methods, compared to membrane distillation, that are able to produce water for irrigation or other define purposes, including safely releasing it to the environment. Overall, this study recommends the need to compare the viability of using other types of membranes and other treatment processes for water purification, mainly keeping in mind the need to minimize treatment costs.

ACKNOWLEDGEMENTS

The project team wishes to thank the following members who served as reference group members for the project.

Reference Group	Affiliation
Prof John Ngoni Zvimba	Water Research Commission (Chairperson)
Mr Buyisile Kholisa	Water Research Commission
Prof Caliphs Zvinowanda	University of Johannesburg
Prof Elvis Fosso-Kankeu	University of South Africa
Dr Godfrey Madzivire	Council for Geosciences
Mr Hennie Kotze	City of Cape Town
Mr James Topkin	Ekurhuleni Water Care Company
Prof Jannie Maree	University of South Africa
Mr Mluleki Mguni	Umgeni Water
A/Prof Sheena Pillai	Durban University of Technology
Dr Swastika Surujlal-Naicker	City of Cape Town
Dr Zakhele Khuzwayo	Johannesburg Water

TABLE OF CONTENTS

EXECUTIVE SUMMARY	III
ACKNOWLEDGEMENTS	V
CHAPTER ONE: INTRODUCTION AND BACKGROUND	1
1.1 Introduction	1
1.2 Structure of the report	3
CHAPTER 2: STRUVITE RECOVERY	4
2.1 Introduction	4
2.2 Methodology	4
2.2.1 Materials	4
2.2.2 Optimisation studies	5
2.2.3 Percentage removal	5
2.2.4 Aqueous samples analyses	6
2.2.5 Solid samples characterization of the synthesized struvite	6
2.2.6 Nutrient recovery pilot plant	6
2.2.7 Synthesis of struvite	7
2.3 Results and discussion	8
2.3.1 Optimisation of operational parameters	8
2.3.2 Treatment of municipal effluents at optimised conditions	17
2.3.3 Parameters affecting struvite crystallisation and precipitation	20
2.3.4 Solid samples characterisation	23
CHAPTER 3: WATER RECLAMATION USING MEMBRANE DISTILLATION	31
3.1 Reclamation of clean water	32
3.2 Membrane properties	33
3.3 Experimental Apparatus	34
3.3.1 Pre-Treatment Apparatus	34
3.3.2 Membrane distillation bench scale unit	35
3.4 Optimisation of operational parameters	36
3.4.1 Effect of temperature	36
3.4.2 Effect of flowrate	36
3.5 Characterisation of the samples	36
3.5.1 Aqueous sample analysis	36
3.5.2 Solid sample analyses	37
3.6 Results on membrane distillation	37
3.6.1 Physico-chemical properties	37
3.6.2 Water recovery and membrane flux	41
3.6.3 Permeate solution recovery and solute retention	46
3.7 Characterisation of the membrane surfaces	47
3.7.1 SEM-EDS Characterisation	47
3.7.2 Fourier Transform Infrared Spectroscopy	49

CHAPTER 4: FIRST ORDER COST BENEFIT ANALYSIS FOR INTEGRATED PROCESS	52
4.1 First order cost benefit analysis	52
4.2 Capital cost	53
4.3 Operation and Maintenance Costs	54
4.4 Projected sales and benefits	55
4.4.1 Revenue from struvite as a fertiliser	55
4.4.2 Revenue of clean water	56
4.4.3 Reduced operational costs	56
4.5 Environmental and regulatory benefits	56
4.6 Evaluation of Benefits and Costs	56
4.7 Discounting method	56
4.8 Benefit-Cost Ratio	57
4.9 Costs estimation.....	57
4.9.1 Capital costs	57
4.9.2 Operational costs	62
4.10 Cost benefit analysis	63
4.10.1 Product price and revenue.....	63
4.10.2 Projected cash flow	64
4.10.3 Net present value	66
4.10.4 Benefit-cost ratio	68
CHAPTER 5: CONCLUSION AND RECOMMENDATIONS.....	69
5.1 Conclusions.....	69
5.2 Recommendations	71
REFERENCES.....	72

CHAPTER ONE: INTRODUCTION AND BACKGROUND

1.1 Introduction

Wastewater treatment facilities, in South Africa in particular, have garnered significant attention due to the observed adverse effects on receiving environments, where high nutrient loadings degrade water quality, diminish aesthetic values, and disrupt human activities such as agriculture, aquaculture, and recreation (Edokpayi et al., 2017). Historically, these treatment facilities were designed to remove nutrients and organic matter derived from domestic (households) sources. However, the high influx of nutrients along with chemicals and emerging contaminants, both from households and from other sources such as industry, have become a pressing challenge to address since these systems were not built to handle such compounds or such high nutrient influxes (Petrie et al., 2015). This issue is compounded by aging infrastructure, insufficient design capacity, and inadequate maintenance, resulting in non-compliant effluent discharges that can greatly affect aquatic ecosystems. Consequently, there is an urgent need to adopt innovative, best practice management approaches to mitigate these environmental impacts effectively (Mavhungu et al., 2020a).

The environmental and health repercussions of untreated or inadequately treated wastewater are substantial, encompassing ecological toxicity, human health risks, and socio-economic impacts (Singh et al., 2023), among others. High concentrations of nutrients such as nitrogen (N) and phosphorus (P) contribute to eutrophication, leading to harmful algal blooms and oxygen-depleted dead zones that directly threaten aquatic biodiversity (Wurtsbaugh et al., 2019). Toxic metals and persistent organic pollutants, both from households and particularly from industrial sources, can bioaccumulate in aquatic organisms, leading to biomagnification within the food chain and ultimately affecting human health (Zaynab et al., 2022). This risk is further exacerbated by rapid population growth and industrialization, as well as inadequate waste management practices, all of which contribute to significant environmental challenges (Lukhele and Msagati, 2024). Furthermore, the discharge of non-compliant effluents exacerbates these threats, thus rendering many water bodies unsafe for both human use and ecological support (Mugwili et al., 2023).

To achieve sustainable municipal wastewater management, there is a need to change from viewing wastewater as a 'nuisance' and to rather view it as an important 'resource'. In this regard, a significant shift from end-of-pipe treatment to reuse and resource recovery is required. In support of resource recovery, techniques for nutrient recovery, such as struvite crystallization have proven beneficial for producing fertilizers from wastewater nutrients (Guan et al., 2023). However, this is limited by calcium and magnesium interferences,

resulting in decreased struvite yield and purity (Capdevielle et al., 2013). On the other hand, membrane distillation (MD) is one innovative approach that can be integrated with struvite crystallization and allow for the potential reclamation of clean water. Recent studies in MD have focused on developing hydrophobic nanocomposite membranes and integrating MD with other processes to enhance flux and reduce energy requirements (Efome et al., 2016, Prince et al., 2014). Generally, commercial MD membranes are typically made from materials such as PTFE (polytetrafluoroethylene), PP (polypropylene), and PVDF (polyvinylidene fluoride), each contributing specific properties related to hydrophobicity, thermal stability, and mechanical strength (Alkhudhiri et al., 2012). The optimization of these membranes and module configurations is essential to address challenges related to flux recovery, pore wetting, and scalability. Furthermore, challenges relating to fouling, module design, and energy consumption must be overcome to enhance scalability and cost-effectiveness.

While technological maturity in resource recovery from wastewater has greatly progressed, comprehensive economic energy consumption and efficiency still require further exploration (Zhu et al., 2024). In this regard, the economic and environmental advantages of struvite recovery through nutrient recovery units (NTU) paired with direct contact membrane distillation has been emphasized (Vinardell et al., 2023).

Building on these recent advances, this study aims to investigate the feasibility of using activated cryptocrystalline magnesite for struvite crystallisation from municipal wastewater and the reclamation of clean water using membrane distillation. The specific objectives are:

- To evaluate the physico-chemical and microbial properties of raw and treated water, after struvite crystallisation, as to gain insight on factors influencing the quality of treated MWW effluents.
- To investigate the feasibility of struvite crystallisation/synthesis from MWW intermediary streams using activated magnesite at bench scale
- To optimize conditions suitable for the reclamation of clean drinking water using product water from the struvite synthesis process.
- To test the viability of clean water recovery from Nutrient Recovery Unit effluent stream at laboratory-scale.
- Develop a CBA for the proposed struvite and clean water recovery system from MWW.
- To suggest upscaling strategies for integrated struvite and clean water reclamation systems and develop recommendations for the pilot testing of the developed process in a relevant environment.

1.2 Structure of the report

This bespoke report comprises five (5) chapters that are linked to the specific objectives and deliverables of the project. Specifically:

Chapter 1: Introduction and background

This chapter provides a detailed background of the advancement in the body of knowledge in relation to the subject under investigation, and subsequently highlights the primary objectives of the project.

Chapter 2: Struvite recovery using activated cryptocrystalline magnesite

This chapter focuses on the recovery of phosphate and ammonia from real municipal wastewater and their valorisation for the synthesis of struvite, after the addition of activated cryptocrystalline magnesite.

Chapter 3: Water reclamation using membrane distillation

This chapter is devoted to the use of novel and highly promising filtration technology, namely membrane distillation, for the polishing of product water from the struvite synthesis process.

Chapter 4: First order cost benefit analysis for integrated process

This chapter endeavours to demonstrate the financial requirements for the synthesis of struvite using activated cryptocrystalline magnesite and membrane distillation for clean water reclamation.

Chapter 5: Conclusion and recommendations

This chapter distils final conclusions and recommendation from the synthesis of struvite using activated cryptocrystalline magnesite and from reclaiming clean water using membrane distillation. The recommendations are derived from the deficiencies that were identified from the integration of these technologies, while upscaling strategies for struvite and water reclamation are further provided, including recommendations for pilot testing of the developed process in a relevant environment along with avenues of consideration for future research.

CHAPTER 2: STRUVITE RECOVERY

2.1 Introduction

Municipal wastewater is well endowed with nutrients which can be problematic when released to receiving water bodies, but they could also be recovered for beneficial use. Raw municipal wastewater typically contains 20 – 70 mg/L of nitrogen and 4 – 12 mg/L of phosphorus (Tchobanoglous et al., 2003), while biological processes are employed for removing these nutrients from wastewater. However, these processes concentrate the nutrients in the sludge, which need to be treated prior to disposal. In fact, approximately 90% of phosphorus in the influent wastewater can be transferred into the sludge (Tarayre et al., 2016). However, during sludge anaerobic digestion, the nutrients are released back into the aqueous stream, eventually reaching receiving environments which further increases the nutrients loads of biological process. Several technologies have been developed for nutrients recovery from wastewater. These technologies are based on chemical, biological, and filtration (membrane and advanced membrane systems) methods (Ye et al., 2020). The chemical method of nutrients recovery through struvite synthesis and precipitation has been shown to be commercially viable for streams with orthophosphate concentration above 50 mg/L (Mehta et al., 2015, Krishnamoorthy et al., 2021). In addition, various commercial technologies have been developed for treatment of digested sludge liquor (Desmidt et al., 2015). However, these technologies do not address struvite scaling in pipelines from anaerobic digesters. On the other hand, cryptocrystalline magnesite, a low-cost magnesium source that is abundant and readily available in South Africa (Masindi et al., 2015) has been found effective, when activated (Mavhungu et al., 2020b), in the recovery struvite from MWW. Yet, the dilute nature of nutrients in MWW can impose on the process cost and effectiveness, among others, while existing biological treatment plants should be retrofitted for the chemical precipitation of nutrients in the form of struvite, which can raise questions about cost and feasibility. For this reason, here the recovery of struvite from digested sludge, an already existing waste stream from biological treatment plants, was examined using activated cryptocrystalline magnesite (ACM).

2.2 Methodology

2.2.1 Materials

Industrial grade cryptocrystalline magnesite was obtained from Syferfontein Carbonates Pty (Ltd). ACM was produced from magnesite through activation in a muffle furnace at 700°C for 4 hours, with a temperature increase rate of 10°C/minute. The sludge samples were collected from the digested sludge holding tank (open tank with fitted stirrer) at one of Johannesburg Water's sewage treatment plant. In more detail, the sludge samples comprised waste

activated sludge (WAS), which was anaerobically digested at temperature of 35 ° C for a hydraulic retention time of 15 days.

2.2.2 Optimisation studies

To understand the factors that influence the removal of phosphate and ammonia from MWW, a number of operational parameters were evaluated, and these include contact time, ACM dosage, chemical species (phosphate and ammonia along with calcium (Ca) and magnesium (Mg)) and total dissolved solids (TDS) concentrations in the treated effluent, pH, and temperature. All experiments were performed in high-density polyethylene (HDPE) flasks using an overhead stirrer moving at 500 rpm. For a thorough understanding of struvite crystallisation process monothetic analysis was employed. Specifically, the effect of a wide array of parameters were explored by varying one parameter and fixing all the other parameters, i.e., one-factor-at-a-time (OFAT) method was employed. The parameters that influence the removal of phosphate and ammonia from MWW and were thoroughly examined. Factors that influence the removal of phosphate and ammonia from aqueous solutions, which were examined herein through monothetic analysis that comprise the varying of mixing time (min) with 1; 5; 10; 30; 60;120; 150; 180; 240; and 300, dosage (g in 100 mL volume) with 0.1; 0.5; 1; 2; 3; 4; 5; 8; and 10, concentration (mg/L or ppm) with 2; 4; 8; 12; 16; 21; 33; 41; 82; and 123, pH with 1, 2, 3, 4, 5, 6, 7, 8, 9, 10, and 11, and temperature (°C) with 25; 45; 55; 65; and 75.

The OFAT experiments were performed in a 500 ml volumetric flask. The effect of the initial phosphate and ammonia concentration was studied by diluting the MWW with pure water to the desired concentration. The effect of initial pH of the MWW was examined by using 0.1 M NaOH and/or 0.1 HCl to adjust the pH to the required level. The effect of ACM dosage on the pH and on nutrients removal from the MWW was determined by weighing varying ACM masses on a 4-decimal point mass balance and then add them into reaction vessels, while the effect of contact time was studied by agitating the mixture (MWW and ACM) at different specified time intervals. Finally, the effect of temperature was determined by using a beaker with a heater at controlling the temperature of the mixture at specified values.

2.2.3 Percentage removal

The percentage of phosphate and ammonia removed from MWW was estimated using **Equation 2.1:**

$$\% \text{ Removal} = \frac{C_0 - C_e}{C_0} \times 100 \quad (2.1)$$

where C_0 is the initial concentration of phosphate and ammonia in mg.L^{-1} and C_e is the corresponding equilibrium concentrations, again in mg.L^{-1} .

2.2.4 Aqueous samples analyses

The pH, electrical conductivity (EC). and TDS were monitored using a multi-parameter probe (HANNA instrument, HI9828). The concentrations of the examined chemical species were analysed by means of inductively coupled plasma mass spectrometry (ICP-MS) (7500ce, Agilent, Alpharetta, GA, USA).

2.2.5 Solid samples characterization of the synthesized struvite

The equipment used for the characterisation both the feed material (ACM) as well as the product material, i.e., struvite. The equipment used for characterisation of feed and product minerals were, according to the quest, mineralogical properties (X-ray Diffraction (XRD))(PANalytical X'Pert PRO-diffractometer equipped with Philips PW 1710 Diffractometer with graphite secondary monochromatic source), functional groups (Fourier Transform Infrared Spectrometer (FTIR))(Perkin-Elmer Spectrum 100 Fourier Transform Infrared Spectrometer (FTIR) equipped with a Perkin-Elmer Precisely Universal Attenuated Total Reflectance (ATR) sampling accessory with a diamond crystal), and Morphology, Mapping and elements (Field Emission Scanning Electron Microscope (FE-SEM) equipped with an Energy-dispersive X-ray spectroscopy (EDS))(Auriga Cobra FIB-FESEM, Carl Zeiss FE-SEM, Germany).

2.2.6 Nutrient recovery pilot plant

The pilot plant trials were carried out in a 300-litre continuously stirred tank reactor (CSTR) commissioned and operating in CSIR Pretoria campus, as illustrated in **Figure 2.1**. The reactor is equipped with a variable speed drive motor, which allows for control of the speed of the stirrer.

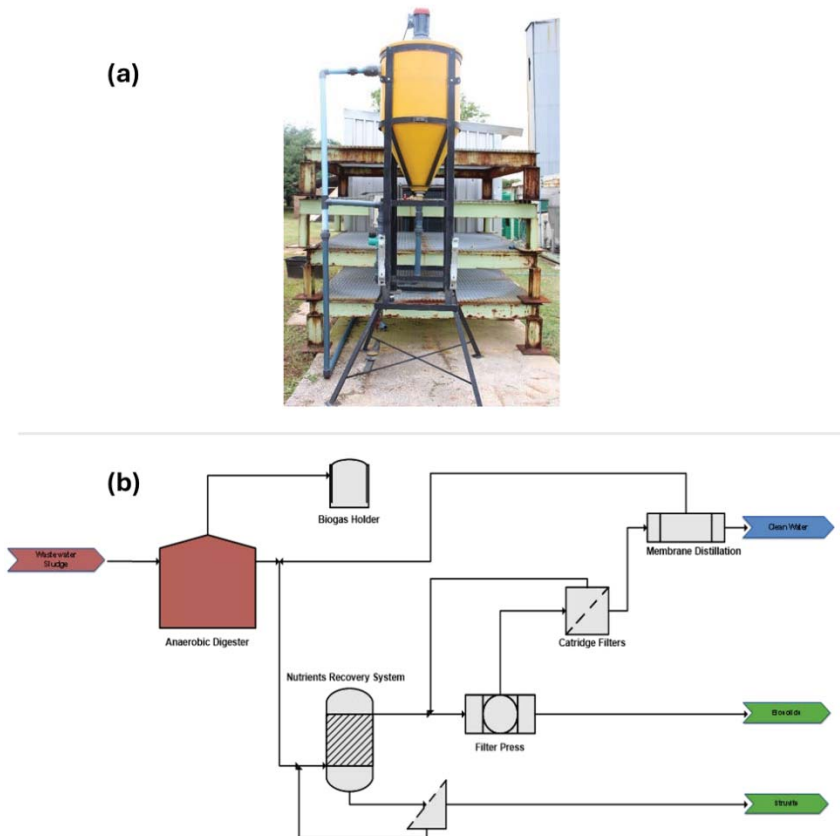


Figure 2.1: (a) The 300-litre CSTR for nutrients recovery system from digested WAS and (b) integrated schematic diagram of mineral recovery and drinking water reclamation system from MWW.

In more detail, the pilot plant was first fed with digested sludge (WAS) from an anaerobic digester that produces biogas. As such, the pathogens count and organic content of the sludge has been greatly reduced compared to the undigested sludge. In more detail, the WAS is first passed through a nutrient recovery unit (NRU), where struvite crystallization takes place. Struvite is then recovered and dewatered, with the excess water being sent back to the NRU, while the nutrients-depleted effluent from the NRU was passed through a belt-filter press and cartridge filters to remove biosolids. The produced biosolids were then air-dried and composted, prior to being disposed, while the filtrate (nutrients-depleted effluent) was sent to a direct contact membrane distillation (DCMD) unit for water reclamation (**Figure 2.1**). More details about the NRU, where struvite crystallisation takes place, are given below.

2.2.7 Synthesis of struvite

In the NRU, first the powdered ACM was delivered by dry-bulk tankers and loaded into hopper for temporary storage, prior to being pumped to the slurry preparation tank. In the preparation tank, dry ACM was mixed with overflow from the sedimentation tank for preparation of slurry.

During start-up, fresh water was used for preparation of the slurry, thereafter, part of the (or once the plant was stable, a fraction of the overflow or supernatant was used) overflow from the sedimentation tank was used. The slurry and anaerobic digester effluent was pumped to the fluidised bed reactor (FBR) at controlled rate. In the FBR, nutrients contained in the sludge were reacted with magnesium to form struvite crystals. Crystals were formed in the FBR until sufficient size was attained and settled against upward fluid motion. Tiny crystals that were washed off with fluid were allowed to overflow into sedimentation tank and collected at the bottom where they were recycled back to the FBR. The FBR underflow was drained into a rotary drum screen for separation of struvite from the sludge. The struvite crystals were then air-dried prior to be sent to a packaging facility. As mentioned above, the overflow from the sedimentation tank and sludge from the drum screen were taken for dewatering, while the produced filtrate was used for water recovery through MD.

2.3 Results and discussion

2.3.1 Optimisation of operational parameters

2.3.1.1 Variation of pollutants removal as a function of contact time

The effect of contact time on TDS and levels is shown in **Figure 2.2**. TDS is a direct indicator of the nutrients that are contained in WAS, and a reduction in its levels suggest the removal of the nutrients and the migration to struvite crystals.

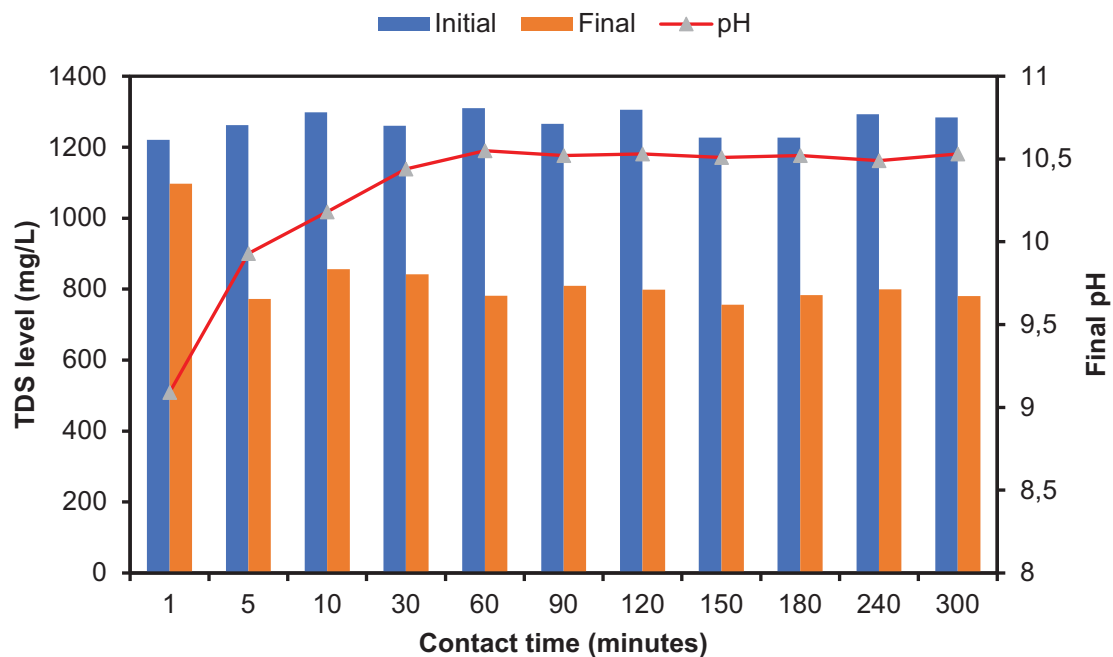


Figure 2.2: Variation of TDS and pH levels with increasing contact times (conditions: 1 g:100 mL (10 g/L S/L ratio) ACM dosage, room temperature (25 °C), and 500 rpm mixing speed)

As shown in **Figure 2.2**, there was a decrease in TDS with increasing contact time. Specifically, a rapid decrease was observed from 0 to 5 min contact time, thereafter, trivial fluctuations in TDS levels were observed, hence suggested that TDS removal reaching a plateau after 5 min contact time. This implies that the system reaches equilibrium in a very short contact time. This assertion was further verified by examining the percentage removal of the nutrients under study and the levels of Ca and Mg with varying contact time, and results are shown in **Figure 2.3**.

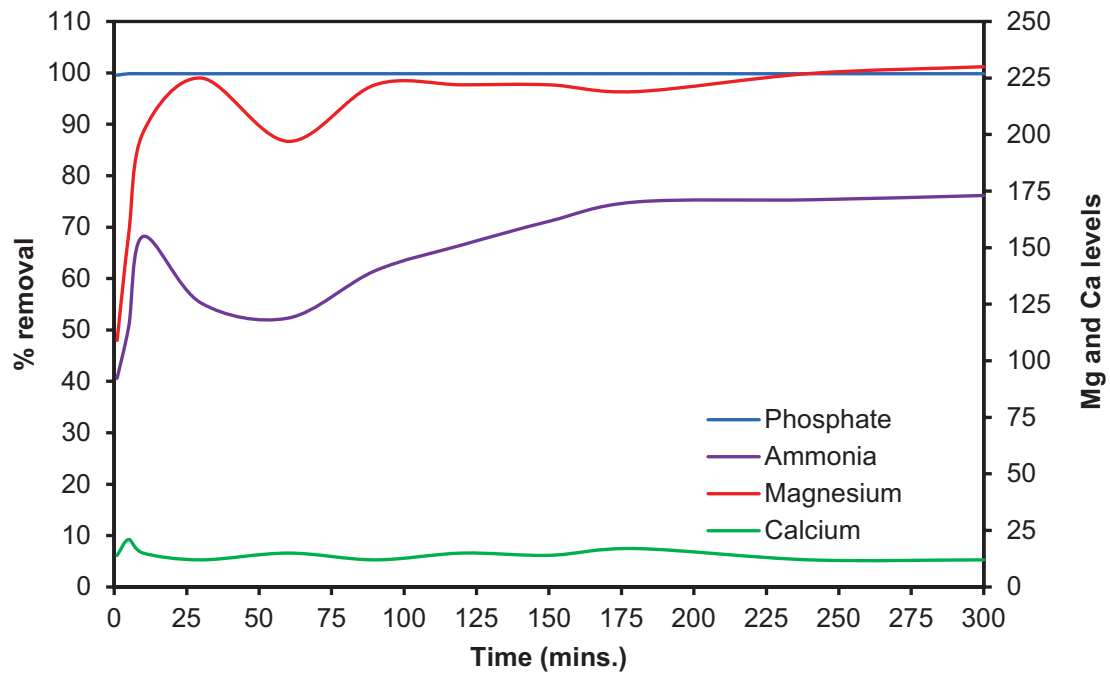


Figure 2.3: Variation in the percentages removal (%) of ammonia and phosphate, and the levels of Ca and Mg with varying contact times (conditions: 1 g: 100 mL S/L ratios, room temperature, 1 g of pre-treated magnesite, and 500 rpm mixing speed)

As was expected, there was an increase in percentage removal of phosphate and ammonia with an increase in contact time (**Figure 2.3**). This is attributed to the reaction of ACM with phosphate and, to a lesser extent, ammonia. An increase in phosphate removal was observed until 5 min and thereafter the removal plateaus since phosphate has been practically removed from the system and migrated to struvite crystals. This corresponds to the observed TDS levels with varying contact times (**Figure 2.2**). A similar trend was observed by Yagi and Fukushi (2012). However, the removal of ammonia was observed to be increasing from 0 to 180 minutes (having spiked in 5 min contact time), thereafter, it commenced to stabilize, thus indicating that the reaction has reached equilibrium. More so, the Ca and Mg levels were observed to increase with an increase in contact time, but again a sharp spike was observed

in 5 min. This is an indication that a rapid reaction between Mg^{2+} , Ca^{2+} , NH_4^+ , and PO_4^{3-} takes place within 5 min of contact time and this leads to the formation of struvite. Therefore, to afford the reaction adequate time, 5 min was taken as the optimum time for the removal of phosphate, while 60 min will be required to optimize ammonia removal as well. However, 5 min can be considered as the ideal time for struvite synthesis, since phosphate is depleted within the first 5 min of contact time, but more focus is given below on the contact time range 0 to 60 min.. Finally, we have to note that this study attained a fast struvite crystallisation time as compared with the literature (Sutiyono et al., 2016).

2.3.1.2 Variation of nutrients removal as a function of both ACM dosage and optimum contact time

The effect of ACM dosage on TDS attenuation is shown in **Figure 2.4**, when both the optimum contact time range (1 to 60 min) and ACM dosage are considered.

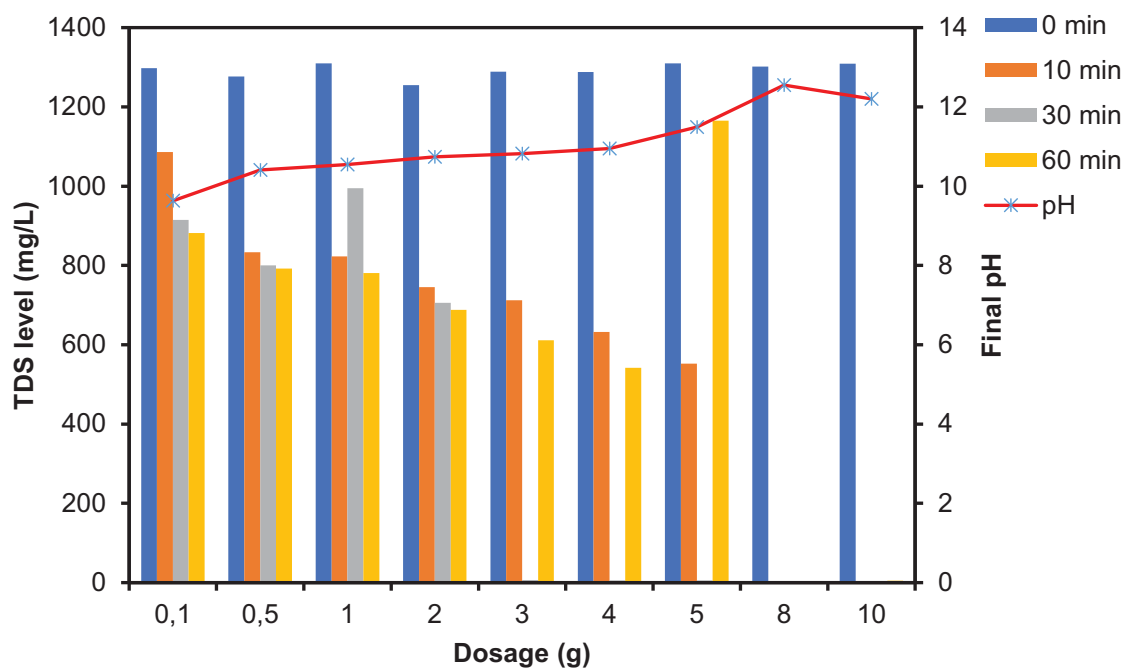


Figure 2.4: Variation in TDS with an increase in dosage (conditions: 100 mL of treated volume, room temperature (25 °C), initial pH > 6.5, and 500 rpm mixing speed).

As shown in **Figure 2.4**, the TDS attenuation was observed to be inversely proportional to both the contact time and the ACM dosage. Specifically, as the contact time and dosage increases, the levels of TDS were observed to decrease. In more detail, for ACM dosages in the range 0.1 to 3 g and contact time up to 30 min, TDS levels appear to decrease and thereafter, at increased contact time TDS levels appear to have been practically removed.

Therefore, excluding an extreme value at 50 g/L dosage, higher ACM dosages and contact times appear not to benefit the struvite crystallisation system. As such, thirty minutes (30 min) and 3 g (per 100 mL) were observed as the most parameters for TDS attenuation and thereby for nutrients removal from WAS to the struvite crystals. To underpin the TDS attenuation results the variations in the percentage removals of phosphate and ammonia, along with variations in the calcium and magnesium levels with varying ACM dosages are shown in **Figure 2.5**.

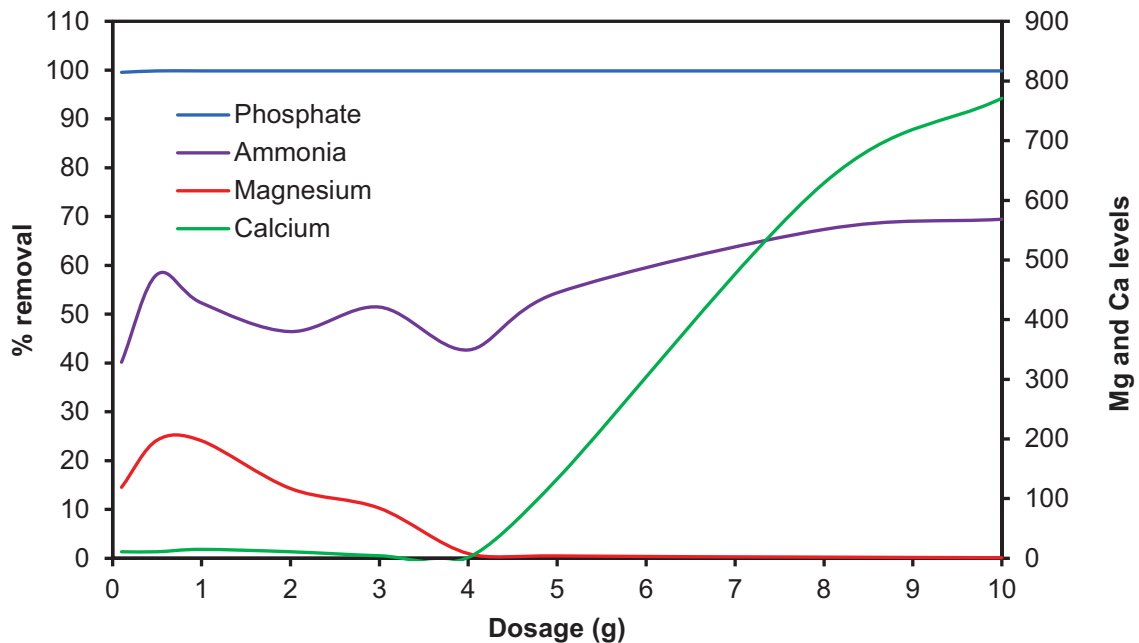


Figure 2.5: Variation in the percentage removal of ammonia and phosphate, and the levels of calcium and magnesium with a varying ACM dosages (conditions: 100 mL volume, room temperature, and 500 rpm mixing speed)

As shown in **Figure 2.5**, phosphate is practically removed even at the first examined dosage whereas ammonia removal spikes at the 1 g (per 100 mL) dosage thereafter the removal efficiency drops and exhibits lower spikes while after the 4 g dosage is appears to steadily increase, albeit reaching again the same removal efficiency (around 60%) that was observed in the 1 g dosage.. The level of Mg was observed to decrease with an increase in dosage whereas the Ca level was increasing with an increase in feed dosage. The reduction in Mg level may be explained by an increase in pH with an increase in Ca, leading to the precipitation of brucite. Moreover, the removal of phosphate was observed to be > 99% from 0.1 g to 10 g hence indicating greater efficiency on the system. It also indicates high affinity of the feed material to phosphate hence very little dosage is required. The level of ammonium also demonstrated an increase in removal efficacy with an increase in dosage. However, it

demonstrated a direct proportional relationship with the Mg levels. As the Mg levels were decreasing, the ammonium removal efficacy was increase hence indicating a possible formation of struvite. The Ca levels were also observed to increase with an increase in dosage; this may be attributed to possible dissolution of Ca and Mg from the ACM matrix into the solution to be precursors for struvite synthesis or minerals attenuation. In light of the obtained results, it appears that the 0.5 g ACM dosage is suitable for the removal of phosphate, whereas 8 g is suitable for the removal of ammonia which will then be used for the synthesis of struvite and the treatment of municipal water in the subsequent experiments. For the purpose of this study, 4 g per 100 mL was taken as the optimum dosage for subsequent experiments.

2.3.1.3 Variation of nutrients removal as a function of chemical species concentration

The variation of the TDS levels with increasing ACM dosages is shown in **Figure 2.6**.

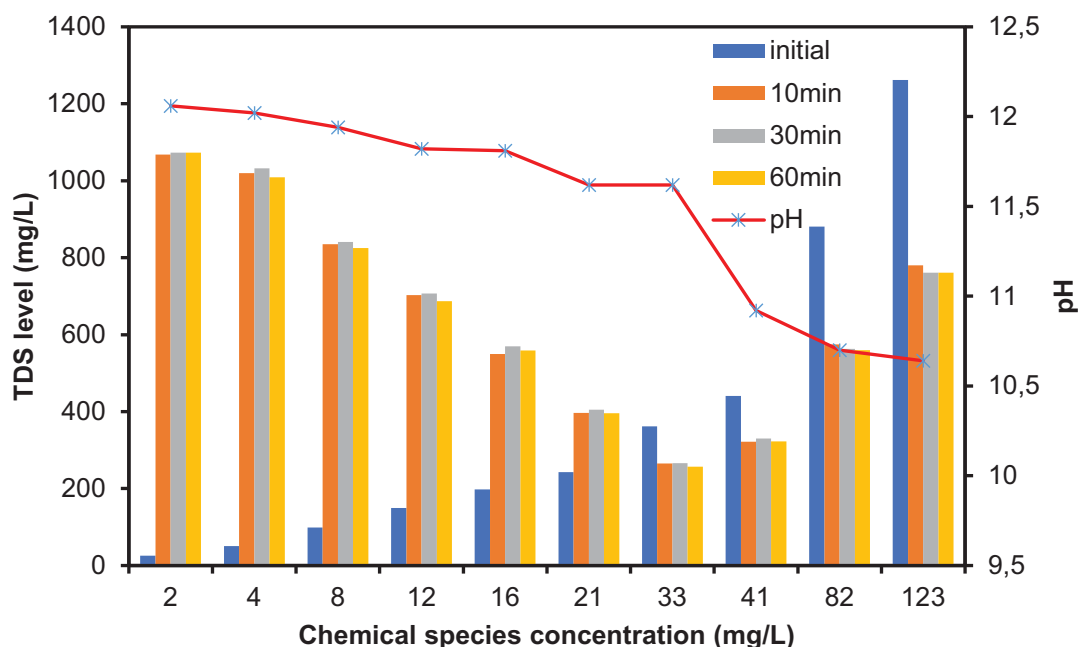


Figure 2.6: Variation in TDS with a variation in chemical species concentration (conditions: room temperature, pH > 6.5, 4 g, and 500 rpm mixing speed)

Specifically, there was an increase in TDS with an increase in chemical species concentration. The pH was also observed to decrease with an increase in concentration. High pH in low concentration indicates the over-saturation of the system with alkaline generating materials hence leading to an increase in alkalinity, however, as the concentration increases, more chemical components are present to react with those chemicals hence a reduction in pH. From 2 to 21 mg/L of phosphate, the TDS was above the initial TDS of feed water. This is an indication that the addition of ACM is increasing the TDS due to dissolution of chemical components in its matrices. From 33 to 123 mg/L of phosphate, the TDS of product water was

observed to be below the initial TDS hence depicting a possible attenuation of chemical components from an aqueous system. In terms of TDS, the system was observed to be independent of concentration. The effect of chemical species concentration on the removal of phosphate and ammonia from aqueous solution is shown in **Figure 2.7**.

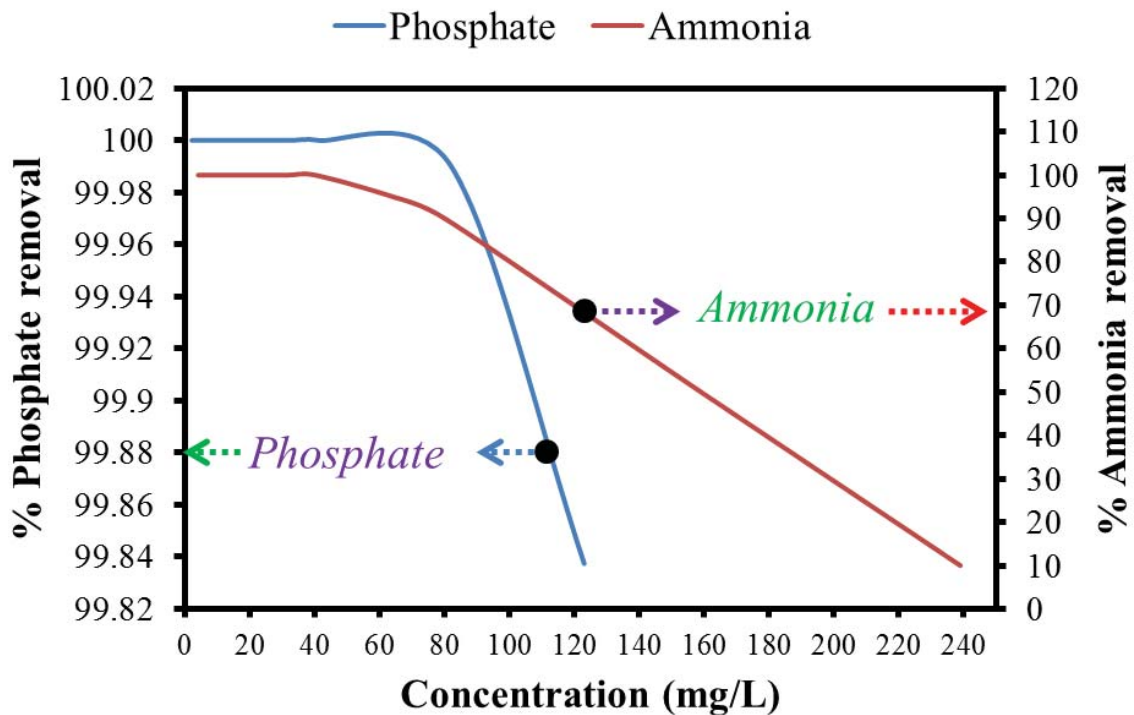


Figure 2.7: Variation in percentage removal of ammonia and phosphate with a variation in chemical species concentration (conditions: room temperature, 4 g of dosage, and 500 rpm mixing speed).

As shown in **Figure 2.7**, the removal of phosphate and ammonia was observed to decrease with an increase in chemical species concentration. This is an indication that the precursors are getting depleted with an increase in concentration, thus leading to a reduction in the removal efficiency. The removal of phosphate from 0 to 123 mg/L concentration was efficient at 4 g: 100 mL S/L ratio, however, at 80 mg/L, the system demonstrated a decrease in the removal efficiency. Contrary, ammonia removal was observed to be more effective and efficient from 0 to 40 mg/L, beyond that, the removal efficiency was observed to gradually decrease. In that regard, it can be concluded that 4 g of pre-treated magnesite can remove \leq 123 and 80 mg/L of phosphate and ammonia respectively.

2.3.1.4 Variation in nutrients removal as a function of pH

The effect of pH on TDS attenuation is shown in **Figure 2.8**.

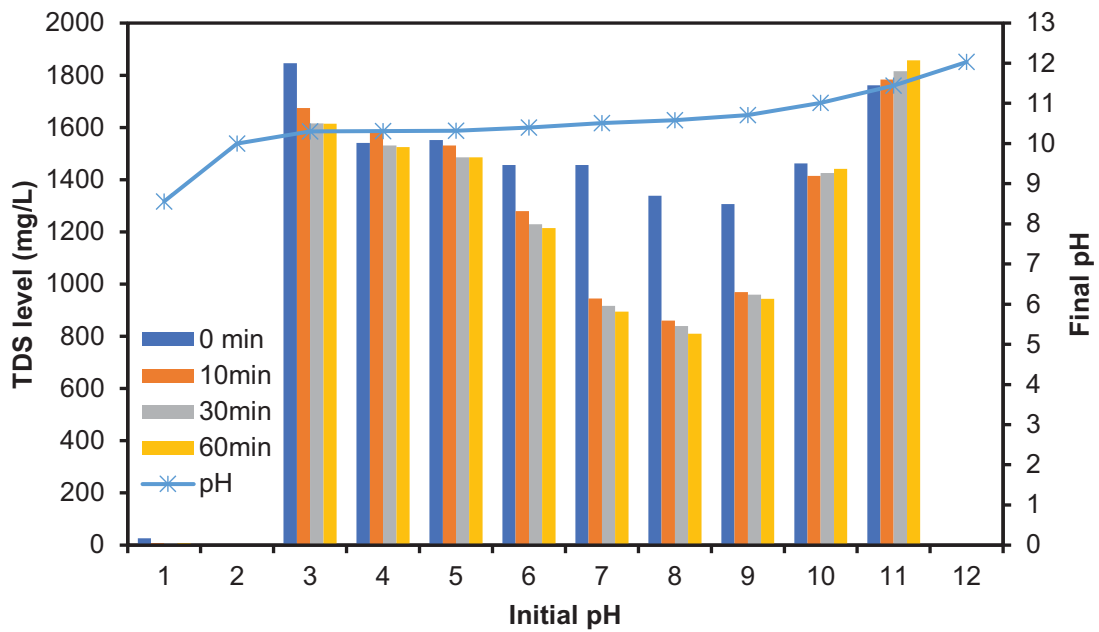


Figure 2.8: Variation in TDS levels with changes in pH (conditions: room temperature, pH > 6.5, 4 g, 500 rpm mixing speed, 123 ppm for phosphate, and 80 ppm for ammonia)

As shown in **Figure 2.8**, there was a decrease in TDS with an increase in pH from pH 3 to 8, thereafter, the TDS was observed to increase with an increase in pH. This may be explained by the precipitation of Mg from an aqueous system, (e.g., brucite will begin to precipitate out at around 9 pH), hence making the system deficient of one of the main components. However, above pH 10, the system is now dominated by Ca ions hence making them the best candidate for anions removal. The system was observed to be dependent on pH. The pH of the final solution was also observed to increase with an increase in initial pH. However, the most effective conditions were observed to be pH 8.5 to 10.

The effect of pH on the removal of phosphate and ammonia from aqueous solution is shown in **Figure 2.9**.

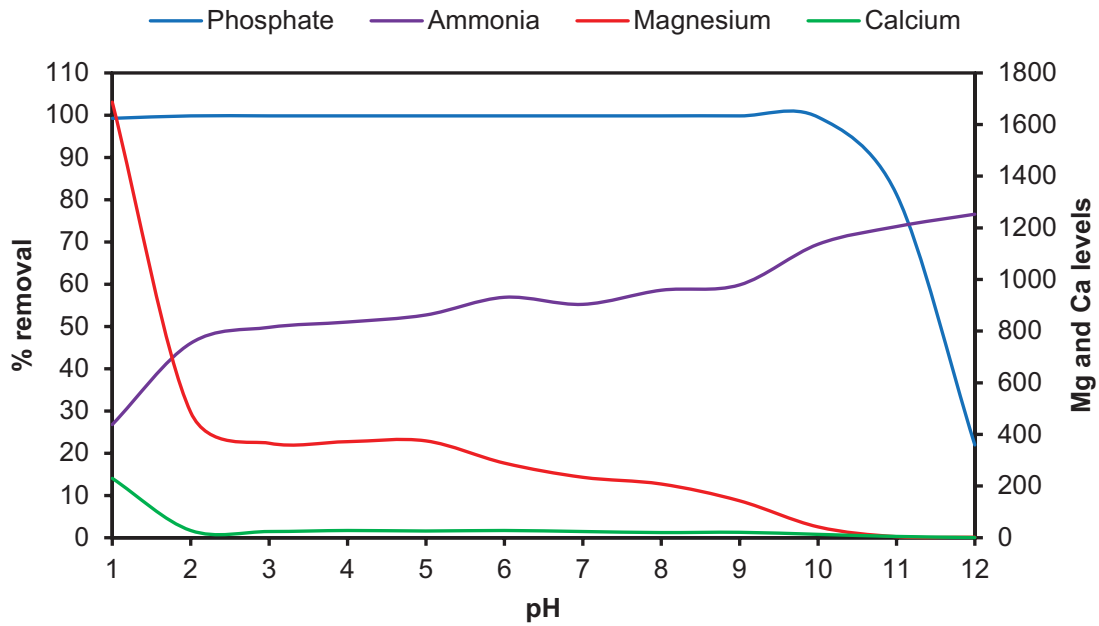


Figure 2.9: Variation in percentage removal of ammonia and phosphate with a variation in chemical species concentration (conditions: 60 minutes, 4 g of dosage per 100 mL, ≤ 123 and 80 mg/L of phosphate and ammonia, and 500 rpm mixing speed).

As shown in **Figure 2.9**, the removal of pollutants was increasing with an increase in pH, from pH 2 to 10. Thereafter, there was a reduction in the removal of phosphate. However, the removal of ammonia was observed to increase with an increase in pH. The removal of phosphate was observed to be $> 99\%$ from pH 1 – 10 and it drastically dropped after pH 10 to 12. The levels of Mg and Ca were also observed to decrease with an increase in pH, however, at pH > 10 , they were observed to have depleted and this is directly proportional to the level of phosphate in solution. Moreover, a rapid decrease at pH 2 – 3 is proportional to the levels of TDS which showed very lowest TDS. As such, pH $> 8 - 10$ was observed to be suitable for the removal of phosphate and ammonia from aqueous solution, and these levels can be achieved directly with the use of ACM, which when dissolves in the solution will increase the initial pH levels to 8.5 – 11.1 (dissolution equilibrium of magnesium hydroxide and oxide). Similar results were reported by Stolzenburg et al. (2015). In addition, pH > 10 promote the loss of ammonia to air due to stripping (Sutiyono et al., 2016). As such, the observed ammonia attenuation at high pH levels is likely not an indication that the produced sludge is further enriched with ammonia but that ammonia has been moved to a gaseous form.

2.3.1.5 Variation of nutrients removal as a function of temperature

The effect of the solution temperature on TDS attenuation is shown in **Figure 2.10**.

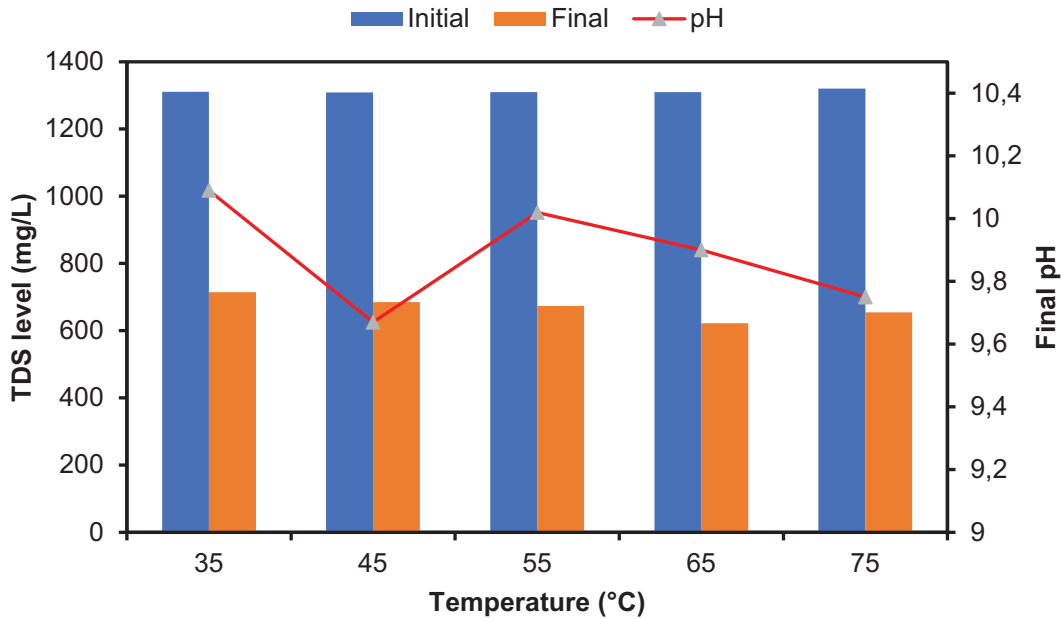


Figure 2.10: Variation in TDS with a variation in pH (conditions: 60 minutes, 4 g, 500 rpm mixing speed, 123 ppm for phosphate, and 80 ppm for ammonia, pH between 8 to 10).

Figure 2.10 shows the effect of temperature on the removal of phosphate and ammonia from the aqueous system. It was identified that TDS is independent of the temperature, since the TDS levels remained the same for all examined temperature gradients. This also indicates that the removal of phosphate and ammonia from the aqueous system is independent of temperature. As such, experiments were conducted at room temperature to make this technology environmentally friendly and less energy intensive.

To further substantiate this claim, the effect of the temperature on the removal of phosphate and ammonia from the aqueous solution was also examined and results are shown in **Figure 2.11**.

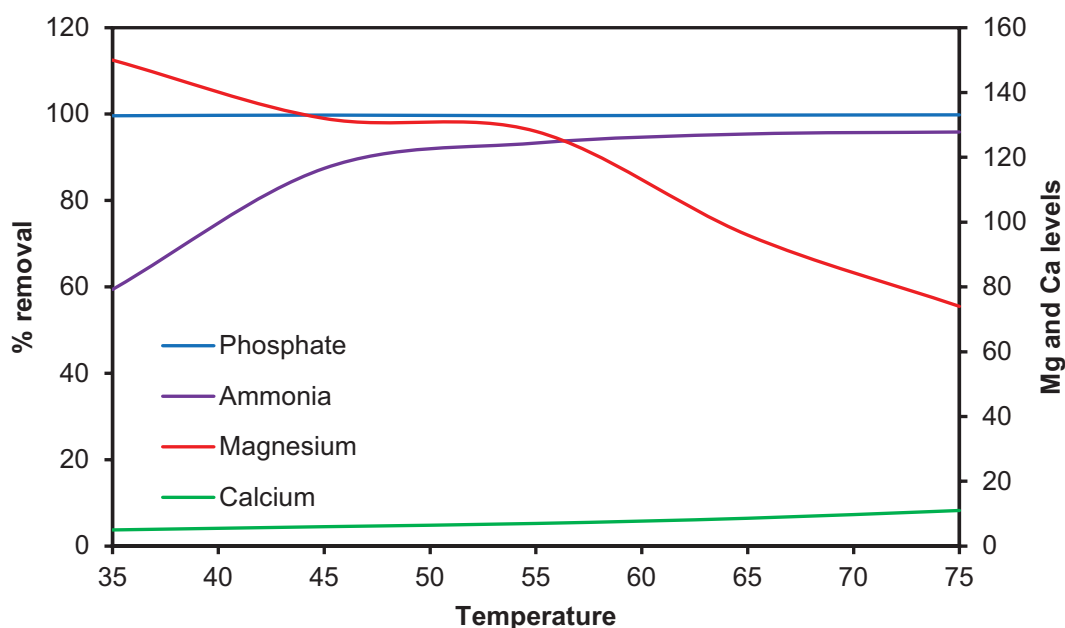


Figure 2.11: Variation in percentage removal of ammonia and phosphate with different temperature gradients (conditions: 60 minutes: room temperature, 4 g of dosage, ≤ 123 and 80 mg/L of phosphate and ammonia, and 500 rpm mixing speed).

As shown in **Figure 2.11**, there was an increase ammonia removal with an increase in temperature. The removal of phosphate was independent of temperature but the removal of ammonia was dependent on temperature, and similar to the effect of pH this is likely reflect ammonia stripping rather than ammonia preconcentration in the struvite sludge. The Mg levels were also observed to be dependent of temperature, as they were observed to significantly decrease with an increase in temperature hence denoting a rapid reaction with the pollutants, and to a lesser extent the retrograde dissolution of both Mg and Ca, i.e., low temperatures favour dissolution. This can be an indication that the synthesis of struvite is endothermic because it requires additional energy for optimal removal of struvite. In light of that, 55°C was taken as the optimum temperature for subsequent experiments. For industrial deployment purposes, the authors opted to room than 55°C temperature. This is attributed to the fact the ammonia evaporate at temperature above 30 °C as reported by Sutyono et al. (2016). The Ca levels were also observed to gradually increase with an increase in temperature hence off-setting the TDS of a defined system.

2.3.2 Treatment of municipal effluents at optimised conditions

The characteristics of the raw (WAS effluent from the MWW under study) and treated (product water) effluent, when treated under the aforementioned optimised conditions, i.e., 60 minutes:

room temperature, 4 g of dosage, ≤ 123 and 80 mg/L of phosphate and ammonia, and 500 rpm mixing speed, are reported in **Table 2.1**.

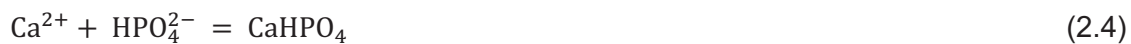
Table 2.1: The feed and product water quality for the municipal effluents treated under optimised conditions.

Parameters	Units	Raw municipal effluents	Treated water
Aluminum	mg/L	<0.00073	<0.00073
Ammonia Nitrogen	mg/L	135	30
Antimony	mg/L	0.0017	0.0011
Arsenic	mg/L	0.0035	0.0034
Barium	mg/L	0.011	0.0058
Boron	mg/L	<0.16	<0.16
Cadmium	mg/L	<0.0002	<0.0002
Calcium	mg/L	200	0.2
Chloride	mg/L	76	81
Chlorine (free)	mg/L	0.07	0.04
Chromium	mg/L	0.00037	0.0013
Color	mg/L	44	33
Copper	mg/L	0.0013	0.0007
Cyanide total	mg/L	<0.010	<0.010
Electrical conductivity	mS/cm	200	120
Fluoride	mg/L	<0.2	1.2
Iron	mg/L	0.015	<0.00088
Lead	mg/L	<0.00011	<0.00011
Magnesium	mg/L	1600	0.5
Manganese	mg/L	0.022	<0.00025
Mercury	mg/L	0.00039	0.00045
Monochloramine	mg/L	0.03	<0.010
Nickel	mg/L	0.017	0.013
Nitrate + Nitrite	mg/L	1.5	1.3
Nitrate Nitrogen	mg/L	1.4	1.3
Nitrite Nitrogen	mg/L	<0.2	<0.2
pH	N/A	7.5	10.82
Phenols	mg/L	<0.01	<0.01
Phosphate	mg/L	120	<0.001
Selenium	mg/L	<0.0021	<0.0021
Sodium	mg/L	77	74
Sulphate	mg/L	150	40
TDS	mg/L	2900	756
Turbidity	NTU	10	2.9
Uranium	mg/L	<0.00008	<0.00008
Zinc	mg/L	0.014	<0.00057

As shown in **Table 2.3**, there was an effective removal of pollutants from WAS effluent when using the produced ACM at optimised conditions. Specifically, the nutrients loading, as well as some other indicators such as electric conductivity (EC) and TDS (see **Table 2.1**) were also removed from the feed water, while the product water quality has also significantly improved. The levels of toxics and harmful contaminants were low to begin with, and many of those remaining relatively stable, indicating the high purity of the generated struvite. As was expected, the pH was observed to increase from 7.5 to 10.8, hence indicating that a reaction took place, i.e., Mg dissolution, leading to this increase. EC and TDS were also observed to decrease after contacting the dissolved ACM, hence depicting that there was attenuation of pollutants from the aqueous media. Sulphate was also reduced from 150 to 40 mg/L. Phosphate was removed from 120 to 0 mg/L, whereas ammonia was removed from 135 to 30 mg/L, hence confirming a possible formation of struvite. The levels of Mg and Ca were also observed to have decreased significantly hence depicting a possible co-precipitation during the struvite formation.

The removal of phosphate and ammonia from water is mainly due to a combination of adsorption and precipitation. Adsorption precedes precipitation and then crystallisation (Li et al., 2017), leading to the formation of a number of struvite and other valuable co-precipitants.

Equations 2.2 – 2.6 depict routes for the formation of a number several final products:



Where $n = 0, 1, 2$, etc., and it corresponds with the solution pH (Peng et al., 2018).

As such, the presence of MgO, and to a much lesser extent of CaO, in the ACM matrix will enable it to effectively treat both raw MWW and WAS effluent via crystallization of struvite and to a much lesser degree of calcium phosphate. These mechanisms of co-precipitation have been also reported by Peng et al. (2018). However, this system cannot be purely defined by adsorption models since the process is not reversible and it is not utterly a surface phenomenon, hence warranting its classification as a precipitation process that led to a crystallization process.

2.3.3 Parameters affecting struvite crystallisation and precipitation

2.3.3.1 Organic contaminants

Digested WAS is composed of significant concentrations of dissolved and particulate organic matter. Thus, it is important to track the fate of this organic matter during nutrient removal from such a stream. **Figure 2.12** shows the solid concentration in the feed and digested sludge, along with the removal efficiency of solids during struvite recovery process under various reaction times.

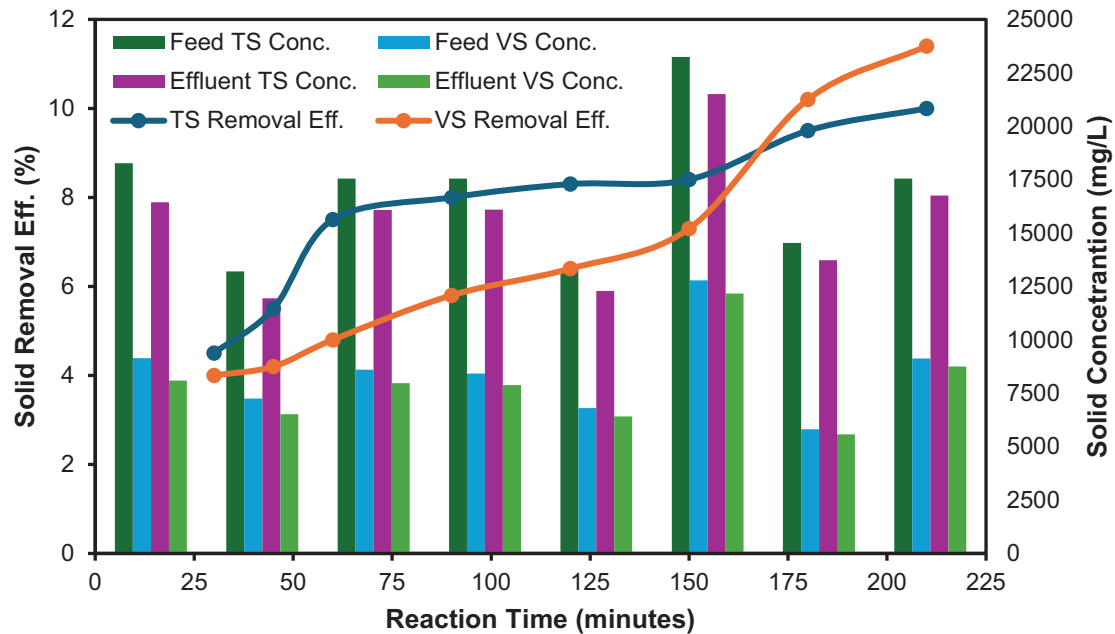


Figure 2.12: Removal efficiency of solids under various retention times

As illustrated in **Figure 2.12**, the total solids (TS) content of the raw sludge varied between 1.31 and 2.32% (13197 – 23248 mg/L), and the volatile solids (VS) content varied between 0.58 and 1.28% (5813 – 12786 mg/L). The TS and VS content of digested sludge varied between 1.19 – 2.15 % and 0.56 – 1.12%, respectively. There is also a variation in the VS/TS ratio in the feed sludge, which indicates the extent of anaerobic digestion and, thus the extent of nutrients release. The removal efficiency of TS and VS is observed to be increasing with increase reaction times. This can be attributed to increased contact time for adsorption to precipitates. The removal efficiency of TS content ranged from 4.5%, at 30 minutes reaction time, to 10%, at 210 minutes reaction time. Liu et al. (2020) observed 4.66% and 13.83% removal efficiency of TS on anaerobically digested WAS and thermally pretreated sludge, respectively.

2.3.3.2 Heavy Metals

Wastewater is composed of a variety of heavy metals (Agoro et al., 2020, Karvelas et al., 2003). Metal concentration is mainly influenced by the source of the wastewater. Treatment works that receive wastewater from industrial sources tend to have elevated concentrations of heavy metals. The treatment works in this study received purely domestic wastewater, and a small fraction of industrial effluent emanating from a beef abattoir. The concentrations of Fe, Mn, Cr, Cu, Ni, Zn, As, Pb and Cd were analysed. In all the trials conducted, no heavy metals were detected in the sludge except for Mn and Cu. Most of the heavy metals were not detected, i.e., their concentrations were below the detection limits of the employed equipment, and this can be attributed to nature of the raw wastewater, i.e., being mainly composed of domestic wastewater. The concentration of the Mn and Cu in the feed sludge varied from undetectable levels to maximum concentrations of 0.196 and 0.123 mg/L, respectively. The source for Mn can be attributed to industrial wastewater received from beef abattoir. Cattle manure is composed mainly of Mn and Zn (Provolo et al., 2018). However, Zn is below detectable limits, and this could be attributed to high affinity for aqueous phase than sludge, whereas Mn accumulates mainly in the sludge (Karvelas et al., 2003). Elevated concentration of Cu can be attributed to use of brass and copper scrubbers for cleaning and corrosion of water supply pipes, while Cu has also the tendency to accumulate more in the sludge (Naja and Volesky, 2017). The concentrations of these metals were significantly low to warrant any calculations for tracing the fate of them during struvite recovery process. This is also a good indication about the safety of using the recovered struvite in agriculture.

2.3.3.2 Organic matter

Given the high content of soluble and particulate organic matter (OM) in the stream which struvite is recovered from, it is important to quantify the OM content of the recovered solids (struvite and co-precipitants). The presence of OM in the struvite is undesirable for cases where the intended application is agriculture. The reason lies to the fact that OM has a microbial content, which can be taken up by the agricultural products, thereby affecting human health if ingested (i.e., consumption of unwashed or not properly washed produce) while at the same time it can also have a negative impact on the receiving environment (Guan et al., 2023). For this reason, the OM content of struvite crystals recovered under various operational conditions was analysed and the results are shown in **Figure 2.13**.

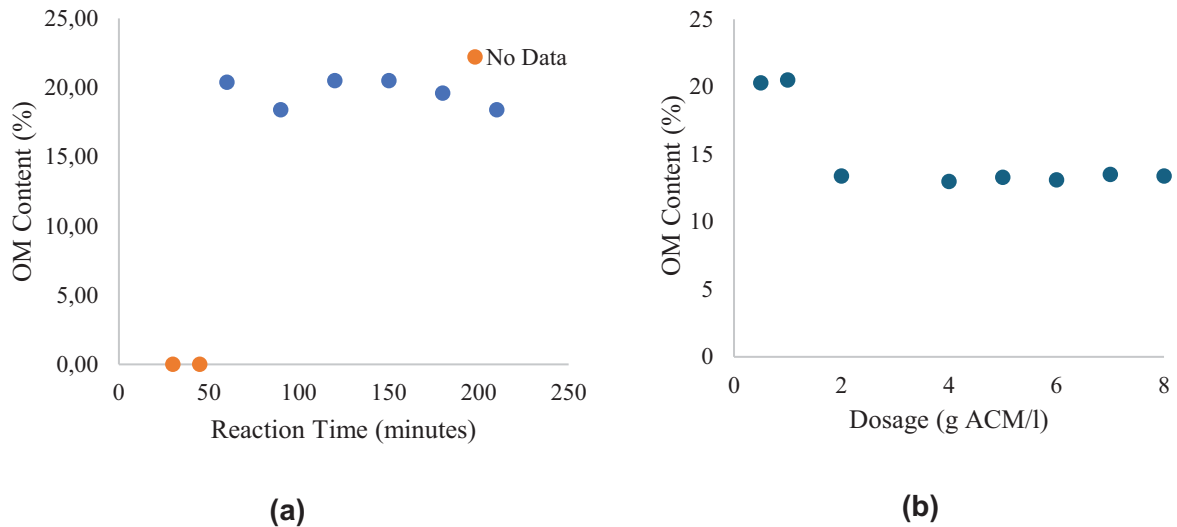


Figure 2.13: Concentration of organic impurities in the recovered struvite crystals under; (a) various contact/reaction/retention times, and (b) different dosages.

Figure 2.13 shows the OM content in the recovered solids at various retention times. Insufficient amounts of struvite crystals were recovered for OM content analysis for contact/reaction times of 30 and 45 min. In **figure 2.11**, it was observed that the removal efficiency of phosphorus was above 99%, which indicates that struvite crystals are formed early on from the reaction of ACM with the wastewater, however, the contact time was not sufficient for the crystal to precipitate out of the solution, i.e., for the agglomeration of the initial struvite crystals into large ones that can be filtered out. This is in accordance with the literature (Y. Wang et al., 2021). Furthermore, for higher (> 45 min) contact times sufficient amounts of precipitates were recovered that could be used of OM quantification, yet only a minimal change in the organic impurities recovered under various reaction time was observed. In more detail, in section 0, TS removal efficiency was observed to increase with increasing reaction time, however, the concentration of organic impurities were not increasing with increasing reaction times. This indicates that some organic solids are not recovered with struvite. These solids could be lumping together due to increased Mg concentration and precipitating out of the aqueous phase, since Mg has shown to increase the dewaterability of sludge (Bergmans et al., 2014). Overall, results are in line with the body of knowledge, where it has been highlighted that the crystal growth of tiny struvite crystals that are initially produced, i.e., when at low reaction times, is inhibited by humic substances (Q. Li et al., 2022) (Azam et al., 2019). This obstacle is lifted at higher reaction times, where sufficient time for crystals interaction is available to allow for the agglomeration into large struvite crystals, while TS removal is through adsorption. This further explains why at higher retention times, VS removal increases markedly compared to TS removal, which is due to adsorption of organics on the surface of struvite crystals (Q. Zhang et al., 2016).

2.3.4 Solid samples characterisation

2.3.4.1 Composition of the raw (feed) sludge from the anaerobic digesters

The proposed integrated resource recovery plant (which includes the Nutrient Recovery Unit and the Direct Contact Membrane Distillation Unit) was fed with effluent sludge emanating from anaerobic digesters. During the batch experimental trials, several samples of the raw sludge were collected and analysed in terms of different physicochemical properties. The results are averaged to give a representative composition of the raw (feed) sludge to the integrated process. The composition of the sludge is shown in **Table 2.2**. Note that the composition of the WAS effluent, i.e., the activated effluent that emanated from this sludge, was given in **Table 2.2**.

Table 2.2: Composition of the raw sludge from the anaerobic digesters.

Constituents	Concentration
Total Ammonium Nitrogen (mg N/L)	350
Orthophosphate (mg P/L)	128
Total Solids (%)	1.70
Volatile Solids (%)	0.85

2.3.4.2 Mineralogical analysis of the raw and activated cryptocrystalline magnesite

The mineralogical properties of the ACM and the synthesized struvite (the mineral product after the treatment of the feed sludge effluent by ACM) are shown in **Figure 2.14**.

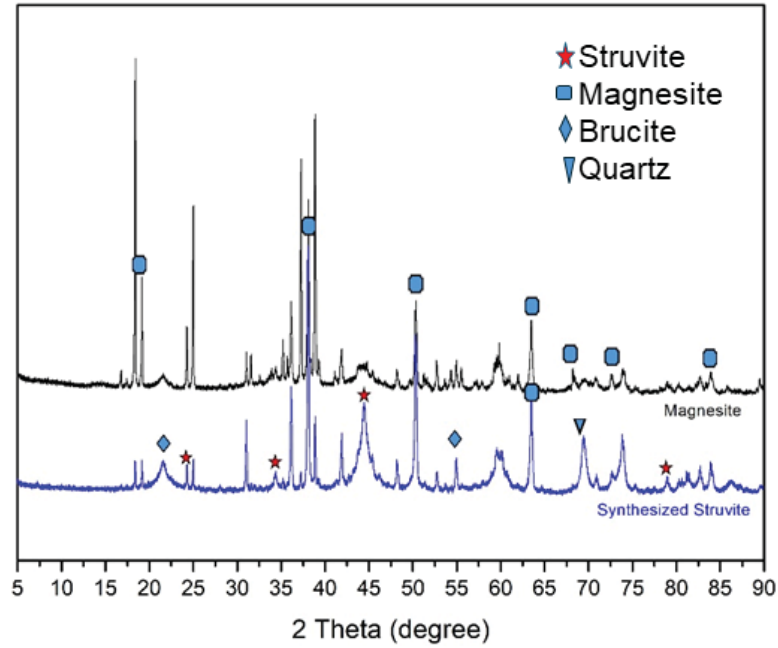


Figure 2.14: The X-ray diffractogram and mineralogical composition of raw magnesite and the synthesised struvite.

As shown in **Figure 2.14**, there was a change in mineral phases after reaction activated magnesite with the phosphate rich effluent. After contacting the municipal effluents, the product mineral was observed to contain struvite, periclase and brucite. This is an indication that phosphate and ammonia are adsorbed to form struvite as denoted by **Equation 2.7**.



Similar results were reported by Sutiyono et al. (2016). The obtained peaks at 21, 23, 31, and 34 2theta degree peaks well match those reported by Li et al. (2017) and Gao et al. (2018). This is a confirmation that the reaction is leading to the formation of Magnesium Ammonium Phosphate (MAP) (struvite). The other components are also essential because the anticipated use of the synthesized material is for agriculture. The presence of Mg and Ca are the contributing factors in an increase in pH. This can be expressed by **Equations 2.8 and 2.9**, where the calcium and magnesium oxides are first reacted with water to form the corresponding hydroxide forms and thereafter these are dissociated into calcium and magnesium ions and hydroxide ions:



This will then scavenge the NH_4^+ and PO_4^{3-} to form a complex (struvite), as denoted by Equation 2.7.

2.3.4.3 Morphological properties

The morphological properties of feed (ACM) and product mineral (struvite) are shown in Figure 2.15.

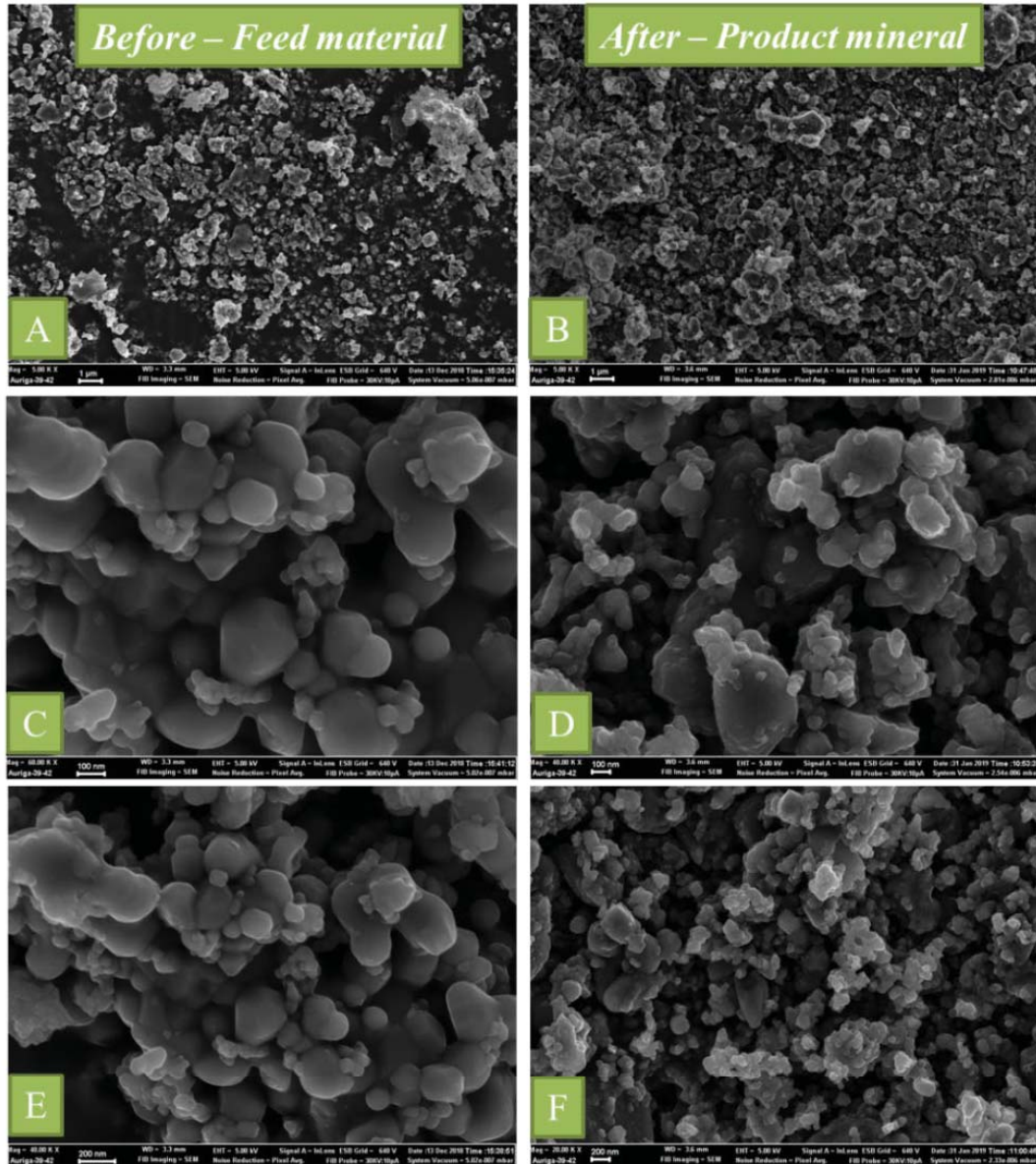


Figure 2.15: The morphological properties of feed and product mineral at 1μm, 100 nm, and 200 nm.

As can be seen, it is clear that ACM contains nano-sheets with hexagonal structures uniformly distributed across its surface, contrary, the product mineral (struvite) portrayed nanosheets-like structures with reduced size. The results are suggesting a possible dissolution of the feed material and the formation of new mineral phases and this is consistent with what has been reported by Herald et al. (2017).

2.3.4.4 Elemental composition of the activated magnesite and produced struvite using XRD

The elemental composition of: (a) ACM (feed) and (b) struvite product mineral is shown in **Figure 2.16**.

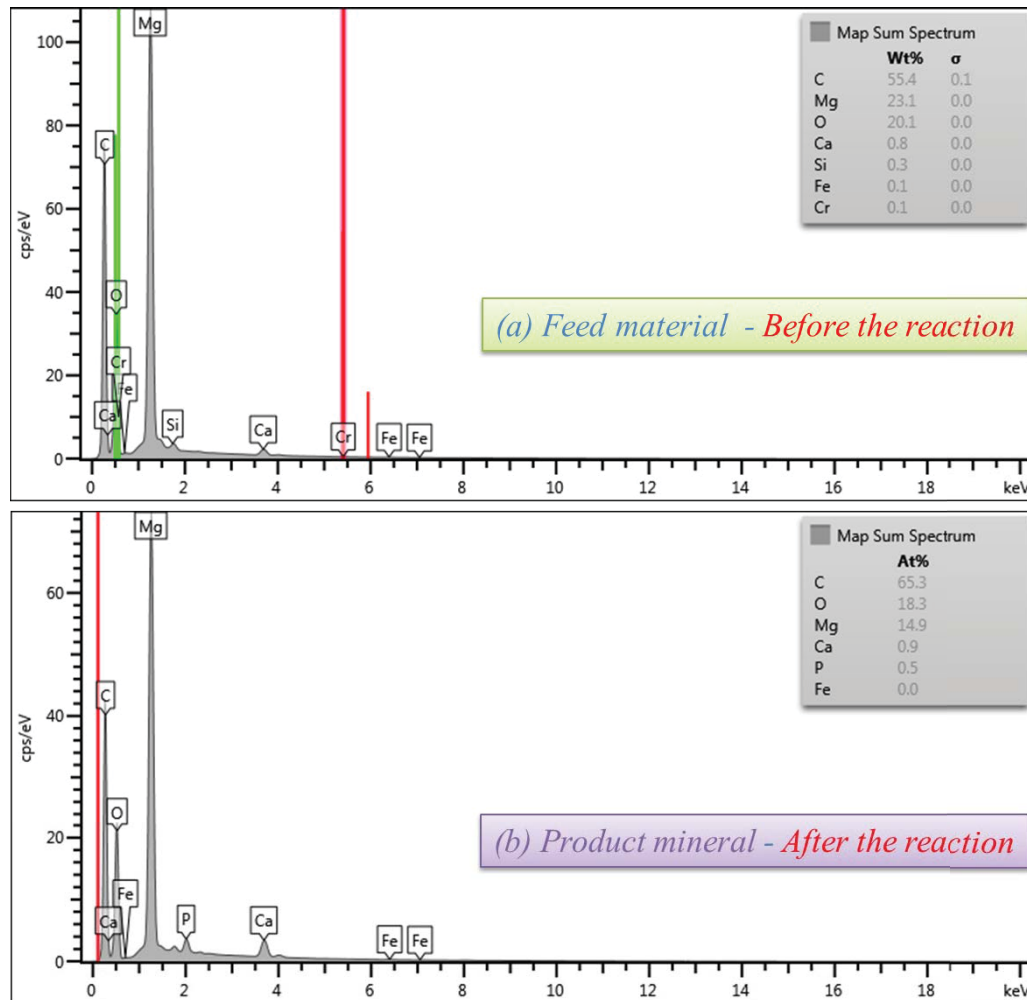


Figure 2.16: Elemental composition of: (a) ACM (feed) and (b) struvite (product mineral).

As depicted in **Figure 2.16a**, ACM was observed to contain Mg, O, and C in addition to traces of Ca, and Si, and this is consistent with the composition of the parent material (raw cryptocrystalline magnesite). This composition is also conducive for increasing the pH. Which is required for the precipitation of the minerals contained in the solution, while Mg and Ca will scavenge NH_4^+ and PO_4^{3-} from the solution. This is evident in **Figure 2.16b**, where the composition of the product sludge is presented, and this was observed to contain Mg, O, C as major components and traces of Ca and P. This is also evident from the water quality since the level of Ca is very low in ACM, but there is correlation with the deposition of phosphate onto the final mineral.

2.3.4.5 Elemental composition of ACM

The elemental mapping of pre-treated magnesite is shown in **Figure 2.17**.

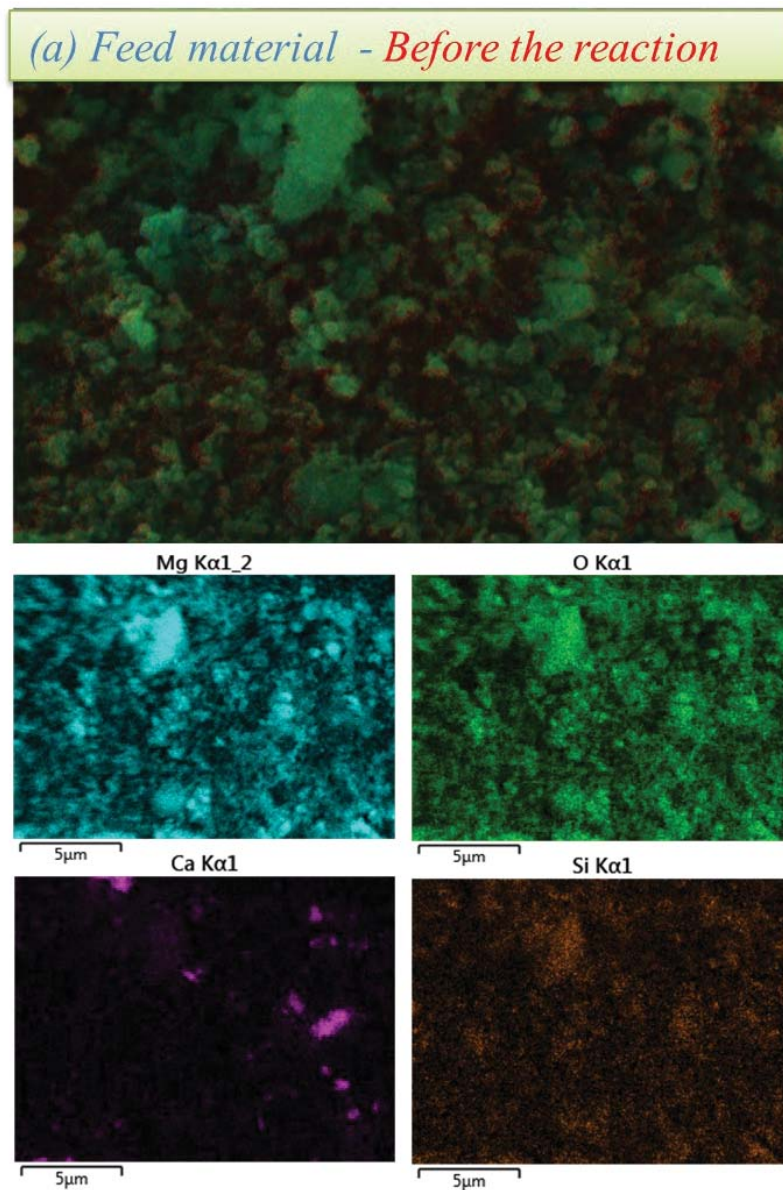


Figure 2.17: The elemental mapping of pre-treated magnesite before contact with MWW

As illustrated in **Figure 2.17**, elemental mapping of the pre-treated magnesite was done. The results confirmed with the elemental analysis, where the pre-treated magnesite was observed to contain Mg, O, Ca and Si. These are elements that contribute to the removal of P and N from an aqueous system.

2.3.4.6 Elemental composition of the produced struvite

The elemental composition of the produced struvite (product mineral), as this was identified using elemental mapping in SEM, is shown in **Figure 2.18**.

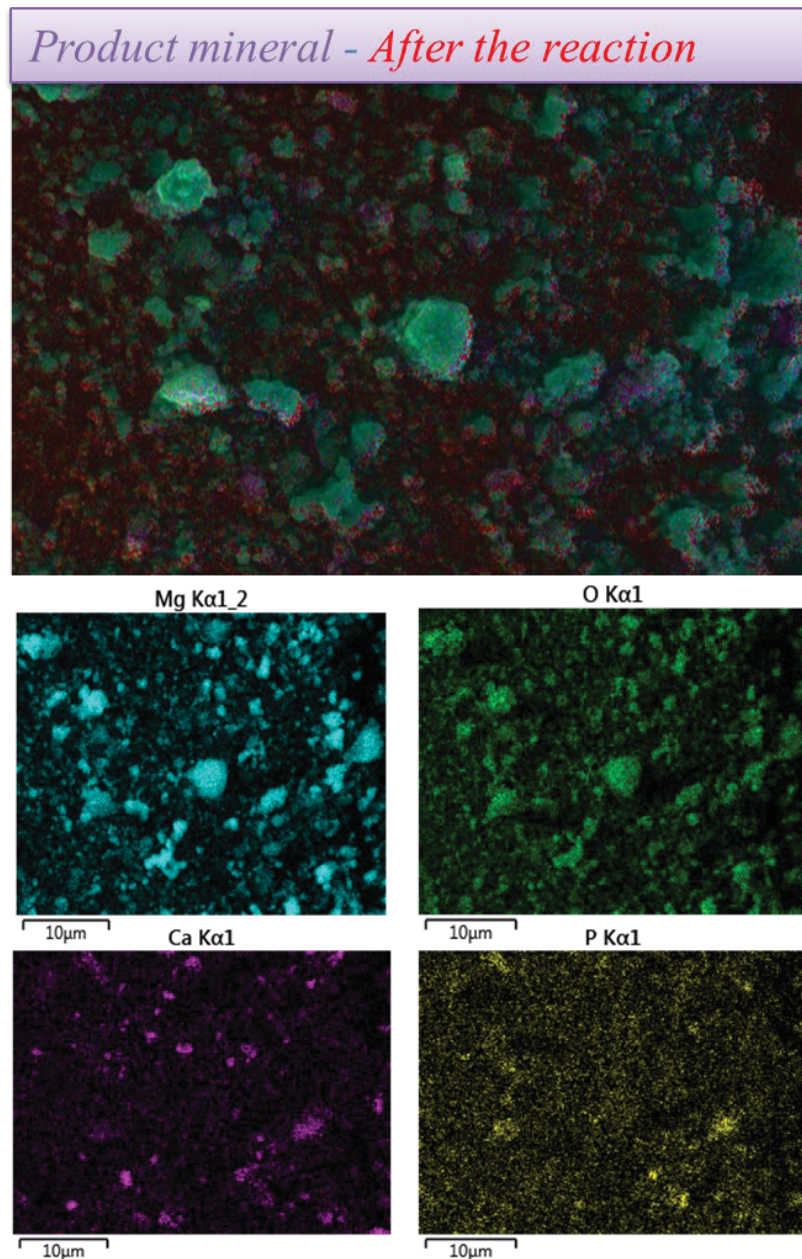


Figure 2.18: The elemental mapping of the product mineral, i.e., the produced struvite from the interaction of ACM with the WAS effluent.

Elemental mapping identified that the product mineral is rich in Mg, O, Ca and P, and this is a strong indication that struvite crystals have been formed.

2.3.4.7 Functional groups analysis using FTIR

To further support the elemental mapping results, functional groups analysis, using FTIR, of the ACM (before interaction) and the product mineral sludge (after interaction) was carried out and results are shown in **Figure 2.19** and **Table 2.5**.

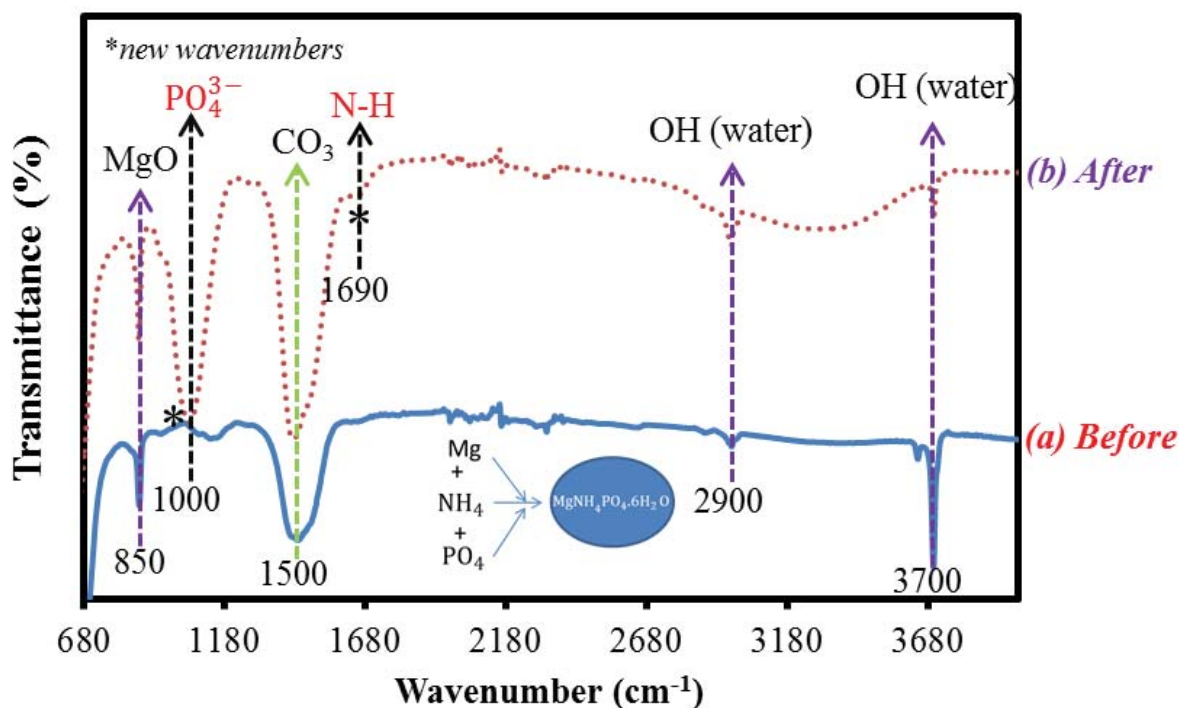


Figure 2.19: The Fourier transforms infrared spectroscopy analysis of the feed (ACM) and product mineral sludge (after interaction).

The identified wavenumbers of the peaks in the FTIR spectrum were duly identified and functionalized as demonstrated in **Table 2.5**.

Table 2.5: The functional groups and wavenumber of identified peaks in the feed (ACM) and product mineral sludge.

Functional group	Wavenumber	Reference
Mg-O	850 cm ⁻¹	(Heraldry et al., 2017)
PO ₄ ³⁻	1000 cm ⁻¹	(Heraldry et al., 2017)
CO ₃	1500 cm ⁻¹	(Heraldry et al., 2017, Magagane et al., 2019)
N-H	1690 cm ⁻¹	(Heraldry et al., 2017)
-OH	2900 and 3700 cm ⁻¹	(Heraldry et al., 2017)

As shown in **Figure 2.18** and **Table 2.5**, the FTIR spectra confirm the existence of water hydration, Mg-O metal-oxygen bond, and carbonate in the ACM (feed material). This is in agreement and further corroborates the XRD results, thus indicating the presence of periclase and traces of brucite (magnesium hydroxide). The presence of carbonate is traced back to the possible carbonation of the Mg and CaO that were initially contained in ACM, and less likely, to carbonate residues (magnesite) from the calcination process. On the other hand, the product mineral was observed to be hydrated or containing water molecules, Mg-O metal-

oxygen bond, N-H bond, and PO_4^{3-} , hence confirming that struvite has been formed. The obtained results are in agreement with both the literature (Herald et al., 2017) and the EDS and XRD results.

CHAPTER 3: WATER RECLAMATION USING MEMBRANE DISTILLATION

This chapter addresses objective three of this research project and therefore its focus is on the reclamation of clean water using product water from struvite synthesis. The methods employed for water reclamation, along with results to support the developed objectives and findings of the used methodologies are also delineated in this chapter.

In more detail, this section is the continuation of the previous work conducted by the CSIR Water Centre group to examine the scaling up of a struvite recovery system under the South African setting. The optimum conditions, both in terms of nutrients removal and environmental relevance, for struvite crystallization, i.e. 30 – 60 minutes of mixing and 0.5 – 1 g dosage of ACM per 500 mL of municipal effluents (Mavhungu et al., 2019), were adopted on a pilot treatment system that could be applied at village level (rural area) in South Africa and other Low- and Middle-income Countries (LMICs). These conditions are also favourable in terms of environmental relevance, as was identified in the group's latest LCA study using the one-factor-at-time (OFAT) method (Mavhungu et al., 2020b). Drinking water reclamation from wastewater has also examined in the previous work using reverse osmosis (RO) (Masindi et al., 2018, Masindi et al., 2019, Masindi et al., 2014). Specifically, a pilot treatment system, able to operate at rural South Africa, was constructed at the CSIR premises in Pretoria and used for struvite recovery and drinking water reclamation.

Noteworthy, the previous work by the CSIR Water Centre focused on optimization of operational parameters (Mavhungu et al., 2020b). The fundamental goal was to identify the dependent, interdependent, and independent variables/parameters for subsequent pilot studies. It was identified that ammonia removal was dependent on phosphate and magnesium concentration, with decreasing phosphate concentration largely affecting the efficacy of the system in ammonia removal (Mavhungu et al., 2020b). In light of that, a fixed system under optimised condition and with balanced stoichiometry, which yielded high efficacy for ammonia removal, was examined, as demonstrated in the subsequent sections below. Therefore, in this industrially orientated study, a problematic liquid waste (municipal wastewater) is valorised in the context of circular economy through a zero liquid discharge (ZLD) process to synthesize struvite and reclaim (drinking) water. As already mentioned, struvite is a valuable process co-product, since it can be used as a slow-release fertiliser in the agricultural industry and address, at least partly, the growing problem of phosphate rock depletion and phosphate shortage (Talboys et al., 2016). The reclaimed water, the other process co-product, has several defined domestic uses and can also address water scarcity concerns, in South Africa and further afield. The system is versatile and is able to be directly installed in rural South

African villages and can therefore be further scaled up to industrial systems. Finally, as this is a ZLD process, the environmental impacts from discharging poorly treated wastewater, a problem in South Africa and other LMICs that are struggling to manage the ever-increasing wastewater volumes, are also addressed.

3.1 Reclamation of clean water

The filtered supernatant from the Nutrient Recovery Unit, referred to here as feed solution (FS), is first stored in a buffer tank. The design capacity of the tank allows the quality control measures for the membrane distillation feed. The feed to the membrane distillation unit is drawn using five (5) peristaltic pumps run at 19.5 LPM (maximum rate of 24 litres per minute, LPM). This allows for modular configuration for the unit, while at the same time optimising hydraulics on the membrane surface. The effluent then passes through a sand filtration bed before is it filtered with activated carbon for residual ammonia removal. The presence of Ca, Mg, and other hard salts suggest that these may get deposited if solubility limit is exceeded, thus affecting the performance of the membranes and final water quality, as observed during experimental trials. To avoid such eventuality, the use of antiscalant dosing (a chemical scale inhibitor) was employed. Typically, an antiscalant agent such as ASWS 101, or a similar chemical, is mixed with the FS after the pre-treatment (sand and activated carbon filtration), at a rate of 4 - 5 mg/L. To this end, an HDPE chemical mixture tank with an electronic diaphragm type disposing pumps was used.

The prepared FS passes through a flowmeter to the heating bath to achieve an outlet temperature of 45 ± 1.5 °C. The permeate solution (PS), a final water product (prepared ultra-pure water during commissioning), is drawn at the same rate from the PS tank through a chiller to achieve a temperature of 20 ± 1.5 °C. The feed streams, i.e. FS and PS, enter the first stage with each of the fifteen (15) direct contact membrane distillation (DCMD) units counter-current at the same flow rate. Each DCMD unit, in hot and cold connections, are fitted with a pressure gauge and temperature transmitter to a data logger. Each DCMD is fitted with a PTFE membrane allowing for 1.25 g/cm².hr (or 12.5L MH) as per experiments performed by the CSIR researchers, which is lower than the RO metric of 17 L/m²/h (LMH). But once hydraulics are optimised, it is possible to achieve 15 LMH, which is the value used in the mass balance. The outflow of the first stage of the DCMD units enters the second stage consisting a further 30 DCMD units. The final clean water is recycled to the PS tank, whilst the concentrated FS (of lower flow) is returned to the FS tank. Each DCMD unit has a cross-sectional area of around 0.9 m² (0.95 m x 0.95 m). Allowance is made for inline conductivity measurement on each line before the combined final water, as PS, and the returned concentrated FS enter the corresponding tanks. The simplified process flow diagram is shown in **Figure 3.1**.

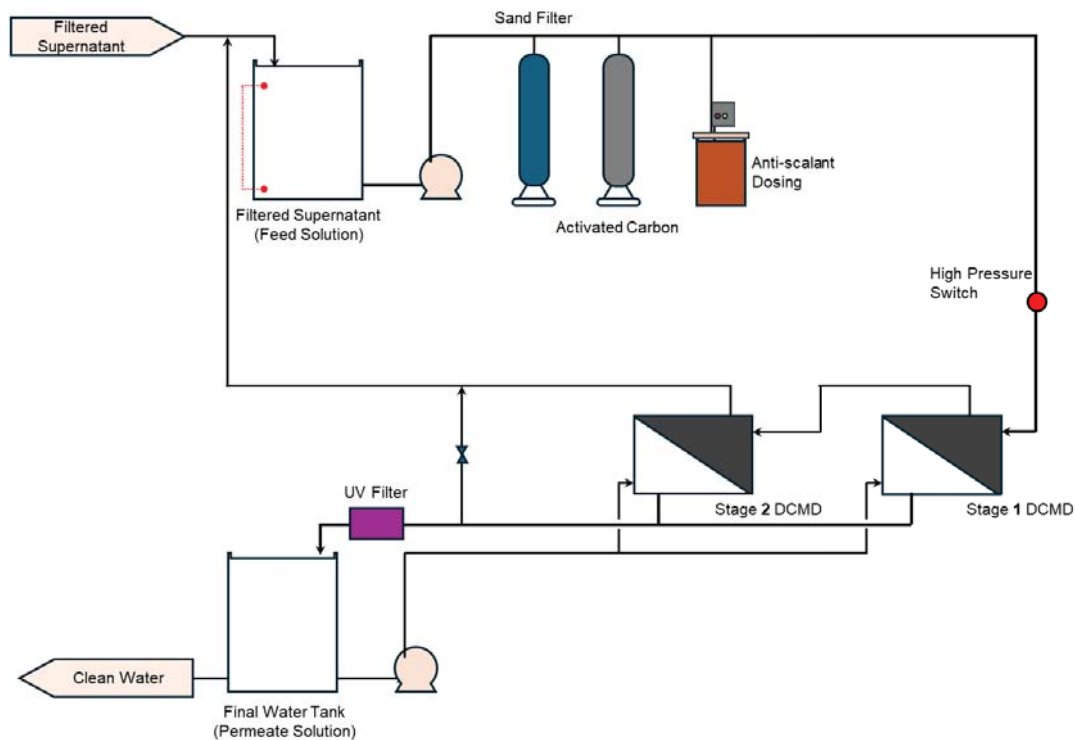


Figure 3.1: Proposed pilot scale flow diagram for clean water reclamation from NRU effluent.

Specific energy consumption (SEC) is a critical metric in evaluating the efficiency of MD systems. It represents the amount of energy required to produce a cubic meter (m^3) of water. SEC values reported in the literature range from 0.52 kWh/ m^3 to 15.36 kWh/ m^3 , depending on the system design and operational parameters (Zarebska-Mølgaard et al., 2022, ve et al., 2024). The SEC of the proposed DCMD unit is 3.4 kWh/ m^3 , which indicates slightly optimised design.

3.2 Membrane properties

The PTFE membranes, with SKU FGLP29325, and spacer for the experiment were purchased from Merck (Pty) Ltd. An additional PVDF membrane, with SKU 88520, was purchased from Thermo Fischer. The properties of the membranes are as shown in **Table 3.1**. A woven mesh spacer was installed on the permeate side of the setup to facilitate flow on the surface of the membrane.

Table 3.1: Properties of the Membranes used in the Membrane Distillation Experiments.

Material	Pore Size (μm)	Porosity (%)	Temperature ($^{\circ}C$)	Thickness, δ (μm)	Liquid Flow ($MI/cm^2 \cdot min$)	LEP (bar)	Effective Area (cm^2)
PTFE (FGLP29325)	0.22	70	130	175	15	1.0	127.41
PVDF (GVHP00010)	0.22	75	85	125	>1		127.41

3.3 Experimental Apparatus

3.3.1 Pre-Treatment Apparatus

The sequence of experiments involves two (2) approaches: (1) direct treatment of the FS, i.e., as received, by mean of MD; and (2) pre-treating the FS before MD. These are described below:

- For direct treatment, composite samples from the NRS effluent are stored overnight in a refrigerator. Minimal settling is achieved, and the sample is portioned daily for the experiments. The bench scale unit (BSU), as illustrated below (**Section 3.3.2**), includes an inline filter which serves to prevent large, suspended solids from entering the membrane cell and damaging the membrane.
- Given the likely presence of ammonia and carbonates in the effluent, the investigation will also include pretreating the FS by means of sand filtration and biological activated carbon (BAC) to remove suspended solids as well as ammonia and nitrates. Residual ammonia is removed by acidification using concentrated hydrochloric acid (HCl). This approach should reduce the concentration of carbonates present in the solution and facilitates the conversion of ammonia into ammonium ions. This mechanism not only serves to maintain the appropriate pH level, but it also alters the speciation of nitrogen molecules, shifting the equilibrium from free ammonia toward the less volatile ammonium form.

Figure 3.5 shows the packing of sand filtration and BAC (in this case coconut shell activated carbon). To maintain enough residence time, flow was managed through the 1000 L unit at 0.1 LPM. The pre-filtered overflow was collected into a 5 L bucket and prepared for acidification.



Figure 3.2: Pre-treatment with sand filtration and coconut-shell activated carbon.

3.3.2 Membrane distillation bench scale unit

The CSIR bespoke DCMD unit was used in the experiments. To standardise operation, a standard operating procedure (SOP) that was developed in 2023 by CSIR was followed.

Figure 3.3 shows the BSU.

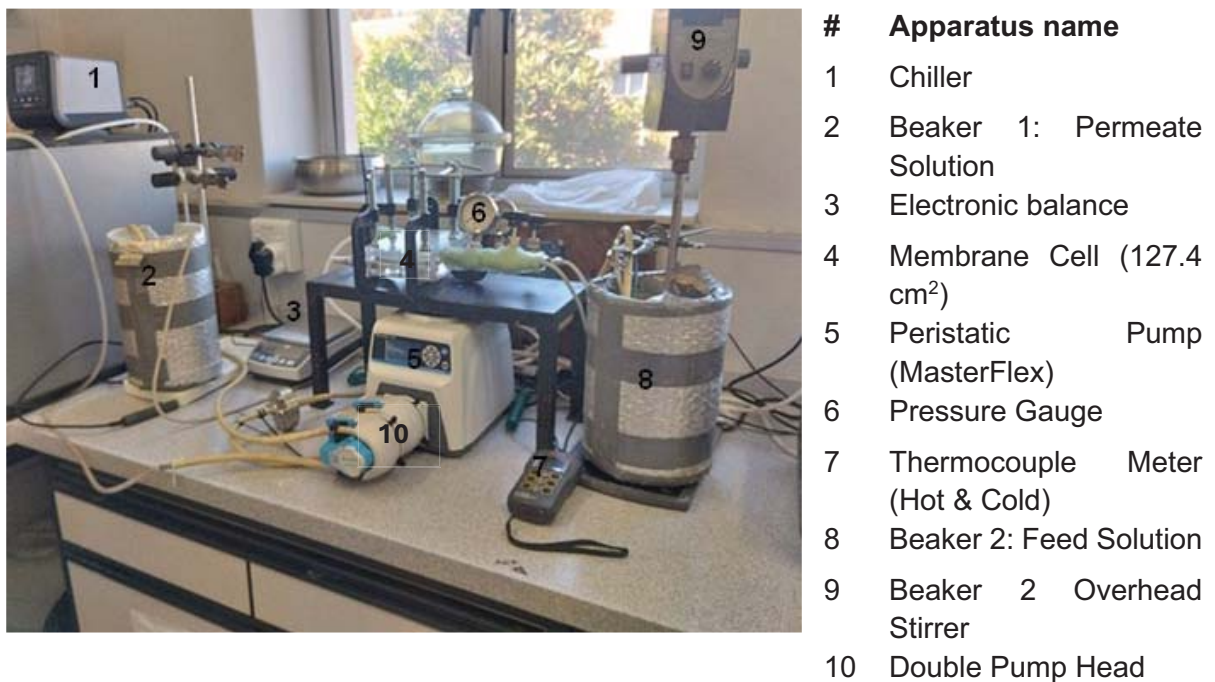


Figure 3.3: The CSIR laboratory setup of the Direct Contact Membrane Distillation (DCMD) Unit.

3.4 Optimisation of operational parameters

To determine the optimum treatment conditions for the effluent under study (i.e., the FS), the main operational parameters were investigated for both the FS stream and as well as for the PS stream. These include the effect of flowrate and temperature. To instil realism, the quality of the FS was not controlled, since in larger systems this will be utilised as received from the NRU. All experiments were performed in triplicate and the obtained data are reported as mean values. Repeat experiments for the same operating conditions were performed. The base experiment was conducted at 400 mL/min using a dual head MasterFlex FS pump, with the PS and FS at $20 \pm 1.5^\circ\text{C}$ and $45 \pm 1.5^\circ\text{C}$, respectively. A PTFE or a PVDF membrane was prepared for each experiment. An overhead stirrer was immersed in the FS at rotated at a constant speed of 300 rpm, to maintain homogenous conditions and uniform temperature.

3.4.1 Effect of temperature

To assess the significance of permeate temperature in improving permeate recovery, the PS temperature was dropped from $20 \pm 1.5^\circ\text{C}$ to $15 \pm 1.5^\circ\text{C}$.

3.4.2 Effect of flowrate

To investigate the benefit of increased flowrate, the MasterFlex FS was set between 400 mL/min and 500 mL/min for the base scenario operating condition of $20 \pm 1.5^\circ\text{C}$ for the PS and $45 \pm 1.5^\circ\text{C}$ for the FS, using the PTFE membrane. It was expected that higher flow rate should increase the flux and reduce or delay the fouling effect on the membrane, thus resulting in improved flux.

3.5 Characterisation of the samples

To understand the physicochemical properties of the feed sample (FS) and the fouling potential of the membranes, state-of-art analytical pieces of equipment were used for materials characterisation, as laid out below.

3.5.1 Aqueous sample analysis

The collected supernatant samples were stored in the refrigerator at 4°C and allowed to acclimate to room temperature before analysis. The TS and VS content was determined thermogravimetrically, according to the APHA methods (APHA, 2017)(APHA et al., 2017). The remaining sludge was centrifuged at 2000 rpm for 5 minutes and then the concentrate was filtered through a $0.45\mu\text{m}$ membrane filter paper to produce a supernatant sample. The supernatant sample was then analysed for inorganic ions. $\text{NH}_3\text{-N}$ and $\text{PO}_4^{3-}\text{-P}$ were analysed using the HACH DR3900 spectrophotometer (Aguilar-Pozo et al., 2023, Ferrari et al., 2019). Calcium (Ca), Magnesium (Mg), Sodium (Na), Potassium (K), Aluminium (Al), Iron (Fe),

Manganese (Mn), Chromium (Cr), Copper (Cu), Nickel (Ni), Zinc (Zn), Arsenic (As), Lead (Pb) and Cadmium (Cd) were analysed in the supernatant using inductively coupled plasma optical emission spectroscopy (ICP-OES). Furthermore, the aqueous samples were also analysed using the inductively coupled plasma mass spectrometry (ICP-MS), Xseries 2, supplied by Thermo scientific, from Hanna-Kunath-Str 11 28199 Bremen, Germany. The pH and conductivity during the experiment was monitored using a Hanna Instruments multi-parameter probe (HI-19828 multi-parameter).

3.5.2 Solid sample analyses

To identify the fouling mechanism and type of compounds deposited on the surface of the membranes from the aqueous media, small samples of the membrane and/or solids materials were assessed. Morphological properties were ascertained using Scanning Electron Microscopy (SEM) coupled with Energy Dispersive Spectroscopy (EDS). For this, an Auriga Cobra FIB- FESEM (Model: Sigma VP FE-SEM with Oxford EDS Sputtering System, make: Carl Zeiss, Supplier: Carl Zeiss, USA) instrument was used. The functional groups were ascertained using a Perkin-Elmer Spectrum 100 Fourier Transform Infrared Spectrometer (FTIR), equipped with a PerkinElmer Precisely Universal Attenuated Total Reflectance (ATR) sampling accessory that uses a diamond crystal. These analytical instruments were used to determine the physicochemical parameters of the solid samples and intensify the mechanisms governing the removal of contaminants from aqueous solutions. These instruments will also be used to determine the fate of inorganic and organic contaminants during the process.

3.6 Results on membrane distillation

3.6.1 Physico-chemical properties

Physical and chemical evaluations of the samples were conducted to assess water quality before and after the MD experiments, as to evaluate both the membrane efficiency and membrane durability. On physical observation, the samples were brown with suspended solids (SS). **Table 3.2** summarises the physicochemical parameters for the feed composites used in the experiments. Ammonia, carbonates, calcium, chlorine, magnesium, phosphates, potassium, silica, sodium, and sulphate were the main constituents in FS, while other constituents were present in trace amounts. The samples are characterised by high pH (above 9.0), varying amounts of sulphates, ammonia at 19 mg/L and carbonates at 278 mg/L for the 50th percentile. The high carbonates are potentially due to magnesite addition in the NRU. The results of the FS constituents when using the PTFE or the PVDF membrane at 400 mL/min flowrate are shown in **Table 3.2**.

Table 3.2: The varying quality of the pilot NRU effluent, as received for the MD experiments

Parameters	Units	Feed solution							Percentile	
		1	2	3	4	5	6	7	50 th	99 th
Ammonia	mg/L	37	18	21	39	24	43	352	19	36
Carbonates	mg/L	215	278	487	282	234	487	273	278	487
Chlorine	mg/L	72	135	95	162	163	95	106	106	162.9
Calcium	mg/L	13	3	19	5	7	12	14	12	18.7
Magnesium	mg/L	169	259	189	224	236	143	207	207	257.6
Phosphates	mg/L	1.4	0.4	1.9	0.9	0.6	1.9	0.5	0.9	1.9
Potassium	mg/L	46	78	51	63	72	39	103	63	101.5
Sodium	mg/L	70	125	81	111	132	76	147	111	146.1
Silica	mg/L	3.6	13.8	0.2	2	6.6	0.2	<0.2	2.8	13.44
Sulphate	mg/L	46	124	7	47	49	7	49	47	119.5
EC	mS/m	142	230	128	166	161	134	178	161	226.8
pH	-	10.0	9.1	10.6	9.7	9.6	10.6	9.7	9.7	10.6
TDS	mg/L	1030	1660	922	1195	1159	965	1282	1159	1637
Turbidity	NTU	24	11	32	12	12	32	3.3	12	32

Table 3.2 delineates the representation of the priming permeate quality by permeate solution (Set 1). Notably, the PS results demonstrate that membrane distillation, especially the PTFE membrane (Merck Millipore FLGP29325), efficiently rejected non-volatile constituents. However, there is a remarkable increase in pH in the PS, which is attributed to the presence of ammonia. This is likely due to the hydrophobic nature of PTFE membrane, which allows for the diffusional transport of volatile compounds, including ammonia, in the vapor phase. Moreover, the EC and TDS of the permeate increased, this observation clearly confirms that certain ionic species were transferred into the PS. These findings are comparable to those reported by (Aquino et al., 2023, Kim et al., 2016).

Further, experiments carried out under the same operating conditions, except that the PS was maintained at $15 \pm 1.5^\circ\text{C}$, showed a similar trend for ammonia and carbonates. Experiments conducted at $20 \pm 1.5^\circ\text{C}$ for the PS and keeping other parameters constant at baseline, where PVDF is used, showed that the membrane is highly selective in rejecting all non-volatile constituents. However, carbonates and ammonia permeated the membrane in substantial amounts resulting in an increase of pH and EC. These findings are very similar to those obtained from experiments using PTFE membrane. Over time, the pH of the PS varied proportionally with the pH of the FS.

The PS results show a significant pH increase when the FS pH was not controlled, as depicted in **Table 3.3**. This increase is due to the selective transfer of volatile and carbonate compounds over the porous membrane. Pre-treatment of the FS with BAC followed by acidification caused the pH of the PS to stabilise below 9.0. The pre-treatment effectively reduced the release of ammonia and sulphates into the PS.

Table 3.3: The permeate solution quality from the lab scale DCMD of 147.2 cm² at varying PS temperature and membrane type.

		Permeate Solution – Set					
		PTFE, 400 mL/min		PTFE, 400 mL/min		PVDF, 400 mL/min	
		20°C	20°C	15°C	15°C	20°C	20°C
Parameters	Units	Set 1	Set 2	Set 1	Set 2	Set 1	Set 2
Ammonia	mg/L	<0.1	20	<0.1	11	<0.1	12
Carbonates	mg/L	<5	<5	<5	<5	<5	28
Chlorine	mg/L	<2	4	<0.2	<0.2	<2	<2
Calcium	mg/L	<1	<1	<1	<1	<1	<1
Magnesium	mg/L	<1	<1	<1	<1	<1	<1
Phosphates	mg/L	<0.2	<0.2	<0.2	<0.2	0.2	0.2
Potassium	mg/L	<0.5	<0.5	<0.5	<0.5	<0.5	<0.5
Sodium	mg/L	<1	2	<1	<1	<1	<1
Silica	mg/L	0.3	<0.2	<0.2	<0.2	<0.2	<0.2
Sulphate	mg/L	3	4	8	7	<2	6
EC	mS/m	0.8	1.5	0.9	3.9	0.8	6.8
pH	-	6.6	9.5	7.9	8.5	8.2	9.9
TDS	mg/L	<10	11	6	28	5.8	71
Turbidity	NTU	2	6	0.1	0.25	0.1	0.6

In all experiments, a consistent pattern in (FS) feed and permeate (PS) composition was noted. After the experiments, FS compositions demonstrated an increase in TDS and EC. The PS compositions showed consistent trends throughout experiments, regardless of the membrane used. Both PVDF and PTFE membranes demonstrated the ability to reject non-volatile components. Treating the FS *as-is* indicated that all PS samples after MD exhibited minor increases in TDS, EC, pH and ammonia content. The existence of ammonia in the permeate is due to its volatile nature, allowing it to pass through the membrane along with the water molecules (i.e., vapour). Interestingly, carbonates were found in the PS of the PVDF experiments. This observation is anomalous considering that carbonates are non-volatile ionic species that should be rejected by the MD membranes. The presence of carbonates indicates potential membrane wetting issues, which could allow non-volatile species to pass through.

To reduce the impact of ammonia and carbonates on the quality of the PS, additional experiments were conducted with the FS subjected to pre-treatment as described in the Materials and Methods (**Section 2.2**). **Figure 3.4** below shows the difference in pH overtime for the FS as received and PS when pre-treated by sand filtration and BAC followed by HCl acidification. When there was no pre-treatment, the pH increased from 8 to 9.36 within 10 minutes of the experiment and remained constant throughout the experiment.

Table 3.4: The permeate solution (PS) quality from the lab scale DCMD of 147.2 cm² at varying pretreated FS.

		Permeate		Permeate		Distillate	
		Set 1	Set 2	Set 1	Set 2	Set 1	Set 2
		20°C - Pre-treated					
Parameter	Unit	PTFE, 400 mL/min		PTFE, 400 mL/min		PVDF, 400 mL/min	
Ammonia	mg/L	<0.1	6	<0.1	8	<0.1	18
Carbonates	mg/L	<5	<5	<5	<5	<5	24
Chlorine	mg/L	<2	<2	<2	<2	<2	<2
Calcium	mg/L	<1	<1	<1	<1	<1	3
Magnesium	mg/L	<1	<1	<1	<1	<1	<1
Phosphates	mg/L	<0.2	<0.2	<0.2	<0.2	<0.2	<0.2
Potassium	mg/L	<0.5	0.6	<0.5	<0.5	<0.5	0.6
Sodium	mg/L	<1	<1	<1	<1	<1	<1
Silica	mg/L	<0.2	<0.2	<0.2	<0.2	<0.2	<0.2
Sulphate	mg/L	2	3	4	7	2	3
EC	mS/m	0.3	9	0.5	8.9	0.7	16.3
pH	-	7.6	8.4	7.0	8.2	7.2	9.0
TDS	mg/L	<1	15	<1	17	<1	26
Turbidity	NTU	0.1	0.3	0.1	0.4	0.1	0.4

When pre-treated, the PS was at a pH of 6, the PS pH steadily increased over time. After 430 minutes, the pH was 8.02. This shows that the acidification of the FS had a positive impact on the PS pH as it can be seen in **Figure 3.4**, as the pH curve was always lower than that without pre-treatment. Therefore, as expected the combination of pH adjustment and BAC treatment improved the overall quality of the PS.

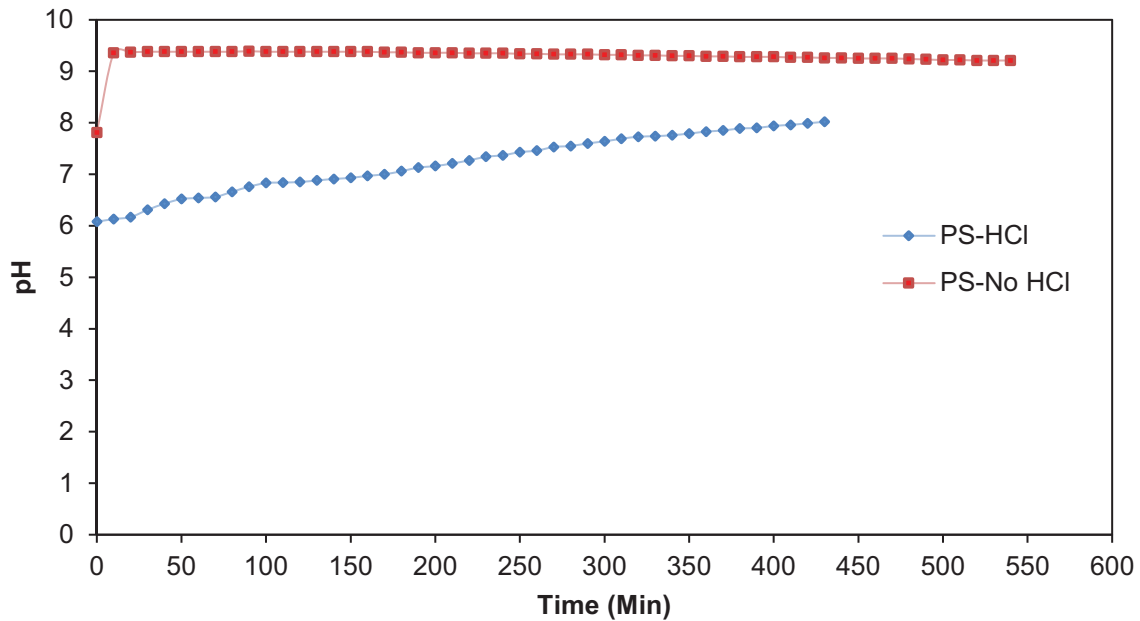


Figure 3.4: The pH of the permeate solution (PS); (1) without any pre-treatment – indicated by PS-No HCl, and (2) with filtration and acidification pre-treatment – indicated by PS-HCl.

3.6.2 Water recovery and membrane flux

The discussion covers experimental results where the PS temperature for each experiment, which was either maintained at 15 ± 1.5 °C or 20 ± 1.5 °C, while the flowrate of the feed (FS) and permeate (PS) was maintained constant at either 400 or 500 mL/min. Two (2) membranes, i.e., PTFE and PVDF, with the same pore size ($0.22 \mu\text{m}$) were compared in terms of efficacy, durability, and flux performance. Finally, a dual head pump was used to circulate the PS and FS at the same flowrate.

3.6.2.1 Effect of treatment time and temperature

Figure 3.5 shows the experimental values of mass flux as function of time, with the PS kept constant at 20°C . The temperature of the FS was kept constant at $45 \pm 1.5^\circ\text{C}$, and the flowrate at 400 mL/min. Three trials were conducted under the same conditions. All the experiments kept increasing after the 60th minute up until the 110th minute. After 110 minutes, the mass flux starts to remain constant, as was also reported by Chew et al. (2017). The average mass flux for experiment 1, 2, and 3 were $1.24 \text{ g/cm}^2\text{h}$ ($12.4 \text{ L/m}^2\text{.hr}$), $1.22 \text{ g/cm}^2\text{h}$ ($12.2 \text{ L/m}^2\text{.hr}$), and $1.20 \text{ g/cm}^2\text{h}$ ($12.0 \text{ L/m}^2\text{.hr}$), respectively. After 300 minutes (~5 hours), there was a decline in average mass flux for experiment 1 and 2 at 0.8% and 4.92% respectively, while experiment 3 showed no decline in average mass flux. This decline in mass flux shows that the FS began to be concentrated and may be prone to cause a decrease in the driving force (Khan & Nordberg, 2018).

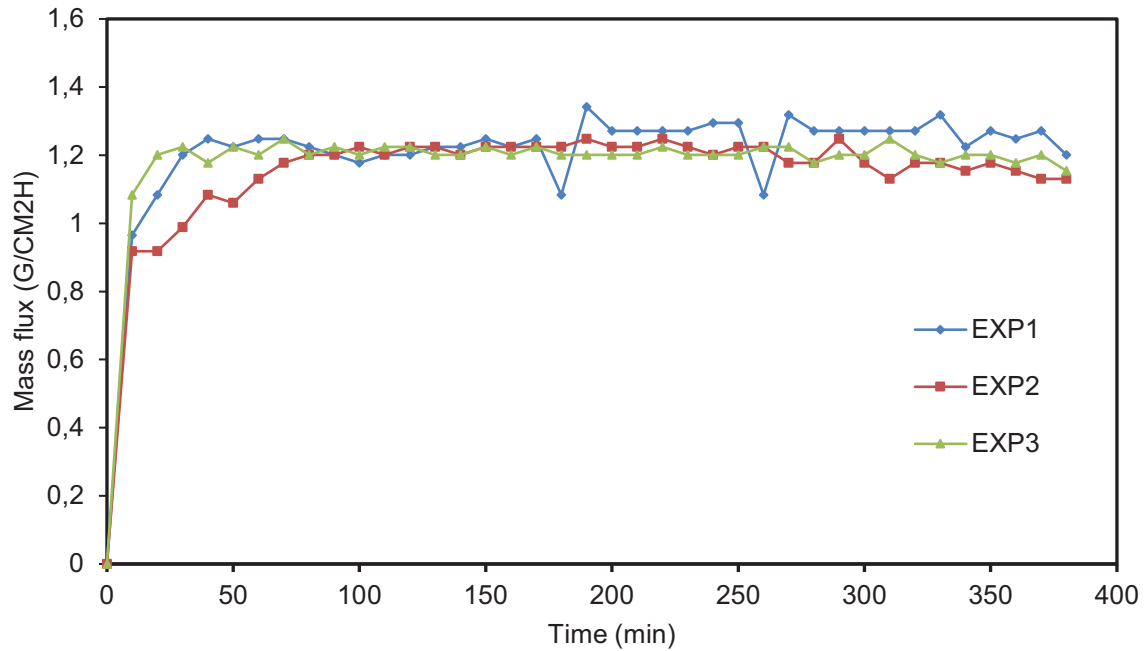


Figure 3.5: Membrane distillation mass flux at base conditions of 400 mL/min, TF=45°C and TP=20°C. NB: EXP stands for experiment).

Figure 3.6 shows the experimental values of mass flux as a function of time, with the PS kept constant at 15 ± 1.5 °C. The temperature of the FS was kept at 45 ± 1.5 °C, and the flow rate at 400 mL/min. The mass flux of experiment 1 and 2 started to increase with an increase in time for the first 100 minutes. After the 100th minute, both experiments showed that overtime they maintain some stability, this is observed by how the mass flux remained relatively constant throughout the experiments. The average mass flux for experiment 1 and 2 was 1.02 g/cm²h and 1.1 g/cm²h respectively.

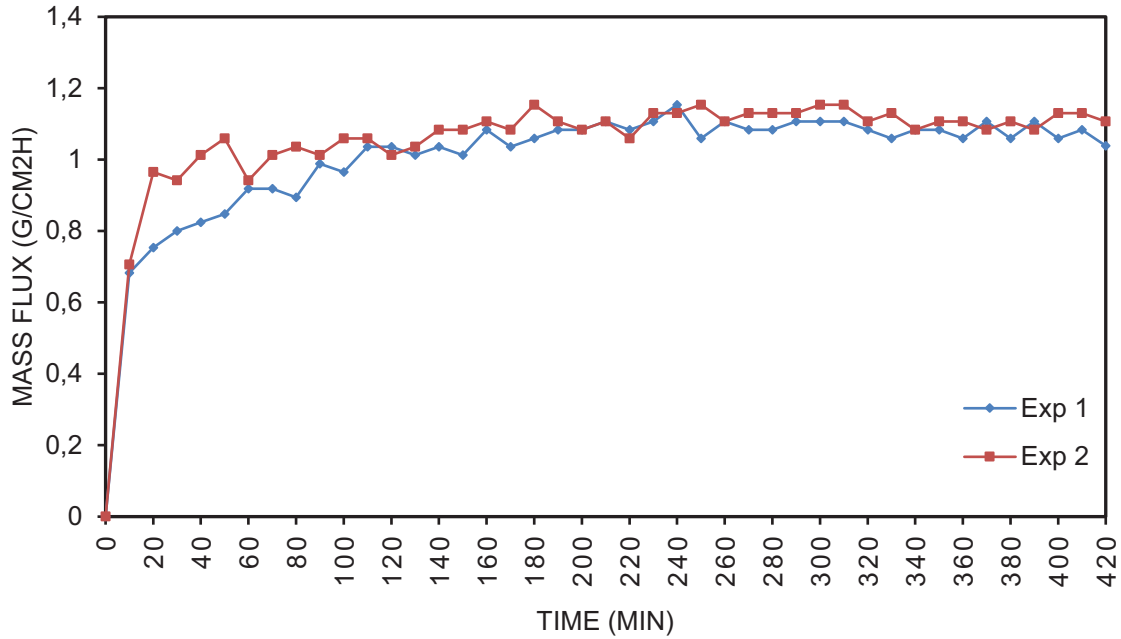


Figure 3.6: Membrane distillation mass flux at flow rate 400 mL /min, TF = 45°C and TP = 15°C.

Similar behaviour can be seen after 100 minutes of run time, where the mass flux remained steady, although the mass flux at PS temperature of 15 ± 1.5 °C was lower than when the conditions were 20 ± 1.5 °C. The difference in the average mass flux at these conditions is not significant and this is similar to observations by Alklaibi and Lior (2005), in that changing the temperature of the PS has twice less effect than FS temperature. The decline in mass flux was only observed in the first two experiments out of the five conducted and the decline was <5%. The effect of temperature is very important in MD since the process is iso-thermal. The trend of the temperature profile for baseline conditions, with the FS at 45 ± 1.5 °C and PS at 20 ± 1.5 °C, and circulation at 400 mL/min are shown in **Figure 3.7**. Results show that the desired temperature conditions and controls were met as both the PS and FS temperature remained constant, thus the average temperature also remained constant.

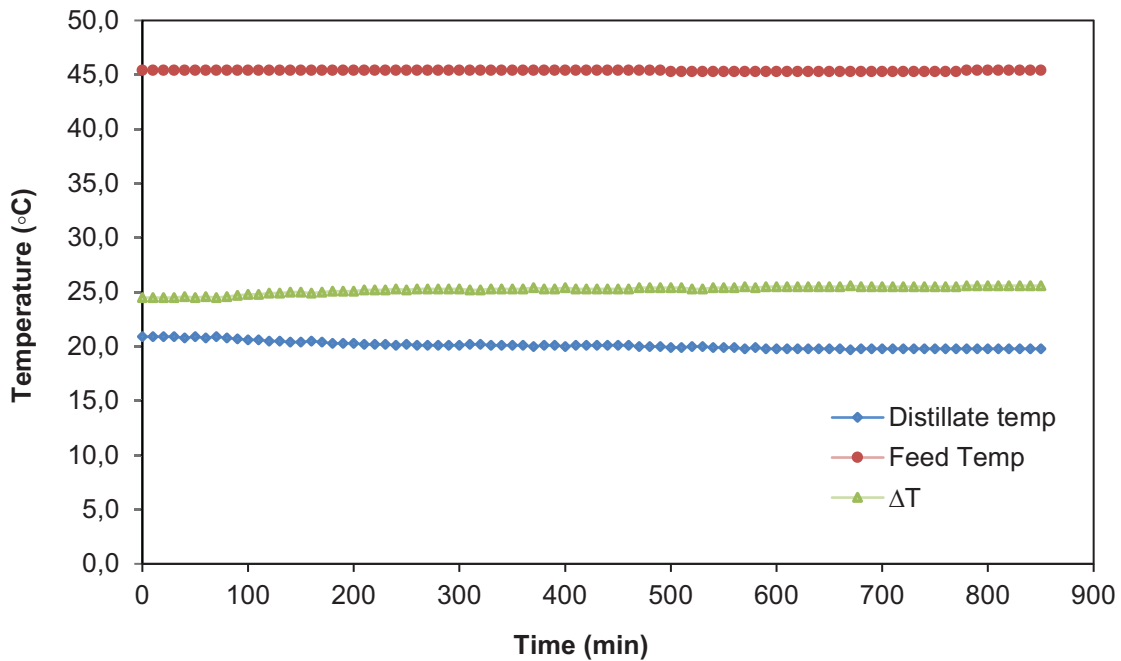


Figure 3.7: Temperature profiles of the DCMD at baseline conditions; FS=45±1.5°C, and PS=20±1.5°C.

3.6.2.2 Effect of the Membrane Material

To evaluate the effect of membrane material on mass flux, a PVDF membrane was used at the same base conditions as the PTFE membrane. **Figure 3.8** shows the mass flux over time using a PVDF membrane at base conditions. Result indicate an initial sharp increase in mass flux to approximately 0.45 g/cm²h. After 60 minutes, the flux stabilises around 0.25 - 0.3 g/cm²h. In contrast, the PTFE membrane, as shown in **Figure 3.9**, demonstrates superior performance, stabilising around 1.2 g/cm²h. The different performances can be attributed to the properties of the membrane material. PTFE is known for its superior chemical resistance and thermal stability compared to PVDF, and this may contribute to the superior performance and stability of the experiments when the PTFE membrane is used.

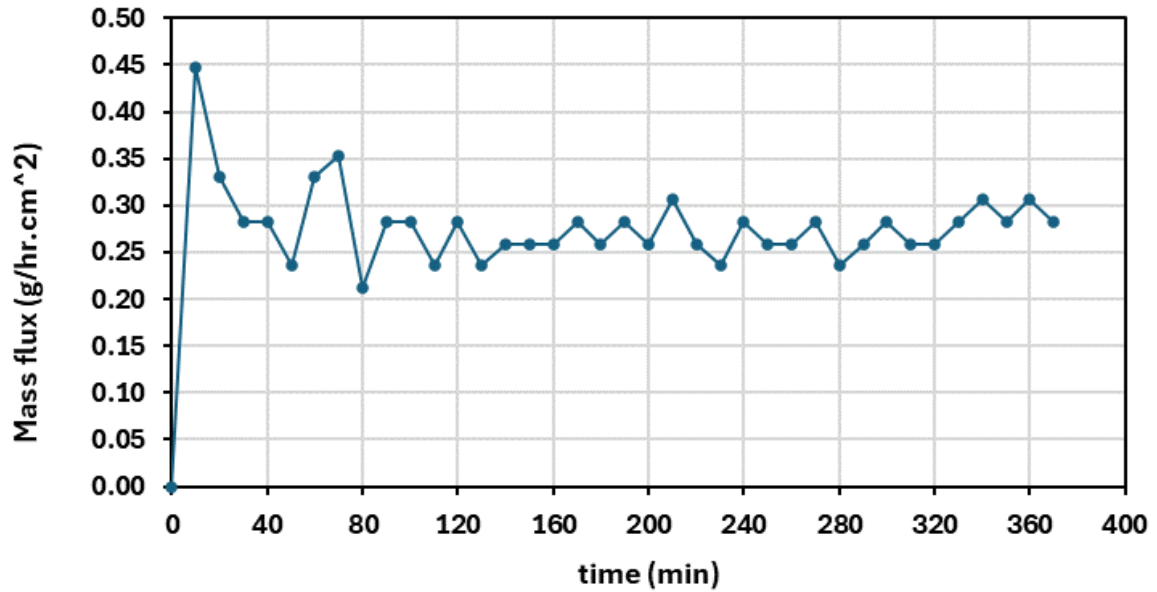


Figure 3.8: Membrane distillation mass flux at base conditions of 400 mL/min, TF =45°C and TP=20°C, using PVDF membrane.

3.6.2.3 Effect of Pre-treatment

To evaluate the effect of pre-treatment, the same baseline conditions were followed. **Figure 3.9** illustrates the mass flux as a function of time after the pre-treatment with a combination of sand filtration and BAC, followed by acidification of the FS, using concentrated HCl. The baseline conditions are flowrate of 400 mL/min, while the FS and PS temperatures at $45 \pm 1.5^\circ\text{C}$ and $20 \pm 1.5^\circ\text{C}$, respectively. The mass flux initially increased in both experiments, but then it starts to decrease over time. After 220 minutes, the mass flux remains stable throughout the duration of the experiment. The decrease in the mass flux might be attributable to the increase in concentration of the FS. The pre-treatment showed that higher flux can be achieved, at $1.4 \text{ g/cm}^2\text{h}$ versus $1.1 \text{ g/cm}^2\text{h}$ when direct FS is used under the same baseline conditions. In more detail, the flux declined, from a peak of $1.4 \text{ g/cm}^2\text{h}$, by 25% after 14 hours with a recovery of over 95%. It must be noted that the flux after 200 minutes remained relatively stable, at a loss of 14%.

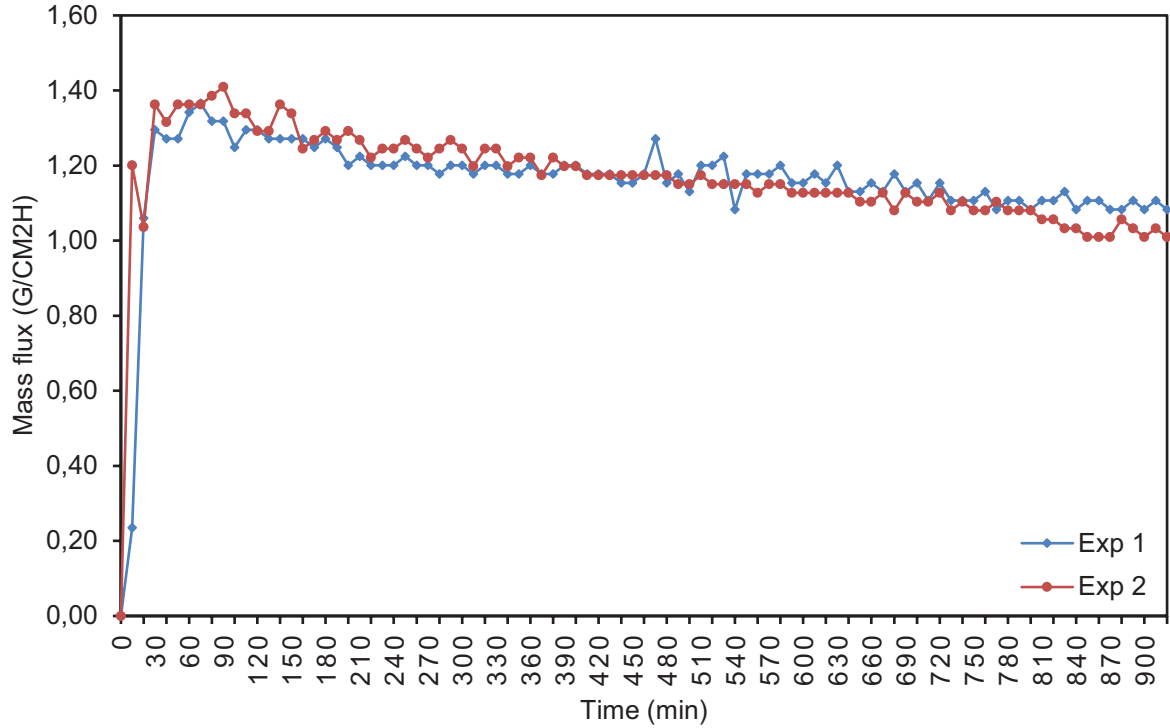


Figure 3.9: Membrane distillation mass flux at a flow of 400 ml/min, TF =45°C and TP=20°C, using PTFE.

3.6.3 Permeate solution recovery and solute retention

Equation 3.1 was used to calculate water recovery percentage.

$$\% \text{water recovery} = \left(\left(\frac{\text{Final permeate water (L)}}{\text{Initial distilled water(L)}} \right) - 1 \right) \times 100\% \quad (3.1)$$

According to (Eykens et al., 2016) the retention coefficient (R) determines how well dissolved compounds are separated from a solvent during membrane distillation and is calculated using

Equation 3.2:

$$R = 1 - \frac{C_p}{C_f} \quad (3.2)$$

where, C_p and C_f are the concentrations (in $\frac{g}{L}$) of the permeate and the feed solution, respectively.

The retention coefficients (R) (based on the TDS of final permeate and initial feed) of the three experimental runs were calculated using **Equation 3.2** and these were used to calculate the percentage (%) retentions, by multiplying by 100% to evaluate the membrane's (all experiments were conducted using the PTFE membrane which was identified to has superior performance over the PVDF membrane) efficiency in retaining particulates.

From the base conditions (400 mL/min, 20 ± 1.5 °C PS, and 45 ± 1.5 °C FS), the average PS recovery is over 90%. The overall water loss for the three experiments was 250 mL from the original volume of 3000 mL. These losses are due to evaporation during the operation. The membrane was only able to reject >95% of the solutes. The remaining solutes, i.e., those that were not rejected by the membrane may have resulted in membrane wetting, concentration polarisation, and/or membrane fouling as evident by the solid deposits observed on the membrane surface.

3.7 Characterisation of the membrane surfaces

3.7.1 SEM-EDS Characterisation

SEM was used to investigate accumulation of salt deposits on the PTFE membrane surface, at different treatment stages, and the obtained images are illustrated in **Figure 3.10**.

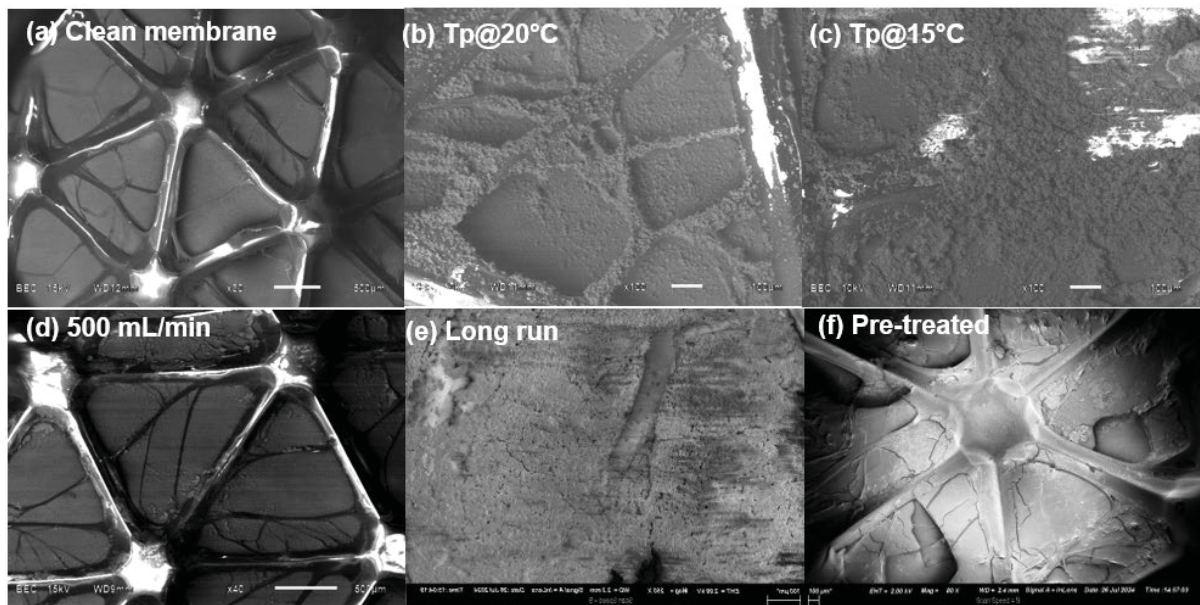


Figure 3.10: SEM images for: (a) clean PTFE membrane, (b) Tp@20°C, (c) Tp@15°C, (d) 500 mL/min, (e) Long run and (f) Pre-treated.

In more detail, **Figure 3.10** demonstrates that the surfaces of the clean and used PTFE membrane varied substantially. The circulation flowrate was set at 400 mL/min and the FS temperature was set at 45 ± 1.5 °C, unless otherwise specified. The clean membrane, is depicted in **Figure 3.10a**, clearly exhibiting a porous surface, while the SEM micrographs of the membrane after treating the effluent revealed different deposits on the membrane surface (**Figure 3.10b-f**). Specifically, the SEM micrographs revealed distinct variations in scale formation throughout the membrane surfaces and under various operating conditions. The membrane exposed to permeate at 20 ± 1.5 °C (Tp@20°C) exhibited minimal scale deposition, as shown in **Figure 3.10b**. On the contrary the membrane used for the permeate

at 15 ± 1.5 °C temperature exhibited a considerable amount of scale deposition, as shown in **Figure 3.10c**. This is not surprising given the retrograde dissolution of calcium and magnesium, while these results suggest that the tendency for scale formation is significantly influenced by temperature. Interestingly, at a high flow rate of 500 mL/min, the membrane surface displayed negligible scale deposition, as shown in **Figure 3.10d**. The findings suggest that high flowrates reduce concentration polarisation by increasing turbulence and mixing, thus minimising scale formation (Gryta, 2008).

The SEM imaging revealed considerable scale formation on the membrane surface for the long-run experiment (runtime > 7 hours), as shown in **Figure 3.10e**. This is due to the feed alkalinity which causes carbonates and magnesium salts to precipitate, leading to increased scaling. On the contrary, **Figure 3.10f** illustrates that the pre-treated experiment had much less scale on the membrane surface after more than 15 hours of operation. This is due to the lower pH of the FS, which prevents the precipitation of sparingly soluble salts, primarily carbonates. These scale-forming components become more soluble in the acidic environment, which inhibits their ability to nucleate and develop on the membrane surface (Antony et al., 2011, Yan et al., 2019). Furthermore, EDS elemental mapping provided insight into the chemical composition of the membrane before (clean) and after treatment (used membrane). **Table 3.5** demonstrates that the clean membrane was predominantly composed of C and F, which are membrane components. In contrast, the membrane surface in run Tp@20°C mainly consisted of C, Mg, and O, indicating the existence of MgCO₃. In addition, inorganic elements including Si and Ca were also identified in this run (Charfi et al., 2021).

When the PS temperature was reduced to 15 ± 1.5 °C (Tp@15°C) the concentrations of C, Mg, and O on the membrane surface increased significantly in comparison to Tp@20°C. This temperature-dependent response demonstrates that scales form on the membrane surface under various thermal conditions (Kayvani Fard et al., 2016). Furthermore, trace amounts of Ca and Si were also discovered, as illustrated. On the other hand, increasing the flow rate to 500 mL/min resulted in lower levels of C, Mg, and O relative to flow rates i.e., 400 mL/min (Tp@15°C and Tp@20°C). Overall, membrane samples demonstrated the consistent presence of Mg, C and O across all conditions, which is typically MgCO₃. It is worth noting that EDS revealed distinct elements in all runs which is due to scales being distributed unevenly on the membrane surface (Nguyen et al., 2017). Moreover, EDS analysis was conducted on both membranes used in pre-treated and direct (untreated) FS. In more detail, the membrane that was used in pre-treated FS exhibited significantly lower levels of C, Mg, and O compared to the membrane that was used in untreated FS. The lower concentrations of these elements suggest that pre-treatment effectively reduced these components. Additionally, trace amounts of other elements were detected in both runs.

Table 3.5: EDS elemental analysis of membrane surface at base conditions for Clean PTFE membrane, Tp@45°C, Tp@15°C, 500 mL/min, Long run, and Pre-treated.

Parameters	Clean	Tp@15°C	Tp@20°C	500 mL/min	Long run	Pre-treated
C	41.59	29.0	11.74	32.61	44.2	66.1
O	0	30.20	47.68	9.93	38.3	14.4
Mg	0	15.50	28.02	1.38	9.6	1.8
F	58.41	23.68	12.12	55.29	5.2	10.4
Si	0	1.7	0.22	0.35	0.7	0.3
Ca	0	0	0.23	0	0.6	0.4
Na	0	0	0	0.34	0.3	0
K	0	0	0	0	0.2	0.3
Na	0	0	0	0	0.2	0.4
Cl	0	0	0	0	0.2	2.5
P	0	0.63	0	0.09	0.1	0.5
Ni	0	0	0	0	0.1	0.1
Fe	0	0	0	0	0.1	0.3
S	0	0	0	0	0	0
N	0	0	0	0	0	2.5

3.7.2 Fourier Transform Infrared Spectroscopy

FTIR studies were carried out to explore the functional groups that are present in both the clean membrane and used (at different experimental conditions) membrane. The FTIR spectra is illustrated in **Figure 3.11**.

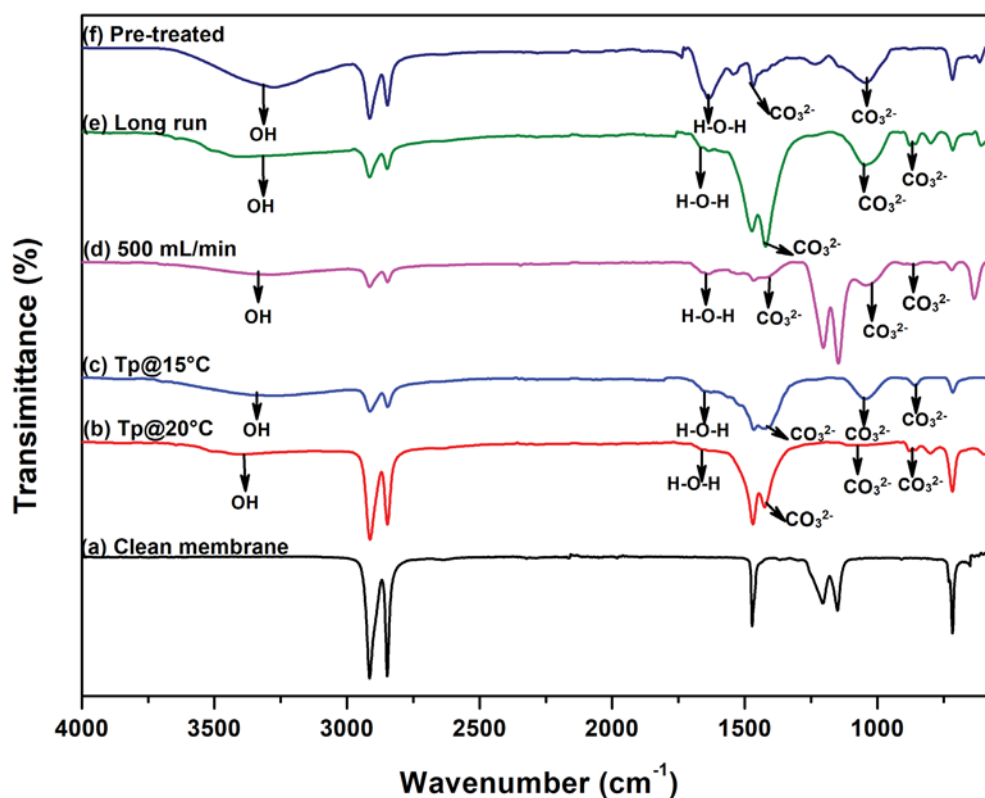


Figure 3.11: FTIR spectrum: (a) Clean membrane, (b) TP@20°C and (c) TP@15°C, (d) 500 mL/min, (e) Long run, and (f) Pre-treated.

Specifically, **Figure 3.11a** illustrates the FTIR spectrum of the clean PTFE membrane, which showed distinct peaks at 1223 cm^{-1} and 1154 cm^{-1} , indicating the stretching vibration of the CF_2 group. The peak at 1471 cm^{-1} is associated with the C-F bending in PTFE.

Figure 3.11b displays the FTIR spectrum for the membrane used at a permeate temperature of $20 \pm 1.5^\circ\text{C}$. The peak at 3494 cm^{-1} corresponds to the stretching vibrations of structural water molecules (O-H) present in the FS. An additional band is observed in the range of 1618 cm^{-1} , representing the bending vibrations of the water molecule itself (H-O-H bending). For the carbonate group, the peak at around 1430 cm^{-1} represents the symmetric stretching vibrations of carbonate (CO_3^{2-}). The bands at 1053 cm^{-1} and 879 cm^{-1} are assigned to the asymmetric stretching and out of plane bending of CO_3^{2-} , respectively (Manni et al., 2022, Xiang et al., 2019).

The FTIR spectrum for the membrane used at a permeate temperature of 15°C (Tp@15°C) is shown in **Figure 3.11(c)**. The peaks at 3394 cm^{-1} and 1620 correspond to water stretching and bending vibrational modes. Similar to the run at $20 \pm 1.5^\circ\text{C}$, the run at $15 \pm 1.5^\circ\text{C}$ exhibits prominent peaks at 1429 cm^{-1} , 1053 cm^{-1} and 864 cm^{-1} which are attributed to the symmetric stretching, asymmetric stretching, and out of plane bending of CO_3^{2-} , respectively.

The FTIR spectrum obtained from the membrane at a flow rate of 500 mL/min exhibited weak bands typical of CO_3^{2-} (**Figure 3.11d**). This observation can be explained by a variety of factors. The primary reason is, most likely, the dilution effect caused by a higher flow rate, which may significantly decrease the amount of chemical species present (Guillen-Burrieza et al., 2016). Inconsistent sample concentration can also have a significant impact on peak intensity. As a result, the concentration may have decreased below the FTIR instrument's detection limit, resulting in missing prominent peaks.

Figure 3.11e illustrates that extended operation resulted in considerable scale formation, as evidenced by prominent FTIR peaks. Conversely, when the FS was pre-treated with acid, the FTIR spectrum revealed negligible scale presence on the membrane surface, despite the extended use duration (**Figure 3.11f**). The FTIR results for both runs revealed prominent peaks at 1430 cm^{-1} , 1052 cm^{-1} and 879 cm^{-1} associated with carbonates. SEM analysis, in conjunction with EDS, successfully determined the types of scales and the components found in FS. Powder, which is typically characteristic of MgCO_3 , was found to have been formed on the surface of the membrane in addition to other elements that were also in trace amounts. EDS further revealed distinct elements in most runs, which could be attributable to spatial variation in salt concentration across the FS, altering the salt distribution across the membrane surface. If the salt concentration varies throughout the solution, various parts of the membrane may be subjected to different salt concentrations during the distillation process. This can cause differences in the type and quantity of salts deposited on different sections of the membrane. Finally, in all runs, FTIR results further confirmed the presence of CO_3^{2-} .

CHAPTER 4: FIRST ORDER COST BENEFIT ANALYSIS FOR INTEGRATED PROCESS

4.1 First order cost benefit analysis

This section seeks to evaluate the monetary value of the benefits that directly derived from the project against the investment for implementing the project. Specifically, the valuable products of the project were restricted to the produced struvite and the reclaimed clean water, against the capital expenditure (CapEx) and operating expenses (OpEx) of a proposed integrated resource recovery plant.

The struvite recovery is dependent on the pH of the feed, since high pH values promote the precipitation of magnesium and calcium phosphate, thus lowering the quality and purity of the struvite. The concentration of Mg^{2+} , NH_4^+ and PO_4^{3-} ions is pH-dependent, which in turn dictates the struvite solubility and this decreases as the pH increases, reaching a minimum solubility at pH values between 9.0 and 10.7 (Simms, 2023). Recent advances in membrane distillation have focused on enhancing membrane materials and configurations to improve performance and reduce fouling. Innovations such as the development of hydrophobic nanocomposite membranes and the integration of membrane distillation with other processes have shown promising results in increasing flux and reducing energy requirements (Efome et al., 2016). These advancements have brought MD closer to commercial viability, with several pilot-scale studies demonstrating its potential for large-scale applications (Hausmann, 2013).

Commercial membranes for MD are typically made from materials like polytetrafluoroethylene (PTFE), polypropylene (PP), and polyvinylidene fluoride (PVDF), each offering different properties in terms of hydrophobicity, thermal stability, and mechanical strength (Alkhudhiri et al., 2012). The choice of membrane material and configuration is crucial for optimizing the performance and longevity of the membranes (Camacho et al., 2013). Furthermore, one major challenge experienced with struvite precipitation is that the crystallisation of struvite is affected by competing positive ions, particularly as calcium ions. Specifically, the calcium ions compete with magnesium ions to form calcium phosphate precipitates, which result in a decrease in both struvite mass and purity. Such an interference depends on the alkalinity and/or molar ratios of the N:P and Ca:Mg (Capdevielle et al., 2013). To prove the viability and sustainability of proposed membrane distillation process for clean water production, a comprehensive technological and economic analysis is essential. This includes evaluating the flux achieved, the cost of water produced, and the overall energy efficiency of the process. Such analyses help in identifying the most cost-effective and energy-efficient configurations, ensuring that MD can be a sustainable solution, particularly when water scarcity issues are concerned (Shokri and Sanavi Fard, 2023). Here, a

preliminary cost analysis of the proposed integrated resource recovery plant, consisting of a batch mode Nutrient Recovery Unit (NRU) and laboratory scale DCMD unit, was carried out to investigate the viability of struvite recovery, clean water reclamation, and possible industrial salts. While this process has been proved viable technically, as laid out in the previous chapters, its economic assessment has not been conducted and this is discussed below.

4.2 Capital cost

Once-off capital injection at the beginning of the project will be required for expansion or retrofitting the current process with proposed new processes. These estimates are used by consulting firms and contractors to calculate the once-off CapEx that is required for the design, construction and commissioning of the new process. Upon completion, the plant can then be handed over to the end-user for operations. There are various classifications for CapEx estimation, with varying degree of accuracy and levels of information for each one. The classification for cost estimation is order-of-magnitude, study, preliminary, definitive, and detailed estimate. The choice on the technique to use will be dictated by the level of information available. In cases where information is limited, order of magnitude or study estimate can be used. Order of magnitude relies on cost information of a complete process, and it is then adjusted using scaling factor, whereas study estimates rely on costing of major equipment (i.e. pumps, compressors, turbines, vessels, columns, vessels and heat exchangers) identified in the process flow diagram (Turton, 2009). The costs information can also be obtained from historical records of similar processes, and the costs is adjusted using the scaling factor to account for inflation and differences in capacities. Rapid capital costs estimation allows for costs estimation using historical data. **Equation 4.1** can be used to account for inflation and different in capacities (Sinnott, 2005):

$$C = C_1 \left(\frac{S}{S_1} \right)^{0.6} \quad (4.1)$$

Where C is the cost for equipment

C_1 is the cost for equipment in the reference data

S is the capacity of the plant

S_1 is the capacity of the plant for the reference data

Total equipment purchasing costs (EPC) can be obtained by summation of all the costs of individual major processing units (Sinnott, 2005). However, the EPC is not inclusive of the following:

- Equipment erection
- Piping
- Instrumentation

- Electrical
- Buildings
- Storages
- Site development
- Ancillary buildings
- Design and engineering
- Contractor's fee
- Contingency
-

To account for the above costs, fixed capital costs is calculated using **Equation 4.2**:

$$FCC = 4.41 \cdot EPC \quad (4.2)$$

Vessels

Conceptual design of tanks and reactors can be based hydraulic retention time (HRT) of similar reactors. If the flow rate (Q) is known, **Equation 4.3** can be used to determine the working volume of that vessel. A safety factor of 10% is considered as headspace of the vessel.

$$V = 1.1 \cdot Q \cdot HRT \quad (4.3)$$

Pumps

The pumps can be designed based on the flowrates requirements of fluids to be pumped. The hydraulic pressure (P_{hyd}) can be computed using **Equation 4.4**. The computed pressure (P_M) can be used for sizing of the motor by computing power requirements of the motor using **Equation 4.5**.

$$P_{hyd}(kW) = \frac{Q\rho gh}{3.6 \times 10^6} \quad (4.4)$$

$$P_M(kW) = \frac{P_{hyd}}{\epsilon_P \cdot \epsilon_M} \quad (4.5)$$

Where Q is the volumetric flowrate of the fluid (m^3/hr)

ρ is the density of the fluid (kg/hr)

g is the gravitational acceleration (m/s^2)

h is the head of the fluid (m)

4.3 Operation and Maintenance Costs

Upon completion of construction, commissioning, and handing over the plant, production of struvite and clean water commences. There are additional costs associated with this process, and these include:

- Electricity for powering electrical equipment in the plant

- Purchase and delivery of ACM
- Purchase of conditioning chemicals, including hydrochloric acid (HCl)
- Replacement of fouled membrane
- Personnel salaries

Furthermore, there were costs associated with maintenance and servicing some of the equipment within the plant.

The full-scale design of the plant is illustrated in **Figure 4.1**.

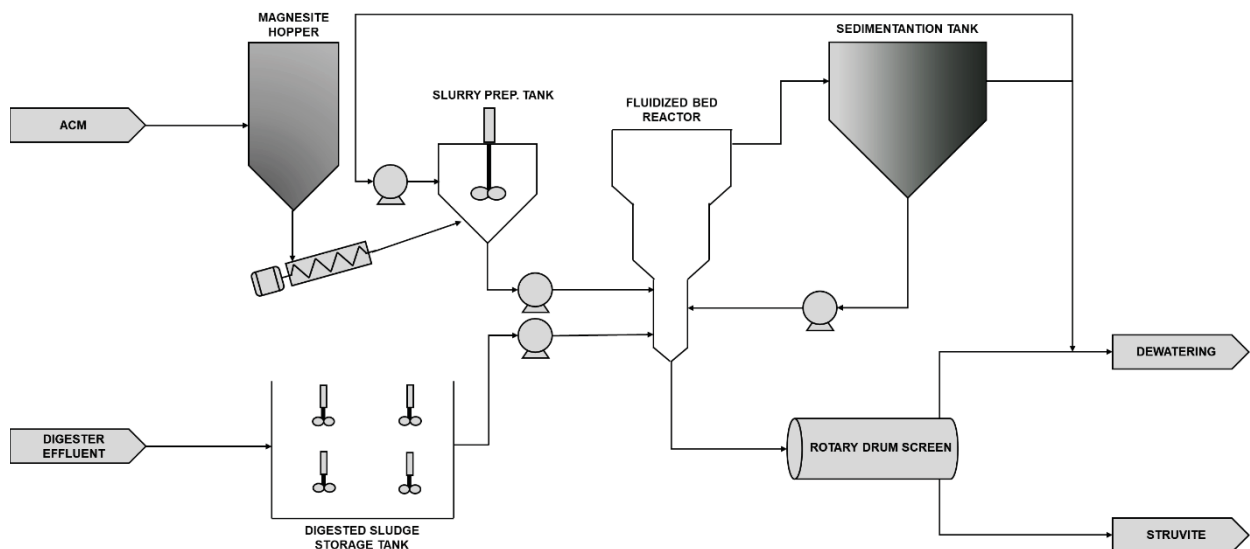


Figure 4.1: Full-scale process flow diagram for struvite recovery from effluent derived from anaerobically digested sewage sludge.

4.4 Projected sales and benefits

4.4.1 Revenue from struvite as a fertiliser

The ability to sell struvite recovery as a slow-release fertiliser is one of its key financial benefits. Phosphorus and nitrogen, two elements necessary for plant growth, are found in struvite. The fertiliser market is well-established in other countries, with phosphorus being a particularly valuable component due to its scarce natural deposits. Struvite provides a sustainable substitute for conventional phosphate fertilisers derived from phosphate ore deposits. Despite the price fluctuations of phosphate fertilisers due to global supply chains, the sale of struvite can provide a supplementary revenue stream for wastewater treatment plants.

4.4.2 Revenue of clean water

South Africa is faced with constrained water resources to fulfil growing demand. The address the forecasted shortages in water supply, the National Water and Sanitation Master Plan (Vol. 3) of 2019 calls on the need for diversification of the water resources. Ultimately, the upgrading of the wastewater treatment works effluent to clean water will achieve dual benefits of avoiding environmental and aquatic degradation and creating a water resource for important economic sectors of the country.

4.4.3 Reduced operational costs

The possibility of reducing operating cost associated with the removal of nitrogen in WWTPs. Struvite removes phosphorus along with nitrogen, this reduces nitrogen load on bioreactors. WWTPs incurs costs for electricity consumption associated with nitrification-denitrification. Thus, the potential savings associated with reduction in electricity consumption.

4.5 Environmental and regulatory benefits

In addition to direct financial advantages, there are various indirect advantages associated to compliance with environmental discharge requirements. Due to concerns about eutrophication in water bodies, numerous nations and areas have imposed strict restrictions on the release of nitrogen and phosphorus. The potential for severe fines or penalties for exceeding these discharge limitations is another incentive for WWTPs to implement nutrient recovery technologies. Plants that recover essential nutrients can potential savings by penalties imposed by regulations.

4.6 Evaluation of benefits and costs

Costs and benefits for each identified part were evaluated by converting them into financial impacts, although this can be very difficult for some categories of impact like environment, health or employment.

4.7 Discounting method

All the evaluated costs and benefits were added by using discounting techniques, to get a single score for the project (the net present value). In this study, discounting part should have a limited effect, as all the impacts should mainly be the same from one year to another. The only impact for which it is not the case (the building of the plant) has been discounted and transformed into an annual cost. The net present value (NPV) is calculated using **Equation 4.6**.

$$NPV = \sum_{t=0}^T \frac{TB}{(1+r)^t} - \sum_{t=0}^T \frac{TC}{(1+r)^t} \quad (4.6)$$

4.8 Benefit-Cost Ratio

Benefit-cost ratio (BCR) compares discounted total benefits realised during the lifespan of the project to the total costs invested into the project. BCR with a negative value indicate project which total investment costs outweighs total benefits that was realised from the project, whereas BCR with a positive value indicates an economically feasible project. The benefit-cost ratio is calculated using **Equation 4.7**.

$$BCR = \frac{\sum_{t=0}^T \frac{TB}{(1+r)^t}}{\sum_{t=0}^T \frac{TC}{(1+r)^t}} \quad (4.7)$$

4.9 Costs estimation

4.9.1 Capital costs

4.9.1.1 Pilot Plant Conceptual Design

A conceptual design for major units of the integrated resource recovery process was prepared. This allows for rough order of magnitude (ROM) cost estimation. The design specifications are shown in **Table 4.1** and **4.2**.

Table 4.1: Basic design for full-scale struvite recovery plant.

Reactor			
Retention Time	1	hours	<ul style="list-style-type: none"> Experimental data has shown that reaction time of 1 hour is optimal. Safety factor of 10% has been incorporated into the total volume design.
Reactor Working Volume	5.83	m ³	
Reactor Total Volume	6.5	m ³	
Slurry Prep. Tank			
Dilution Factor	1	%	<ul style="list-style-type: none"> ACM will added as slurry and prevent dilution of phosphate from the sludge, the dilution is kept at less than 1%. The solid content of ACM in the slurry is below 60%, which is the maximum solid content for slurry to be pumpable. The tank is allowed to keep slurry sufficient to be fed to the reactor for 1.5 day.
Volume	2.03	m ³	
Hopper			

Volume	15	m ³	<ul style="list-style-type: none"> Dry-bulk trucks have various loading capacities; however, the minimum size is 15 m³. Thus, sufficient storage capacity must be ensured while minimising the capital cost of the unit, the dry magnesite hopper must accommodate at least 1 load of dry-bulk truck.
Digested Sludge Storage Tank			
Retention Time	1	days	<ul style="list-style-type: none"> Digested storage tank is to ensure constant flowrate from of the digester effluent is pumped to the struvite recovery system, this is because digester is de-sludged at a particular time in a day. Sufficient capacity for containing sludge for 1 day.
Volume	140	m ³	
Sedimentation Tank			
Hydraulic Retention Time	6	hours	<ul style="list-style-type: none"> Minimum hydraulic retention time for sedimentation tanks is 3 hours, in this study, the retention time will be increased 2-folds to improve solid removal.
Volume	35	m ³	

Table 4.2: Design specifications for the proposed 140kL/d direct contact membrane distillation plant.

Feed/Product Water Tanks			
Retention Time	5	hours	<ul style="list-style-type: none"> Sizing is based on a membrane flux of 15LMH as per experiments conducted by the CSIR researchers.
Tank Working Volume	6	m ³	
Feed Tank Volume	6.5	m ³	
No. of tanks	5	–	
Total Feed Tank Volume	30	m ³	<ul style="list-style-type: none"> Safety factor of 10% has been incorporated into the total volume design. Allowance is made for 6-hr feed per pump, as per effluent flow from the NRU
Sand Filtration and Activated Carbon Filtration Basins			
Filtration Rate	200	m ³ / m ² /day	

Total Filtration Area	0.14	m ²	<ul style="list-style-type: none"> The filtration rate is based on a rapid sand filter with a bed depth of between 0.6 and 1.9. Backwashing will be considered without using air. Environmental discharge for backwashing is based on backwash rate of 6 m³/ m²/hr, for sand filters and given the quality of feed solution (FS).
Filter Area	0.07	m ²	
Daily Backwash Volume	1.6	m ³	
	2.3	%	
No. of filtration basins	5	–	
HCl Antiscalant Dosing Unit			
Quantity of HCl required	1.95	L/hr	<ul style="list-style-type: none"> The HCl dosing rate is based on experiments conducted by the CSIR researchers, for optimised conditions.
Unit Pump Size Available	2.5	L/hr	
Total HCl required	9.75	L/hr	
Peristaltic Pumps			
Unit Pump Size	19.5	LPM	<ul style="list-style-type: none"> The pump sizes are selected based on the volume of the supernatant received from the NRU.
No. of Pumps	5	–	
Total Plant Capacity	97.5	LPM	
	140	m ³ /day	
DCMD Cell			
DCMD Cell Dimensions	0.95 x 0.95	m x m	<ul style="list-style-type: none"> The size of each DCMD is set to allow for improved hydraulics on the membrane surface whilst maximised to limit total installed units. Each of the five (5) pumps, at 19.5LPM, will have 69 DCMD installed in series for single pass. The maximum recovery is set to limit scaling on the membrane surface.
Number of DCMD Cells	69 * 5	–	
Number of Stages	1	–	
Number of Passes	1	–	
Expected Recovery	80	%	

4.9.1.2 Costings

Using the specifications of major units in the conceptual design, rapid cost method was used for determination of the equipment purchasing costs. The factor was then included to calculate the total fixed costs of establishing an integrated resource recovery process from municipal wastewater digestate. Some of the unit costs for equipment were provided in foreign currencies, thus, the average exchange rates (US\$ 1 = ZAR 18.45 and €1= ZAR 19.96) for 2023 were used (Nedbank, 2024). The costs for NRU and DCMD units are shown in **Table 4.3** and **Table 4.4**, respectively. The CapEx for the DCMD unit is R8 663 875. Accounting for indirect costs for engineering & supervision cost, construction costs, contractor’s fee at a flat rate of 10% (i.e., R866 388) brings the total CapEx to R 9 530 263.

Table 4.3: CapEx for major equipment for the 140 kL/d Nutrient Recovery Unit.

	Processing Unit	Costs Estimates (ZAR)	Unit Costs	References
Nutrient Recovery Unit (NRU)	Reactor	R475 941	US \$10 700/kg P	(Vinardell et al., 2023)
	Slurry Prep. Tank	R12 098	US \$235 /m ³	(Vinardell et al., 2023)
	ACM Hopper	R22 297	€220 /m ³	(Yetilmezsoy et al., 2017)
	Digested Sludge Storage Tank	R84 089	US\$ 235/m ³	(Vinardell et al., 2023)
	Sedimentation Tank	R153 692	€220/m ³	(Yetilmezsoy et al., 2017)
	Magnesite screw pump	R14 077	-	(Alibaba, 2024)
	Slurry dosing pump	R7 027	-	(AquaAeroVitae, n.d.)
	Sludge Pump	R38 800		(AfriPumps, 2024)
	Industrial Mixers (motors for scrappers and mixers)	R13 981	<ul style="list-style-type: none"> • 2x3 kW for homogenisation of the feed • 1x motor for the sedimentation tank 	(M Bond Pumps, 2024; RS Components, n.d.)
	Rotary Drum Screen	R156 473	-	(JX Filtration, 2024)

	Packaging Equipment	R65 843	-	(Yetilmezsoy et al., 2017)
	Drier	R217 076	€65625 /10 ton	(Yetilmezsoy et al., 2017)
	EPC	R1 261 394		
	Total 140kL/d NRU FCC	R5 562 748		

Table 4.4: CapEx for major equipment for the 140 kL/d Direct Contact Membrane Distillation.

	Processing Unit	Costs Estimates (ZAR)	Unit Costs	References
Membrane Distillation	Peristaltic Pumps	R1 387 500	R165 000 for 14LPM (2022)	Merck Millipore
	Membrane Cells	R3 975 500	Discounted at R11 500/unit	Marinus Manten (Pty) Ltd
	Chiller (-20°C to 100°C)	R593 750	R95 000/unit (2022)	United Scientific (Pty) Ltd
	Hot Bath (0°C to 100°C)	R425 000	R68 000/unit (2022)	United Scientific (Pty) Ltd
	Mechanical & Piping	R787 687		
	Instrumentation & Control	R1 495 000	Includes conductivity & pH meters, datacells, and flow sensors	Burkett Systems
	Sub-Total DCMD CapEx	R8 663 875		

Table 4.5: CapEx for the integrated 140kL/d integrated resource recovery plant.

Plant Unit	Costs Estimates (ZAR)
Nutrient Recovery Unit	R5 562 748
Direct Contact Membrane Distillation (DCMD)	R9 530 263
Working Capital (3 months)	R390 778

Total Capital Costs (ZAR)	R 15 483 787
----------------------------------	---------------------

4.9.2 Operational costs

The operational (OpEx) costs for running the integrated process were estimated using historical data from literature and specifications from the conceptual design. The OpEx for the plant is shown in **Table 4.6**. Maintenance, which defines the activity to maintain any condition of the facility and/or equipment and make repairs to maximise the process performance, is assumed at 2.5% of the inside battery limits (ISBL) capital investment due to low level of moving parts in the process.

Table 4.6: Annual operational costs for the integrated treatment process.

	Cost Item	Cost Estimates	Unit Costs	Comments	References
Nutrient Recovery Unit (NRU)	Labour	R110 718	€462.25 /month	-	(Yetilmezsoy et al., 2017)
	ACM	R357 333	R4000 per ton	89.3 tons of ACM required annually	Syferfontein Carbonates Pty Ltd
	Transportation	R20 892	R10 446	2 trips annually	Syferfontein Carbonates Pty Ltd
	Electricity Consumption	R168 923	R2.95/kWh		Eskom Tariff
Membrane Distillation	Labour	R468 000		2 plant operators	Municipal Ranking
	Electricity consumption (heater, chiller and pump)	R518 881	R2.95/kWh		Eskom Tariff
	Membranes	R58 800	R700 per membrane		Merck Millipore
	Hydrochloric Acid	R93 560			

	Sub-total OPEX Costs	R1 563 112			
	Maintenance costs	R355 683		2.5% ISBL CapEx	(Towler and Sinnott, 2021)
	Total O&M Costs	R1 918 795			

4.10 Cost benefit analysis

In this section, the economic analysis including profitability analysis (IRR, NPV, PP) and sensitivity analysis are discussed. Some of the assumptions used in this economic analysis are summarised:

- Plant construction is 1 year (Total project)
- Plant lifetime is 20 years, started from Year 1
- Plant working time is 24 hours in a day and 330 days in a year
- Plant production capacity is 140kL/d (46 200 kL/year) of clean water, and 5.1 tonnes of struvite per year.
- Prime interest rate is 9.5% at Year 0, with the loan interest rate discounted at prime -0.5%.
- Product inflation is kept constant at 11% annually
- The DCMD plant is modular and has negligible site development costs.

The total CapEx for the investment is R15 483 787 which is a 100% capital loan and includes 3 months working capital and other fees such as indirect costs for engineering & supervision cost, construction costs, contractor's fee.

4.10.1 Product price and revenue

The production capacity of integrated resource recovery plant is 46 200 kL/year of clean water, and 5.1 tonnes of struvite / year. Over the simulation duration, the capacity of the plant remains fixed whilst the sales price is projected to increase at an inflation rate of 11%. The price of clean water is not regulated in South Africa but rather based on contract negotiations with the end-user, whilst the market for agricultural struvite is not yet mature. Price of struvite varies in different research papers, the price can range from US \$ 200 – 1855/ton of struvite (Yetilmmezsoy et al., 2017, Vinardell et al., 2023, Gaterell et al., 2000). A conservative price of R 18.45/kg (US \$ 1000/ton) was assumed for struvite at Year 0 in this work.

Three valuable resources were identified in the CBA, and expected returns from the sale of these resources were calculated. Furthermore, financial savings due to reduction of nitrogen load from the integrated processes was also identified and costed. The identified benefits from the project and their expected returns are shown in **Table 4.7**.

Table 4.7: Annual revenue from the sale of valuable products.

	Unit Selling Price/Potential Savings (ZAR)	Annual Production Quantities	Revenue (ZAR)
Struvite	R 18 450 per tonne of struvite	40.77 tons struvite	R 752 268.78
Clean water	R 18.50 per kL of water	51 072 kL water	R 987 500.00
Electricity savings for removal of nitrogen	R13 870 per tonnes of N	16,17 tonnes N	R 67 256.34
Saleable salt	R 4 059 per tonne of salt	11.08 tonnes salt	R 44 984.37
Total (ZAR)			R 1 809 341

4.10.2 Projected cash flow

Cash flow consists of income and outcome flow. Income flow consists of revenue, before tax income, after tax income, and salvage value. Outcome flow consists of capital cost, operational cost, loan payment, and interest payment.

4.10.2.1 Depreciation

The depreciation cash-flow and salvage value, on an annual basis, is calculated and shown in **Table 4.8**. Depreciation value affect fixed cost and salvage value.

Table 4.8: Depreciation and Salvage value for the integrated resource recovery plant.

Year	Depreciation (ZAR)	Salvage (ZAR)
1	1 422 662	12 803 959
2	1 280 396	11 523 563
3	1 152 356	10 371 207
4	1 037 121	9 334 086
5	933 409	8 400 678
6	840 068	7 560 610
7	756 061	6 804 549

Year	Depreciation (ZAR)	Salvage (ZAR)
8	680 455	6 124 094
9	612 409	5 511 685
10	551 168	4 960 516
11	496 052	4 464 464
12	446 446	4 018 018
13	401 802	3 616 216
14	361 622	3 254 595
15	325 459	2 929 135
16	292 914	2 636 222
17	263 622	2 372 599
18	237 260	2 135 340
19	213 534	1 921 806
20	192 181	1 729 625

4.10.2.2 Before tax and after-tax cash flow

Based on revenue and expenses calculations, the resultant cash flow of the proposed plant can be seen on the **Figure 4.2**. In the cash flow calculation, it is assumed that all products (clean water, and struvite) have a market. The after-tax cash flow (ATCF) is the cash flow calculation including tax, so the value will be lower than before tax cash flow (BTCF). The income tax value is 25% based in average tax for business enterprise. Based on cash flow, the IRR 8.4%, when the product pricing is R18.5/kL for clean water and R18.45/kg for struvite.

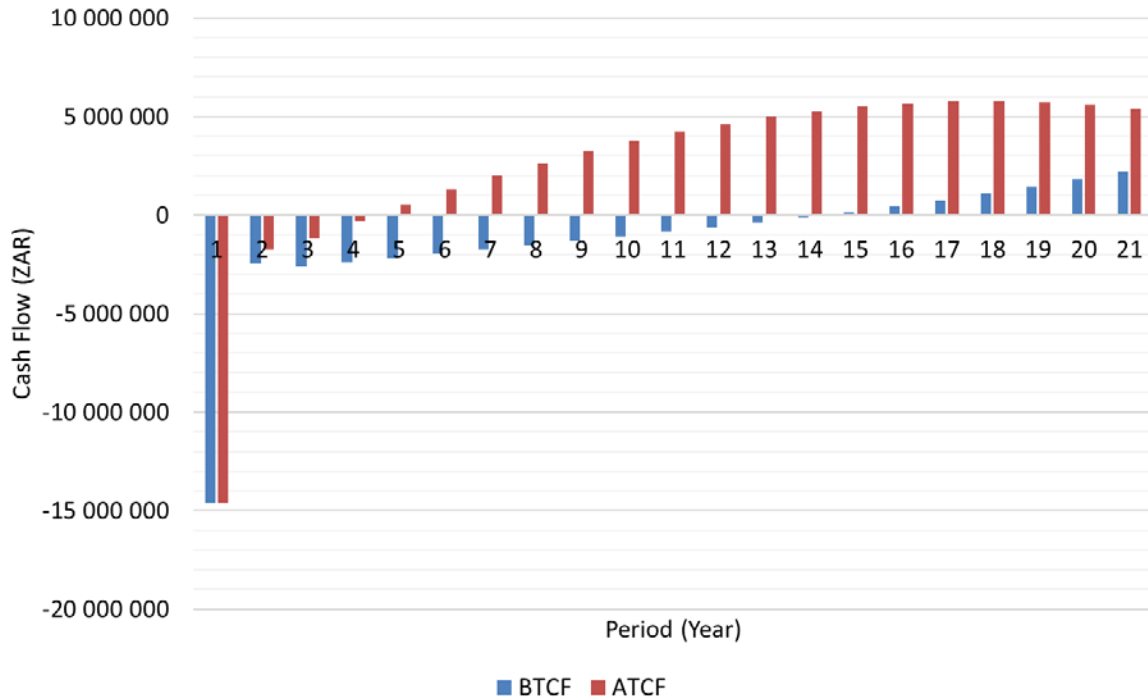


Figure 4.2: Cash Flow as BTCF and ATCF for the integrated resource recovery plant.

4.10.3 Net present value

The Net Present Value (NPV) of the project was calculated over a period of 20 years, based on typical lifespan for some of some of major equipment in chemical processing plants. The NPV over 10 years period is shown in **Figure 4.3**. As present worth means the sum of money at the present time which is the equivalence of cash flow for the certain period of time with a specified minimum acceptable rate of return (MARR), so that if the value of NPV is positive, it means that the plant is feasible to establish. In this instance, the NPV of the project for the base case scenario is decreasing for the first 13 years reaching a minimum of -R 27 822 929, after which it is projected to increase but remaining on a negative.

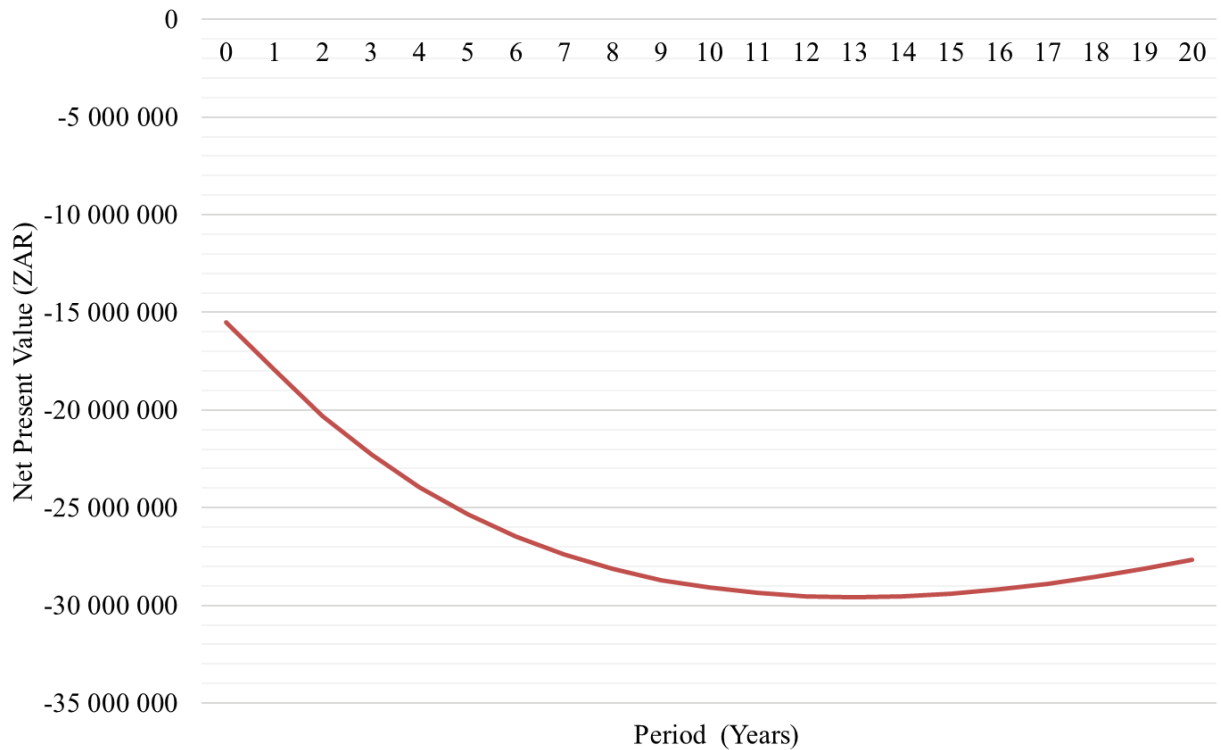


Figure 4.3: Net Present Value for the project over a period of 20 years.

The project is expected to produce struvite and clean water, which are the two key resources of which the returns will be released from. As shown in **Figure 4.3**, struvite and clean water were estimated to generate revenue of R18.45/kg and R 18.50/kL, respectively. This is against estimated production costs of R16.13/kg and 17.72/kL. Thus, the net revenue is R2.02/kg and 78 cents/kL. The production costs determined in this work is comparable to that obtained by other researchers. Sikosana et al. (2017) found the production for high- and low-quality struvite to be R22.10/kg and R 9.01/kg, whereas Seymour (2009) ranged between R12.34 – R19.0 (US \$ 2.40 – US \$ 3.70/pound of P). However, these values will need to be adjusted for inflation. The electrical savings will be made due to the reduction of nitrogen load on bioreactors, and production of saleable salt from DCMD unit. An electrical savings of R13.87/kg N was projected to be made and further revue generation of R3.85/kg sellable salt. The total annual revenue and savings is R1.809 million. The total operating costs is R2.316 million. The project will be anticipated to further cover maintenance costs of the units and repayment of the loan for financing the investment. The base case scenario has considered the project to be financed through a loan. It is not expected that municipalities can have capital reserves for retrofitting infrastructure with innovative technologies. However, the scenario will be considered in the sensitivity analysis. The project

does not break even during the period, indicating the inability of the project to generate returns to payback the initial investment made into the project.

4.10.4 Benefit-cost ratio

The project is estimated to incur total costs of R137,9 million over the 20 years period and generate R25,6 million in returns over the same period. The BCR during the period is 0.19, indicating that that project is not economically feasible. This BCR is agreement in with NPV, which is also less than 0. The BCR of the project for 20 years is shown in **Table 4.9**.

Table 4.9: BCR of the project over 20 years period.

Total Present Value Costs (ZAR)	R 137 855 986.00
Total Present Value Benefits (ZAR)	R 25 616 892.00
BCR	0.19

A close analysis of the Internal Rate of Return (IRR), it is about -9.3% whilst the NPV is always negative for the first 20 years of the project. The investment may not be attractive without consideration of other arbitrary economic metrics such as social and environmental benefits. Further, having a secondary energy source for heating and cooling for the DCMD unit, and the reduction of transport and reagent requirement has potential to reduce operating costs. In another study, the authors researching viability of DCMD as a desalination technology concluded that its current economic viability is limited by high costs, particularly related to cooling (Jawed et al., 2024). In a study by Zarebska-Mølgaard et al. (2022), using FO-MD hybrid system shows potential for water recovery from anaerobically digested (AD) effluents, its current performance in terms of water flux is inadequate for industrial applications. The capital expenditure for the DCMD unit is higher due to limitations in scaling for the DCMD cells which eventually affect negatively the hydraulics and membrane flux. Future improvements in membrane performance and cost reduction are necessary to make the process economically viable.

CHAPTER 5: CONCLUSION AND RECOMMENDATIONS

This chapter will focus on the concluding remarks in light of the terminal objectives of this study, along with the recommendations that precisely suggest upscaling strategies for struvite recovery and water reclamation from the effluent under study and the pilot testing of the developed process in a relevant environment.

5.1 Conclusions

This study aimed to investigate the feasibility of using activated cryptocrystalline magnesite (ACM) and membrane distillation (MD) for the recovery of struvite and the reclamation of water from effluent derived from waste activated sludge (WAS) from municipal wastewater. The focus on struvite recovery and water reclamation was necessitated by their potential applications in agriculture and the industry. As part of the study, a first-order Cost-Benefit Analysis (CBA) was conducted to assess the financial viability of the investigated process.

A bespoke (custom-designed) reactor system was able to effectively removed phosphate and ammonia from WAS effluent, with optimal conditions for struvite recovery being identified as 60 minutes of a contact/reaction time, 2 g/L ACM dosage, and a pH of 9. Complete phosphate removal occurred within 40 minutes, with approximately 71% ammonia removal after 210 minutes. The purity of the recovered struvite was identified through comprehensive characterization. The findings provide insight into resource recovery potential from municipal wastewater, supporting a sustainable approach to wastewater management by facilitating nutrient recovery. The nutrients recovery unit (NRU) effluent, i.e., the supernatant/filtrate after struvite recovery, was initially unsuitable for direct agricultural or industrial use due to elevated levels of magnesium and residual ammonia. For this reason, this was treated using membrane distillation (MD). Composite samples were fed into a direct contact membrane distillation (DCMD) process, employing PTFE and PVDF hydrophobic membranes. To test membrane durability, samples were treated with sand filtration, biologically activated carbon (BAC), and acidification with hydrochloric acid (HCl). Different experimental conditions were varied, including flow rate and permeate temperature, as follows:

- Set flow conditions (400 mL/min or 500 mL/min) at fixed permeate temperatures.
- Set permeate temperatures (15 ± 1.5 °C or 20 ± 1.5 °C) at fixed flow rates.

Analysis through SEM-EDS and FTIR revealed superior durability and average mass flux for PTFE membranes ($1.2 \text{ g/cm}^2\cdot\text{h}$) compared to PVDF membranes ($0.5 \text{ g/cm}^2\cdot\text{h}$). Pretreatment of

the feed solution (acidifying the solution) further increased flux to 1.4 g/cm²·h, a 16.7% improvement. While scaling and pore wetting on the PTFE membrane surface remained a concern, the quality of the permeate met different prescribed wastewater discharge standards, making it suitable for agricultural use after re-mineralization. Industrial applicability will require case-by-case assessment, potentially involving additional polishing for residual ammonia and carbonate removal.

Results further indicated that temperature had a greater impact on mass flux than flow rate, with a 20 ± 1.5°C permeate temperature yielding an average flux of 1.22 g/cm²·h, compared to 1.02 g/cm²·h at 15 ± 1.5°C. We note the retrograde dissolution of the main ions of concern for scaling, i.e., calcium and magnesium, which translates to their precipitation out of the solution with higher temperatures. Furthermore, higher flow rates (500 mL/min) decreased mass flux by 15% compared to 400 mL/min. PTFE membranes consistently performed better than PVDF, aligning with Cheng et al. (2010), who demonstrated PTFE's superior longevity and lower scaling propensity. Pretreated (sand filtration and biological activated carbon (BAC)) feed solutions yielded a mass flux of 1.4 g/cm²·h under baseline conditions, an improvement from 1.22 g/cm²·h with untreated feed. SEM-EDS analyses confirmed that the scaling on membranes comprised non-volatile and inorganic components, with deposition irregularities attributed to bench-scale design issues. Overall, over 95% of permeate solution (PS) was recovered with a mass flux loss below 21%. As mentioned above, PS quality met environmental discharge standards and was suitable for direct agricultural application, though industrial usage may require further treatment.

The integrated system's total fixed capital cost was at R15,093,009, requiring a total capital injection of R15,483,787 (including three months of working capital). The system's annual production capacity is projected at 46,200 kL of clean water and 5.1 tonnes of struvite. Over the simulation period, production capacity remains stable, while the sales price increases at an assumed inflation rate of 11%. Initial sales prices were hedged at R18.5/kL for water and R18.45/kg for struvite. The system's revenue is projected at R1,809,341 against operational expenses of R2,316,982, yielding a net margin of R507,641. However, the NPV and BCR of -R21.0 million and 0.19, respectively, indicate the project is currently economically unfeasible. Sensitivity analysis highlighted utility costs, product pricing, and equipment costs as critical factors impacting feasibility. Based on the proposed pricing, the 140 kL/day resource recovery system does not meet economic viability requirements, primarily due to high capital CapEx) and operational (OpEx) expenses.

Overall, this study emphasised the importance of advanced wastewater treatment technologies, which can potentially support South Africa's goals for water security, food security, and environmental resilience. By integrating resource recovery into municipal wastewater treatment, the project supports National Development Plan (NDP) 2030 and the Water and Sanitation Master Plan. At the same time, it improves service delivery and enterprise stimulation in support of economic development, addressing pollution reduction and sustainable infrastructure. Finally, the study further aligns with UN's Sustainable Development Goals (SDGs), particularly SDG 6 and 12, and the circular economy principles on waste reduction and continual resource use.

5.2 Recommendations

The following research gaps and potential avenues for further research and development were identified, along with upscaling strategies for struvite recovery and water reclamation and these include:

- Evaluating the impact of municipal wastewater treatment works performance, in terms of influent volumes and biological reactor efficiency, on the quality of digested WAS and the resulting quality of struvite recovered. This implies that the study of different WAS effluent qualities as well as of different effluents should be prioritise.
- Improving the design of the DCMD module to enhance distribution across the membrane surface and increase flux.
- Investigating the recovery of PTFE membrane flux by washing the membrane with various methods, such as acid or distilled water.
- Assessing the scalability of membrane distillation technology and its potential energy consumption.
- Further investigating pore wetting on the membrane as it relates to potential precursors based on mineral synthesis chemicals.
- Enhancing module design and exploring alternative cooling/heating methods to improve the economic feasibility of large-scale DCMD systems.
- Conducting research on improved membrane flux and related cost reductions.
- Exploring the market opportunity for selling clean water at a higher price point, above R25/kL, to reflect the true cost of water production relative to the current market rate.
- Investigating actual market prices for struvite, given its superior performance compared to conventional agricultural fertilizers.
- Optimizing the designs for the nutrient recovery unit reactor and the sedimentation tank to reduce capital expenditure.

REFERENCES

- AGORO, M., ADENIJI, A., ADEFISOYE, M. & OKOH, O. 2020. Heavy Metals in Wastewater and Sewage Sludge from Selected Municipal Treatment Plants in Eastern Cape Province, South Africa. *Water*, 12, 2746.
- AGUILAR-POZO, V. B., CHIMENOS, J. M., ELDUAYEN-ECHAVE, B., OLACIREGUI-ARIZMENDI, K., LÓPEZ, A., GÓMEZ, J., GUEMBE, M., GARCÍA, I., AYESA, E. & ASTALS, S. 2023. Struvite precipitation in wastewater treatment plants anaerobic digestion supernatants using a magnesium oxide by-product. *Science of The Total Environment*, 890, 164084.
- ALKHUDHIRI, A., DARWISH, N. & HILAL, N. 2012. Membrane distillation: A comprehensive review. *Desalination*, 287, 2-18.
- ALKLAIBI, A. M. & LIOR, N. 2005. Transport analysis of air-gap membrane distillation. *Journal of Membrane Science*, 255, 239-253.
- ANTONY, A., LOW, J., GRAY, S., CHILDRESS, A., LE-CLECH, P. & LESLIE, G. 2011. Scale formation and control in high pressure membrane water treatment systems: A review. *Fuel and Energy Abstracts*, 383, 1-16.
- APHA 2017. *Standard Methods for the Examination of Water and Wastewater*. Washington DC: American Public Health Association.
- AQUINO, M., SANTORO, S., DI PROFIO, G., LA RUSSA, M., LIMONTI, C., STRAFACE, S., D'ANDREA, G., CURCIO, E. & SICILIANO, A. 2023. Membrane distillation for separation and recovery of valuable compounds from anaerobic digestates. *Separation and Purification Technology*, 315, 123687.
- CAMACHO, L. M., DUMÉE, L., ZHANG, J., LI, J.-D., DUKE, M., GOMEZ, J. & GRAY, S. 2013. Advances in Membrane Distillation for Water Desalination and Purification Applications. *Water*, 5, 94-196.
- CAPDEVIELLE, A., SÝKOROVÁ, E., BISCANS, B., BÉLINE, F. & DAUMER, M.-L. 2013. Optimization of struvite precipitation in synthetic biologically treated swine wastewater—Determination of the optimal process parameters. *Journal of Hazardous Materials*, 244-245, 357-369.
- CHARFI, A., KIM, S., YOON, Y. & CHO, J. 2021. Optimal cleaning strategy to alleviate fouling in membrane distillation process to treat anaerobic digestate. *Chemosphere*, 279, 130524.

- CHEW, N., ZHAO, S., LOH, C. H., PERMOGOROV, N. & WANG, R. 2017. Surfactant effects on water recovery from produced water via direct-contact membrane distillation. *Journal of Membrane Science*, 528, 126-134.
- DESMIDT, E., GHYSELBRECHT, K., ZHANG, Y., PINOY, L., VAN DER BRUGGEN, B., VERSTRAETE, W., RABAEY, K. & MEESCHAERT, B. 2015. Global Phosphorus Scarcity and Full-Scale P-Recovery Techniques: A Review. *Critical Reviews in Environmental Science and Technology*, 45.
- EDOKPAYI, J., ODIYO, J. & DUROWOJU, O. 2017. Impact of Wastewater on Surface Water Quality in Developing Countries: A Case Study of South Africa.
- EHOME, J. E., RANA, D., MATSUURA, T. & LAN, C. Q. 2016. Enhanced performance of PVDF nanocomposite membrane by nanofiber coating: A membrane for sustainable desalination through MD. *Water Research*, 89, 39-49.
- FERRARI, F., PIJUAN, M., RODRIGUEZ-RODA, I. & BLANDIN, G. 2019. Exploring Submerged Forward Osmosis for Water Recovery and Pre-Concentration of Wastewater before Anaerobic Digestion: A Pilot Scale Study. *Membranes*, 9, 97.
- GAO, Y., LIANG, B., CHEN, H. & YIN, P. 2018. An experimental study on the recovery of potassium (K) and phosphorous (P) from synthetic urine by crystallization of magnesium potassium phosphate. *Chemical Engineering Journal*, 337, 19-29.
- GATERELL, M. R., GAY, R., WILSON, R., GOCHIN, R. J. & LESTER, J. N. 2000. An Economic and Environmental Evaluation of the Opportunities for Substituting Phosphorus Recovered from Wastewater Treatment Works in Existing UK Fertiliser Markets. *Environmental Technology*, 21, 1067-1084.
- GRYTA, M. 2008. Alkaline scaling in the membrane distillation process. *Desalination*, 228, 128-134.
- GUAN, Q., LI, Y., ZHONG, Y., LIU, W., ZHANG, J., YU, X., OU, R. & ZENG, G. 2023. A review of struvite crystallization for nutrient source recovery from wastewater. *Journal of Environmental Management*, 344, 118383.
- GUILLEN-BURRIEZA, E., MAVUKKANDY, M. O., BILAD, M. R. & ARAFAT, H. A. 2016. Understanding wetting phenomena in membrane distillation and how operational parameters can affect it. *Journal of Membrane Science*, 515, 163-174.
- HAUSMANN, A. 2013. *Membrane Distillation in Dairy Processing*
- HERALDY, E., RAHMAWATI, F., HERIYANTO & PUTRA, D. P. 2017. Preparation of struvite from desalination waste. *Journal of Environmental Chemical Engineering*, 5, 1666-1675.

- JAWED, A. S., NASSAR, L., HEGAB, H. M., VAN DER MERWE, R., AL MARZOOQI, F., BANAT, F. & HASAN, S. W. 2024. Recent developments in solar-powered membrane distillation for sustainable desalination. *Heliyon*, 10, e31656.
- KARVELAS, M., KATSOYIANNIS, A. & SAMARA, C. 2003. Occurrence and fate of heavy metals in the wastewater treatment process. *Chemosphere*, 53, 1201-1210.
- KAYVANI FARD, A., RHADFI, T., KHRAISHEH, M., ATIEH, M. A., KHRAISHEH, M. & HILAL, N. 2016. Reducing flux decline and fouling of direct contact membrane distillation by utilizing thermal brine from MSF desalination plant. *Desalination*, 379, 172-181.
- KIM, S., LEE, D. W. & CHO, J. 2016. Application of direct contact membrane distillation process to treat anaerobic digestate. *Journal of Membrane Science*, 20–28.
- KRISHNAMOORTHY, N., DEY, B., UNPAPROM, Y., RAMARAJ, R., MANIAM, G. P., GOVINDAN, N., JAYARAMAN, S., ARUNACHALAM, T. & PARAMASIVAN, B. 2021. Engineering principles and process designs for phosphorus recovery as struvite: A comprehensive review. *Journal of Environmental Chemical Engineering*, 9, 105579.
- LI, Z., SUN, X., HUANG, L., LIU, D., YU, L., WU, H. & WEI, D. 2017. Phosphate adsorption and precipitation on calcite under calco-carbonic equilibrium condition. *Chemosphere*, 183, 419-428.
- LIU, X., LI, A., MA, L., JING, Z., YANG, J., TANG, Y. & HU, B. 2020. A comparison on phosphorus release and struvite recovery from waste activated sludge by different treatment methods. *International Biodeterioration & Biodegradation*, 148, 104878.
- LUKHELE, T. & MSAGATI, T. A. M. 2024. Eutrophication of Inland Surface Waters in South Africa: An Overview. *International Journal of Environmental Research*, 18, 27.
- MAGAGANE, N., MASINDI, V., RAMAKOKOVHU, M. M., SHONGWE, M. B. & MUEDI, K. L. 2019. Facile thermal activation of non-reactive cryptocrystalline magnesite and its application on the treatment of acid mine drainage. *Journal of Environmental Management*, 236, 499-509.
- MANNI, A., BOUMBIMBA, R., MIKDAM, A., BOUARI, A., ADDIEGO, F., MEZIANI, J. & MARC, W. 2022. Magnesite and dolomite micro-particles: preparation, physical properties and application in bio-based polymer composite. *Polymer Bulletin*, 79.
- MASINDI, V., CHATZISYMEON, E., KORTIDIS, I. & FOTEINIS, S. 2018. Assessing the sustainability of acid mine drainage (AMD) treatment in South Africa. *Science of the Total Environment*, 635, 793-802.
- MASINDI, V., GITARI, M. W., TUTU, H. & DE BEER, M. 2014. Neutralization and attenuation of metal species in acid mine drainage and mine leachates using magnesite: a batch

- experimental approach. *An Interdisciplinary Response to Mine Water Challenges*, 640-644.
- MASINDI, V., GITARI, W. M. & PINDIHAMA, K. G. 2015. Adsorption of phosphate from municipal effluents using cryptocrystalline magnesite: complementing laboratory results with geochemical modelling.
- MASINDI, V., OSMAN, M. S. & SHINGWENYANA, R. 2019. Valorization of acid mine drainage (AMD): A simplified approach to reclaim drinking water and synthesize valuable minerals - Pilot study. *Journal of Environmental Chemical Engineering*.
- MAVHUNGU, A., MASINDI, V., FOTEINIS, S., MBAYA, R., TEKERE, M., KORTIDIS, I. & CHATZISYMEON, E. 2020a. Advocating circular economy in wastewater treatment: Struvite formation and drinking water reclamation from real municipal effluents. *Journal of Environmental Chemical Engineering*, 8.
- MAVHUNGU, A., MASINDI, V., FOTEINIS, S., MBAYA, R., TEKERE, M., KORTIDIS, I. & CHATZISYMEON, E. 2020b. Advocating circular economy in wastewater treatment: Struvite formation and drinking water reclamation from real municipal effluents. *Journal of Environmental Chemical Engineering*, 8, 103957.
- MAVHUNGU, A., MBAYA, R., MASINDI, V., FOTEINIS, S., MUEDI, K. L., KORTIDIS, I. & CHATZISYMEON, E. 2019. Wastewater treatment valorisation by simultaneously removing and recovering phosphate and ammonia from municipal effluents using a mechano-thermo activated magnesite technology. *Journal of Environmental Management*, 250, 109493.
- MEHTA, C. M., KHUNJAR, W. O., NGUYEN, V., TAIT, S. & BATSTONE, D. J. 2015. Technologies to Recover Nutrients from Waste Streams: A Critical Review. *Critical Reviews in Environmental Science and Technology*, 45, 385-427.
- MUGWILI, M. E., WAANDERS, F. B., MASINDI, V. & FOSSO-KANKEU, E. 2023. An update on sustainabilities and challenges on the removal of ammonia from aqueous solutions: A state-of-the-art review. *Journal of Environmental Management*, 347.
- NAJA, G. M. & VOLESKY, B. 2017. Toxicity and sources of Pb, Cd, Hg, Cr, As, and radionuclides in the environment. *Handbook of advanced industrial and hazardous wastes management*. Crc Press.
- NEDBANK 2024. Daily Exchange Rates for 2024.
- NGUYEN, Q.-M., JEONG, S. & LEE, S. 2017. Characteristics of membrane foulants at different degrees of SWRO brine concentration by membrane distillation. *Desalination*, 409, 7-20.

- PENG, L., DAI, H., WU, Y., PENG, Y. & LU, X. 2018. A comprehensive review of phosphorus recovery from wastewater by crystallization processes. *Chemosphere*, 197, 768-781.
- PETRIE, B., BARDEN, R. & KASPRZYK-HORDERN, B. 2015. A review on emerging contaminants in wastewaters and the environment: Current knowledge, understudied areas and recommendations for future monitoring. *Water Research*, 72, 3-27.
- PRINCE, A., RANA, D., MATSUURA, T., NEELAMEGAM, A., T.S, S. & SINGH, G. 2014. Nanofiber based triple layer hydro-philic/-phobic membrane - A solution for pore wetting in membrane distillation. *Scientific reports*, 4, 6949.
- PROVOLO, G., MANULI, G., FINZI, A., LUCCHINI, G., RIVA, E. & SACCHI, G. A. 2018. Effect of Pig and Cattle Slurry Application on Heavy Metal Composition of Maize Grown on Different Soils. *Sustainability*, 10, 2684.
- SEYMOUR, D. 2009. 10-Year Commodity Price Chart for Phosphate Rock – Phosphate Rock (\$/metric ton). Kennedy/Jenks Consultants.
- SHOKRI, A. & SANAVI FARD, M. 2023. Techno-economic assessment of water desalination: Future outlooks and challenges. *Process Safety and Environmental Protection*, 169, 564-578.
- SIKOSANA, M., RANDALL, D. & VON BLOTTNITZ, H. 2017. A technological and economic exploration of phosphate recovery from centralised sewage treatment in a transitioning economy context. *Water SA*, 43, 343.
- SIMMS, T. 2023. Electrochemically Precipitated Struvite Effects on Soil Property and Crop Response. . Doctoral dissertation, University of Arkansas.
- SINGH, B. J., CHAKRABORTY, A. & SEHGAL, R. 2023. A systematic review of industrial wastewater management: Evaluating challenges and enablers. *Journal of Environmental Management*, 348, 119230.
- STOLZENBURG, P., CAPDEVIELLE, A., TEYCHENÉ, S. & BISCANS, B. 2015. Struvite precipitation with MgO as a precursor: Application to wastewater treatment. *Chemical Engineering Science*, 133, 9-15.
- SUTIYONO, S., EDAHWATI, L., PERWITASARI, D. S., MURYANTO, S., JAMARI, J. & BAYUSENO, A. P. 2016. Synthesis and Characterisation of Struvite Family Crystals by An Aqueous Precipitation Method. *MATEC Web of Conferences*, 58, 01006.
- TALBOYS, P. J., HEPPELL, J., ROOSE, T., HEALEY, J. R., JONES, D. L. & WITHERS, P. J. 2016. Struvite: a slow-release fertiliser for sustainable phosphorus management? *Plant Soil*, 401, 109-123.

- TARAYRE, C., DE CLERCQ, L., CHARLIER, R., MICHELS, E., MEERS, E., CAMARGO-VALERO, M. & DELVIGNE, F. 2016. New perspectives for the design of sustainable bioprocesses for phosphorus recovery from waste. *Bioresource Technology*, 206, 264-274.
- TCHOBANOGLIOUS, G., BURTON, F. L. & STENSEL, H. D. 2003. *Wastewater Engineering, Treatment and Reuse*, Boston, McGraw-Hill.
- TOWLER, G. & SINNOTT, R. 2021. *Chemical engineering design: principles, practice and economics of plant and process design*, Butterworth-Heinemann.
- TURTON, R. 2009. *Analysis, Synthesis, and Design of Chemical Processes*, Prentice Hall.
- VE, L., CUONG, D., NGUYEN, T., NGUYEN, Q., NGUYEN, L., HOANG, M. & MAHMOUDI, F. 2024. Mass Transfer Mechanism Within Commercial PTFE Membranes In Spacer-Filled Direct Contact Membrane Distillation. *International Journal of Membrane Science and Technology*, 11, 281-295.
- VINARDELL, S., CORTINA, J. L. & VALDERRAMA, C. 2023. Environmental and economic evaluation of implementing membrane technologies and struvite crystallisation to recover nutrients from anaerobic digestion supernatant. *Bioresour Technol*, 384, 129326.
- WURTSBAUGH, W., PAERL, H. & DODDS, W. 2019. Nutrients, eutrophication and harmful algal blooms along the freshwater to marine continuum. *Wiley Interdisciplinary Reviews: Water*, 6, e1373.
- XIANG, W., YE, Y., WU, X., SMYTH, J., YANG, Y., ZHANG, Z. & ZHONGPING, W. 2019. High-temperature Raman and FTIR study of aragonite-group carbonates. *Physics and Chemistry of Minerals*, 46.
- YAGI, S. & FUKUSHI, K. 2012. Removal of phosphate from solution by adsorption and precipitation of calcium phosphate onto monohydrocalcite. *Journal of Colloid and Interface Science*, 384, 128-136.
- YAN, Z., YANG, H., QU, F., ZHANG, H., RONG, H., YU, H., LIANG, H., DING, A., LI, G. & VAN DER BRUGGEN, B. 2019. Application of membrane distillation to anaerobic digestion effluent treatment: Identifying culprits of membrane fouling and scaling. *Sci Total Environ*, 688, 880-889.
- YE, Y., NGO, H. H., GUO, W., CHANG, S. W., NGUYEN, D. D., ZHANG, X., ZHANG, J. & LIANG, S. 2020. Nutrient recovery from wastewater: From technology to economy. *Bioresource Technology Reports*, 11, 100425.

- YETILMEZSOY, K., ILHAN, F., KOCAK, E. & AKBIN, H. M. 2017. Feasibility of struvite recovery process for fertilizer industry: A study of financial and economic analysis. *Journal of Cleaner Production*, 152, 88-102.
- ZAREBSKA-MØLGAARD, A., LI, K., NIEDZIELSKA, A., SCHNEIDER, C., YANGALI-QUINTANILLA, V., TSAPEKOS, P., ANGELIDAKI, I., WANG, J. & HELIX-NIELSEN, C. 2022. Techno-economic assessment of a hybrid forward osmosis and membrane distillation system for agricultural water recovery. *Separation and Purification Technology*, 283, 120196.
- ZAYNAB, M., AL-YAHYAI, R., AMEEN, A., SHARIF, Y., ALI, L., FATIMA, M., KHAN, K. A. & LI, S. 2022. Health and environmental effects of heavy metals. *Journal of King Saud University - Science*, 34, 101653.
- ZHU, W., DUAN, C. & CHEN, B. 2024. Energy efficiency assessment of wastewater treatment plants in China based on multiregional input–output analysis and data envelopment analysis. *Applied Energy*, 356, 122462.

